Journal of Materials Science: Materials in Electronics

Editorial board Aims & scope Journal updates

The Journal of Materials Science: Materials in Electronics is an established refereed companion to the Journal of Materials Science. It publishes papers on materials and their applications in modern electronics, covering the ground between fundamental science, such as semiconductor physics, and work concerned specifically with applications. It explores the growth and preparation of new materials, as well as their processing, fabrication, bonding and encapsulation, together with the reliability, failure analysis, quality assurance and characterization related to the whole range of applications in electronics. The Journal presents papers in newly developing fields such as low dimensional structures and devices, optoelectronics including III-V compounds, glasses and linear/non-linear crystal materials and lasers, high Tc superconductors, conducting polymers, thick film materials and new contact technologies, as well as the established electronics device and circuit materials. —

show all

Editor-in-Chief

Safa O. Kasap

Publishing model

Hybrid (Transformative Journal). How to publish with us, including Open Access

2.478 (2020)

Impact factor

2.171 (2020)

Five year impact factor

Sources

Title | Enter title | Find sources

Title: Optical And Quantum Electronics × Optics And Laser Technology × Journal Of Materials Science: Materials In Electronics ×

Improved Citescore

We have updated the CiteScore methodology to ensure a more robust, stable and comprehensive metric which provides an indication of research impact, earlier. The updated methodology will be applied to the calculation of CiteScore, as well as retroactively for all previous CiteScore years (ie. 2018, 2017, 2016…). The previous CiteScore values have been removed and are no longer available.

View CiteScore methodology. >

Filter refine list

Apply Clear filters

Display options

- Display only Open Access journals

Counts for 4-year timeframe

- No minimum selected
- Minimum citations
- Minimum documents

Citescore highest quartile

- Show only titles in top 10 percent
- 1st quartile
- 2nd quartile
- 3rd quartile
- 4th quartile

Source type

- Journals
- Book Series
- Conference Proceedings
- Trade Publications

Apply Clear filters

3 results

Download Scopus Source List | Learn more about Scopus Source List

All | Export to Excel | Save to source list

View metrics for year: 2021

	Source title	Documents 2018-21	% Cited	SNIP	SJR	Publisher
1	Optics and Laser Technology	2,746	84	1.478	0.848	Elsevier
2	Journal of Materials Science: Materials in Electronics	8,844	74	0.637	0.464	Springer Nature
3	Optical and Quantum Electronics	2,064	64	0.922	0.432	Springer Nature

Top of page

About Scopus

What is Scopus

Content coverage

Scopus blog

Scopus API

Privacy matters

Language

日本語版を表示する

查看简体中文版本

查看繁體中文版本

Просмотр версии на русском языке

Customer Service

Help

Tutorials

Contact us

efine Your Search Results

J Mater Sci: Mater Electron Search

rt By: Relevancy

earch Results

ound 2,488 results (Page 1) Share These Results

id you mean this journal?

JOURNAL OF MATERIALS SCIENCE-MATERIALS IN ELECTRONICS

Publisher: SPRINGER , VAN GODEWIJCKSTRAAT 30, DORDRECHT, NETHERLANDS, 3311 GZ

ISSN / eISSN: 0957-4522 / 1573-482X

Web of Science Core Collection: Science Citation Index Expanded

Additional *Web of Science* Indexes: Current Contents Electronics & Telecommunications Collection | Current Contents Engineering, Computing & Technology | Current Contents Physical, Chemical & Earth Sciences | Essential Science Indicators

Share This Journal

View profile page

* Requires free login.

ther Possible Matches

JOURNAL OF MATERIALS SCIENCE & TECHNOLOGY

J Mater Sci: Mater Electron

Enhanced thermoluminescence properties of $CaSrAl_2SiO_7:Ce^{3+},Tb^{3+}$ phosphor

Shweta S. Sharma[1,*], Nameeta Brahme[2], D. P. Bisen[2], Pradeep Dewangan[3], Ishwar Prasad Sahu[4], Suresh G. Onkar[1], Vijay S. Thool[1], Shilpa G. Vidhale[1], and Girish S. Mendhe[1]

[1] Department of Physics, Adarsha Science, J. B. Arts and Birla Commerce College, Dhamangaon, Maharashtra 444709, India
[2] School of Studies in Physics and Astrophysics, Pt. Ravishankar Shukla University, Raipur, Chhattisgarh 492010, India
[3] Department of Physics, Faculty of Science, Shri Rawatpura Sarkar University, Raipur, Chhattisgarh 492010, India
[4] Department of Physics, Indira Gandhi National Tribal University, Amarkantak, Madhya Pradesh 484887, India

Received: 15 April 2021
Accepted: 10 October 2021

ABSTRACT

The application of thermoluminescence technique in radiation dosimetry spans field of health physics, biological and geological sciences and personnel monitoring; this led to the search for new compositions with desirable dosimetric properties. In the present work, $CaSrAl_2SiO_7:Tb^{3+}$ and $CaSrAl_2SiO_7:Ce^{3+},Tb^{3+}$ phosphors were prepared by solid-state reaction method and their TL properties were studied in detail. The comparison of their TL results showed that co-doping of Ce^{3+} ions enhanced TL response of $CaSrAl_2SiO_7:Tb^{3+}$ phosphors; this was also verified from measurement of TL emission spectra of the samples. Optimized glow curves were analysed and TL parameters were extracted from Chen's method. Co-doped $CaSrAl_2SiO_7:Ce^{3+},Tb^{3+}$ phosphor is found to be useful in dosimetric application.

1 Introduction

When an insulating or a superconducting material is exposed to any kind of ionizing radiation, deposited energy is stored in the defect sites and colour centres of the crystal lattice. Due to action of heat energy, a fraction of this stored energy released and emitted as visible light which is called thermoluminescence [1, 2]. Nowadays application of various radiations such as ultraviolet, X-rays, β-rays, γ-rays in the different fields like medical, industrial, agriculture, etc., is increasing [3]. Thermoluminescence (TL) is one of the techniques used in radiation dosimetry [4]. Thermoluminescent materials are more investigated in on-going researches, because they found to have increasing application in thermoluminescence dosimeters. Thermoluminescent dosimeters necessarily have linearity of TL response with exposed radiation dose.

$CaSrAl_2SiO_7$ is one of the members of melilite group; these melilites that are basically silicate-based materials showed their use in TL dosimetry. In this work, thermoluminescence properties of $CaSrAl_2SiO_7:Tb^{3+}$ phosphor are investigated and also

Address correspondence to E-mail: sharma.shweta2812@gmail.com

https://doi.org/10.1007/s10854-021-07260-z
Published online: 25 October 2021

observed that co-doping of Ce^{3+} ions enhanced TL of $CaSrAl_2SiO_7:Tb^{3+}$ phosphor. The effect of different Tb^{3+} concentration in both single and co-doped samples on the TL glow curves has been recorded and glow curve is analysed by computerized glow curve deconvolution method. To the best of our knowledge, there is no earlier report on thermoluminescence investigation on $CaSrAl_2SiO_7:Tb^{3+}$ and $CaSrAl_2SiO_7$: Ce^{3+},Tb^{3+} phosphors.

2 Synthesis and experimental

Phosphors for the study were prepared by solid-state reaction method at high temperature using analytical reagent (AR) grade raw chemicals with more than 99% accuracy. Calcium carbonate, strontium carbonate, aluminium oxide, silicon di-oxide, ceric oxide and terbium oxide were the starting materials. The amounts of the raw chemicals were calculated according to stoichiometric ratio in $CaSrAl_2SiO_7:Ce^{3+}$ (0.5 mol%),Tb^{3+} (y mol%), where y = 1.0, 3.0, 5.0, 7.0, 10.0 mol%. Required quantities of raw materials were mixed homogeneously using agate mortar and pestle for 3 h. The resultant mixtures were fired at high temperature 1300 °C for 5 h. It was then slowly cooled to room temperature inside the closed furnace. The powders so formed were collected by crushing the prepared samples. Now the samples were ready for all other characterization studies.

Phase of synthesized phosphor was confirmed by X-ray diffraction (XRD) technique using Cu-Kα radiation with the help of D2 phaser Bruker diffractometer. Thermoluminescence investigation of phosphor was performed by TLD reader, Nucleonix TL 1009I with constant heating rate of 5 °C/s. As sample must be exposed to any kind of radiation before measurement of TL, UV cabinet is used, where the samples were exposed to UV radiation of 254 nm. Band pass filters of different wavelengths have been used to record TL emission spectrum. To record TL emission spectrum, the processes used in recording TL glow curves were repeated; here the sample that is placed in canthal strip was covered with band pass filter. The band pass filter allows the signals of selected range of wavelengths; hence in TL emission spectrum, characteristic emission peaks were observed.

3 Results and discussion

3.1 XRD investigation

To verify the preparation of phosphors, they were analysed by XRD tool that reveals the phase composition. Figure 1 shows the XRD patterns of Tb^{3+} singly doped and Ce^{3+},Tb^{3+} co-doped $CaSrAl_2SiO_7$ phosphors along with JCPDS file. It is clear that phosphors have good crystallization with no any impurity phase, as experimental diffraction patterns well matched with JCPDS file 26-0327 of $CaSrAl_2SiO_7$. Hence, the as-prepared phosphors have tetragonal crystallographic structure whose space group is $P\bar{4}2_1$ m [5].

3.2 Thermoluminescence investigation

Thermoluminescence (TL) is light emission due to moderate heating of a solid, previously exposed to ionizing radiation. The absorption of the ionizing radiation (UV, X-, β- or γ-rays, high-energy particles) creates traps, and fills them (or those already exist) with electrons and/or holes even at low temperatures. The subsequent heating migrates the electrons

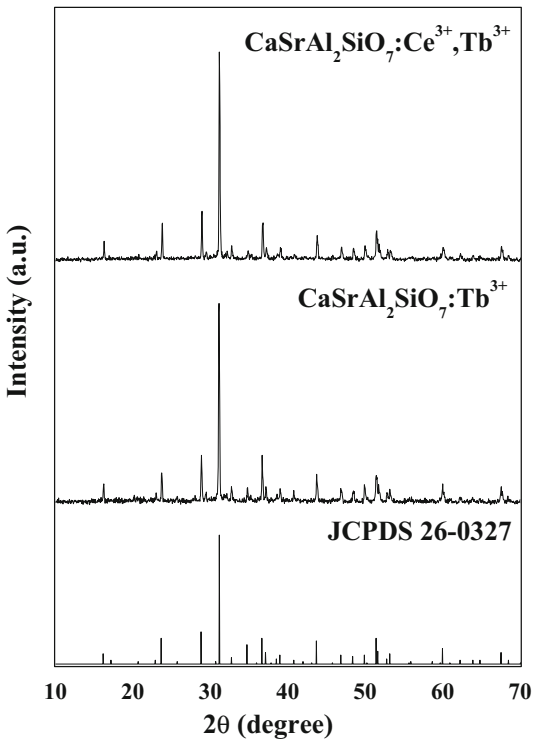

Fig. 1 Diffraction patterns of $CaSrAl_2SiO_7:Tb^{3+}$ and $CaSrAl_2SiO_7:Ce^{3+},Tb^{3+}$ phosphors

and/or holes in the lattice, until they fall into other traps (or recombine) with a consequent photon emission [6]. Thermoluminescent emission from TL materials is very sensitive to the amount and nature of dopant element and radiation effect. So in the present research work, we used Ce^{3+} and Tb^{3+} as single and co-dopant ions with their various concentrations; after that TL measurement was performed for each sample with optimized dopant and co-dopant concentration with various ultraviolet (UV) exposure time and then TL kinetic parameters were extracted from the Chen's peak shape method.

3.2.1 *Thermoluminescence of $CaSrAl_2SiO_7:Ce^{3+}$*

Let us first focus on the investigated thermoluminescence properties of $CaSrAl_2SiO_7:Ce^{3+}$ phosphor; this was already discussed in our previous work in which Ce^{3+} concentration was varied as 0.1, 0.3, 0.5, 1.0, 2.0, 3.0 and 4.0 mol% [7]. The optimized glow curve was obtained for 0.5 mol% Ce^{3+}-doped $CaSrAl_2SiO_7$ phosphor. This optimized phosphor showed an increment in TL intensity up to 35 min of UV irradiation time. As we further increased UV exposure time, saturation in TL intensity was found.

3.2.2 *Thermoluminescence of $CaSrAl_2SiO_7:Tb^{3+}$*

At the second attempt, TL properties of $CaSrAl_2SiO_7:Tb^{3+}$ phosphor was seen and this report is dealing here for the first time. Figure 2 represents a series of Tb^{3+} concentration (1.0, 3.0, 5.0, 7.0, 10.0 mol%)-dependent TL glow curves of $CaSrAl_2SiO_7:Tb^{3+}$ samples. TL peak position is independent of the concentration of Tb^{3+} element and exhibits no shift with change in doping concentration. The only variation obtained in the TL peak intensity while increasing Tb^{3+} concentration. It can be understood from the inset of Fig. 2 that TL intensity of sample first increased with rise in Tb^{3+} concentration, attained a highest value at 5.0 mol% of Tb^{3+} ions and then decreased with further increase in Tb^{3+} concentration; this behaviour arises from concentration quenching process after a particular Tb^{3+} concentration. As we increase impurity concentration, there is an increase in the number of defects/traps which in turn implies a growth in the density of charge carriers being trapped upon irradiation. Therefore the initial rise in the TL peak intensity or area of the glow curves. Furthermore, on being thermally stimulated,

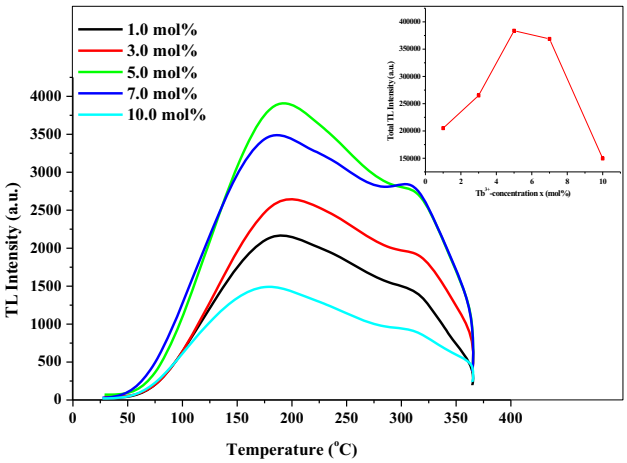

Fig. 2 Concentration-dependent TL glow curves of $CaSrAl_2SiO_7:yTb^{3+}$ phosphors with 10-min UV exposure time

these charge carriers release from traps which in turn recombine with their counterparts at the recombination centre and yield diverse TL glow peaks with elevated height [8].

As thermoluminescence properties are greatly affected by exposure time, TL property of $CaSrAl_2SiO_7:Tb^{3+}$ (5.0 mol%) phosphor was measured with different UV exposure time. For variable UV exposure time, some of the selected TL glow curves of $CaSrAl_2SiO_7:Tb^{3+}$ (5.0 mol%) are represented in Fig. 3. Spectral behaviour was same with increase in length of UV exposure time but peak TL intensity or glow curve area altered with increase in exposure time. The growth in TL response was observed as exposure time was boosted and after 60 min of UV exposure TL response diminished with more added exposure time. With increasing irradiation dose more and more trapping centres or luminescent centres responsible for the TL glow peaks are getting filled. Upon thermal stimulation, these traps liberate their charge carriers and they get recombine with their counterparts, giving rise to different glow peaks. When all the trapping centres that are subjected to desired TL emission get filled, the saturation or decrease in the TL intensity starts appearing [8–10].

3.2.3 *Thermoluminescence of $CaSrAl_2SiO_7:Ce^{3+},Tb^{3+}$*

Thermoluminescence experiments were performed on the series of $CaSrAl_2SiO_7:xCe^{3+}$ and $CaSrAl_2SiO_7:yTb^{3+}$ phosphors that the results point out optimal concentration of Ce^{3+} as x = 0.5 mol% and of Tb^{3+} as y = 5.0 mol%. In the present work, co-doping

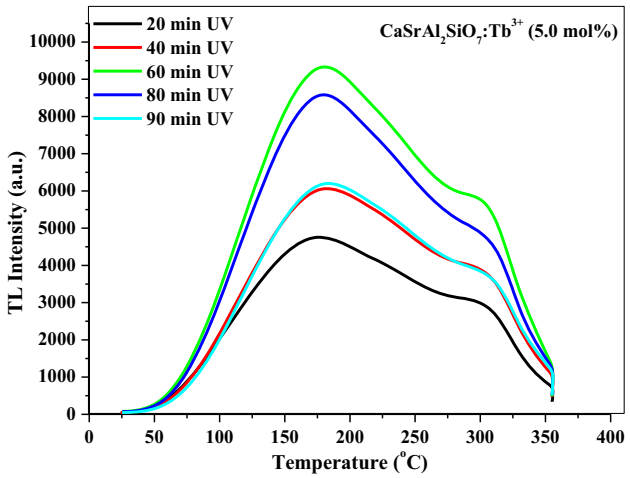

Fig. 3 Effect of UV exposure time on the TL glow curve of $CaSrAl_2SiO_7:Tb^{3+}$ (5.0 mol%) phosphor

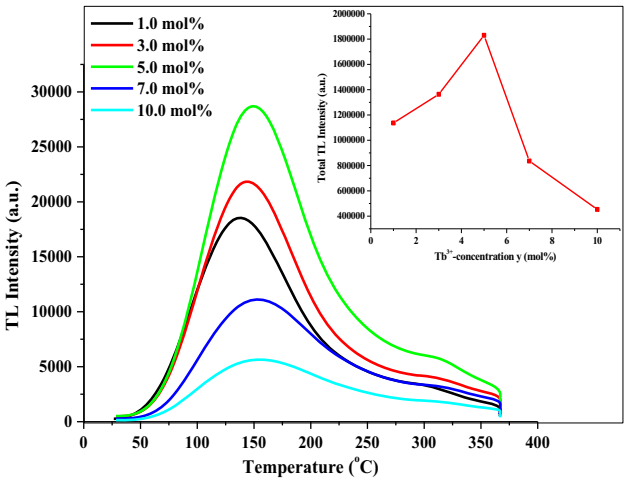

Fig. 4 Tb^{3+} concentration-dependent TL glow curves of $CaSrAl_2SiO_7:Ce^{3+},Tb^{3+}$ phosphor with 30-min UV exposure time

of Ce^{3+} and Tb^{3+} was also performed in $CaSrAl_2SiO_7$ host and TL properties of this co-doped sample were also investigated and compared with TL of singly doped samples. Co-doping was performed with fixed concentration of Ce^{3+} (x = 0.5 mol%) and variable concentration of Tb^{3+} (y = 1.0, 3.0, 5.0, 7.0, 10.0 mol%).

Figure 4 shows TL glow curves of $CaSrAl_2SiO_7:Ce^{3+}$ (x = 0.5 mol%), Tb^{3+} (y = 1.0, 3.0, 5.0, 7.0, 10.0 mol%) phosphors with fixed UV irradiation time. Glow curves for all samples had similar shape but with change in glow curve area. Concentration quenching occurred at 5.0 mol% of Tb^{3+} ions (see inset of Fig. 4). Like Ce^{3+} and Tb^{3+} singly doped samples, impact of various UV irradiation time on the TL glow curve of optimized co-doped $CaSrAl_2SiO_7:Ce^{3+}$ (0.5 mol%),Tb^{3+} (5.0 mol%) sample was seen and this result is depicted in Fig. 5. It can be clearly seen from Fig. 5 that TL intensity of optimized co-doped phosphor increased up to 100 min of UV exposure and then decreased.

3.2.4 *Evaluation of TL parameters*

To determine TL parameters, broad glow curves of 60-min UV exposed $CaSrAl_2SiO_7:Tb^{3+}$ (5.0 mol%) and 100-min UV exposed $CaSrAl_2SiO_7:Ce^{3+}$ (0.5 mol%),Tb^{3+} (5.0 mol%) samples were first applied to computerized glow curve deconvolution (CGCD) method. Both samples were found to have four overlapping peaks in their parent glow curves. The position of constituent peaks is shown in Fig. 6. TL parameters like geometrical shape factor (μ_g),

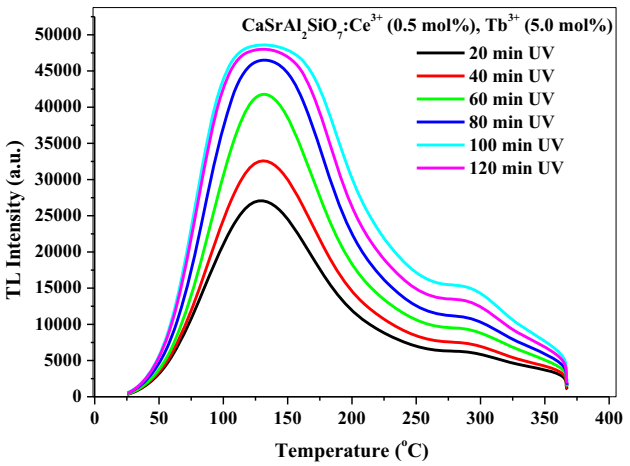

Fig. 5 Effect of UV exposure time on the TL glow curve of $CaSrAl_2SiO_7:Ce^{3+},Tb^{3+}$ phosphor

order of kinetics (b), frequency factor (S) and activation energy (E) were extracted using Chen's peak shape method. The calculated TL parameters of Tb^{3+}-doped and Ce^{3+},Tb^{3+} co-doped $CaSrAl_2SiO_7$ phosphors are listed in Table 1.

3.2.5 *TL emission spectra*

Figure 7 represents comparison of TL emission spectra of $CaSrAl_2SiO_7:Ce^{3+}$, $CaSrAl_2SiO_7:Tb^{3+}$ and $CaSrAl_2SiO_7:Ce^{3+},Tb^{3+}$ phosphors. Emission spectra were recorded using interference band pass filters of various wavelengths from 400 to 700 nm. Emission spectra of Ce^{3+}-doped sample was already discussed in our previous article [7], here it is shown for comparison only. The three samples have characteristic

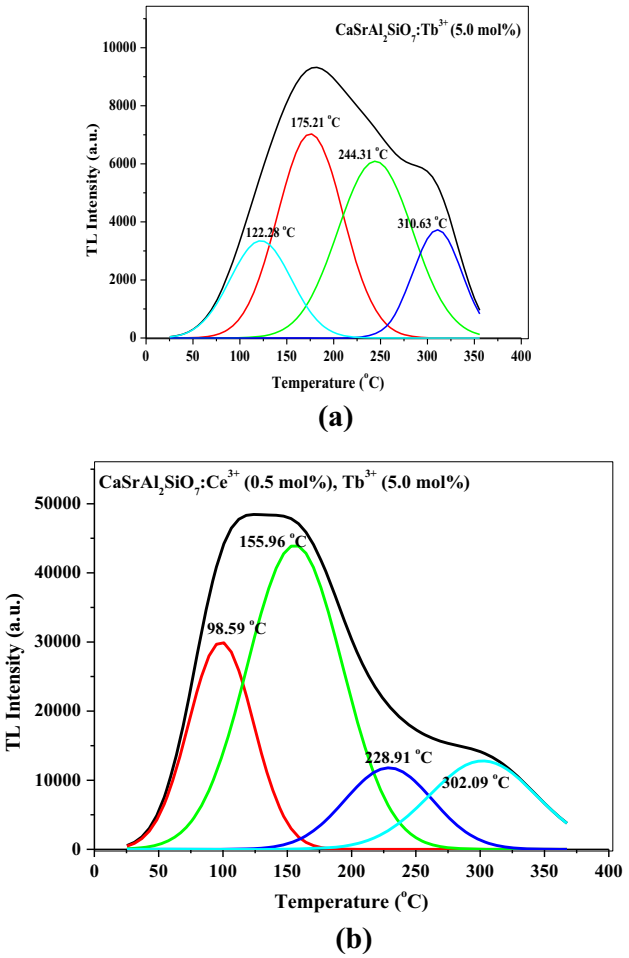

Fig. 6 Representation of peak deconvolution on parent glow curve of **a** $CaSrAl_2SiO_7:Tb^{3+}$ and **b** $CaSrAl_2SiO_7$: Ce^{3+},Tb^{3+} phosphors

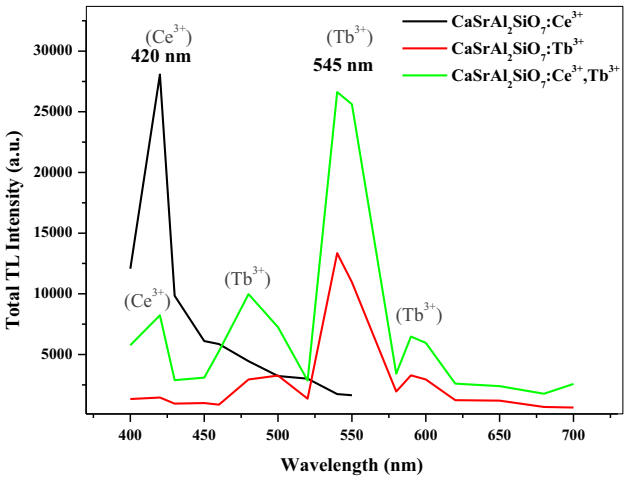

Fig. 7 TL Emission spectra of $CaSrAl_2SiO_7:Ce^{3+}$, $CaSrAl_2SiO_7:Tb^{3+}$ and $CaSrAl_2SiO_7:Ce^{3+},Tb^{3+}$ phosphors

emission peaks of respective dopant and co-dopant ions. $CaSrAl_2SiO_7:Tb^{3+}$ sample has emission peaks at around 480, 545 and 590 nm these are due to characteristic transition $^5D_4 \rightarrow {}^7F_6$, $^5D_4 \rightarrow {}^7F_5$ and $^5D_4 \rightarrow {}^7F_4$ of Tb^{3+} ions [11]. $CaSrAl_2SiO_7:Ce^{3+},Tb^{3+}$ sample has characteristic peak of Ce^{3+} ions at around 420 nm, due to 5d ($^5D_{3/2}$) → 4f ($^2F_{5/2}$) [12, 13]and characteristic peaks of Tb^{3+} ions situated at around 480, 545 and 600 nm; these are due to above-mentioned transitions of Tb^{3+} ions.

Figure 8 shows the comparative TL glow curves of the three optimized phosphors. Ce^{3+},Tb^{3+} co-doped phosphor has most intense TL properties among all three. Also from Fig. 7 it is clearly visible that TL emission of cerium ions is decreased, while TL emission of terbium ions is increased in co-doped sample; hence co-doping of small amount of Ce^{3+} ions, i.e., 0.5 mol%, may enhance TL emission of Tb^{3+} ions in $CaSrAl_2SiO_7$ host.

Present study concludes that among the three, Ce^{3+},Tb^{3+} co-doped $CaSrAl_2SiO_7$ phosphor has almost linear increment in total TL intensity with respect to UV exposure time up to 100 min, which is very large range as compared to other UV irradiated silicate, aluminate and aluminosilicate-based phosphors such as $Ca_2Al_2SiO_7:Ce^{3+},Tb^{3+}$ [14]; $Ca_2Al_2SiO_7:Ce^{3+}$[15]; $BaMgAl_{10}O_{17}:Ce^{3+}$ [16]. Hence

Table 1 Calculated TL parameters

Phosphor	T_m (°C)	μ_g	b	E (eV)	S (s^{-1})
$CaSrAl_2SiO_7:Tb^{3+}$ (5.0 mol%)	122.28	0.48	1	0.46	8.07×10^6
	175.21	0.48	1	0.57	2.45×10^7
	244.31	0.49	1	0.75	1.82×10^8
	310.63	0.70	2	1.41	2.12×10^{13}
$CaSrAl_2SiO_7:Ce^{3+}$ (0.5 mol%),Tb^{3+} (5.0 mol%)	98.59	0.49	1	0.54	2.35×10^8
	155.96	0.5	2	0.53	1.4×10^7
	228.91	0.49	1	0.78	7.45×10^8
	302.09	0.49	1	0.82	1.37×10^8

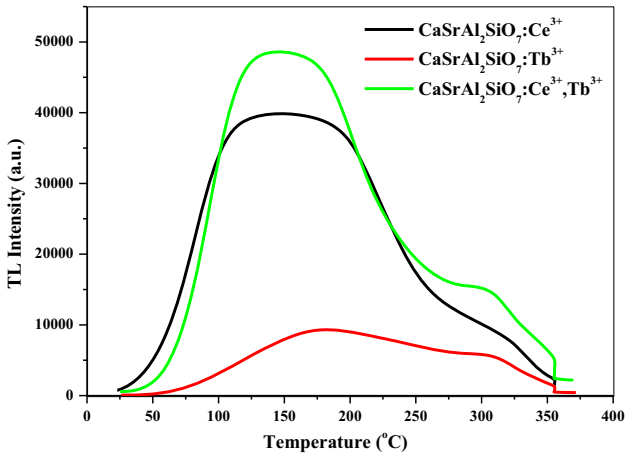

Fig. 8 Comparative TL glow curves of $CaSrAl_2SiO_7:Ce^{3+}$, $CaSrAl_2SiO_7:Tb^{3+}$ and $CaSrAl_2SiO_7:Ce^{3+},Tb^{3+}$ phosphors

$CaSrAl_2SiO_7:Ce^{3+},Tb^{3+}$ phosphor may be most appropriately useful for UV dosimeter application.

4 Conclusions

$CaSrAl_2SiO_7:yTb^{3+}$ and $CaSrAl_2SiO_7:Ce^{3+},yTb^{3+}$ phosphors were prepared by solid-state reaction method. Detail comparative TL study of singly doped and co-doped samples was investigated. Concentration-dependent TL glow curves of $CaSrAl_2SiO_7:yTb^{3+}$ phosphor and $CaSrAl_2SiO_7:Ce^{3+},yTb^{3+}$ phosphors were measured and found that 5.0 mol % is optimized concentration of Tb^{3+} ions in both samples. Tb^{3+} singly doped sample showed linear increment in TL intensity up to 60 min, while Ce^{3+},Tb^{3+} co-doped sample showed this linearity up to 100 min, also TL properties of co-doped sample got enhanced with inclusion of 0.5 mol% of Ce^{3+} ions, this was also verified from TL emission spectra. Hence the optimized $CaSrAl_2SiO_7:Ce^{3+}$(0.5 mol%),Tb^{3+}(5.0 mol%) phosphor may be a potential candidate for UV dosimeter application.

References

1. B.C. Bhatta, M.S. Kulkarni, Thermoluminescent phosphors for radiation dosimetry. Defect Diffus. Forum **347**, 179–227 (2014). https://doi.org/10.4028/www.scientific.net/DDF.347.179
2. T.H. Van, S.N. Manh, Q.V. Xuan, S. Bounyavong, Photoluminescence and thermoluminescence characteristics of $Sr_3B_2O_6:Eu^{2+}$ yellow phosphor. J. Lumin. **31**, 1103–1108 (2016)
3. N.A. Razak, S. Hashim, M.H.A. Mhareba, N. Tamchek, Photoluminescence and thermoluminescence properties of Li_2O-Na_2O-B_2O_3 glass. J. Lumin. **31**, 754–759 (2016)
4. C. Furetta, F. Santopietro, C. Sanipoli, G. Kitis, Thermoluminescent (TL) properties of the perovskite $KMgF_3$ activated by Ce and Er impurities. Appl. Radiat. Isot. **55**, 533–542 (2001)
5. S. Sharma, N. Brahme, D.P. Bisen, P. Dewangan, Luminescence properties of near-UV excitable yellow-orange light emitting warm $CaSrAl_2SiO_7:Sm^{3+}$ phosphors. J. Rare Earths **37**, 365–373 (2019)
6. R. Capelletti, Luminescence, in *Reference Module in Materials Science and Materials Engineering* (2017). https://doi.org/10.1016/B978-0-12-803581-8.012047-9
7. S. Sharma, N. Brahme, D.P. Bisen, P. Dewangan, S. Tigga, G. Tiwari, A. Khare, Study on photoluminescence and thermoluminescence properties of UV-irradiated $CaSrAl_2SiO_7:Ce^{3+}$ phosphors. J. Mater. Sci. **29**, 1412–1419 (2018)
8. K. Sharma, S. Bahl, B. Singh, P. Kumar, S.P. Lochab, A. Pandey, $BaSO_4$: Eu as an energy independent thermoluminescent radiation dosimeter for gamma rays and $^{C6}+$ ion beam. Radiat. Phys. Chem. **145**, 64–73 (2018)
9. D. Joseph Daniel, O. Annalakshmi, U. Madhusoodanan, P. Ramasamy, Thermoluminescence characteristics and dosimetric aspects of fluoroperovskites (NaMgF3:Eu2+, Ce3+). J. Rare Earths **32**(6), 496 (2014)
10. N. Kaur, M. Singh, L. Singh, S.P. Lochab, Investigation of thermoluminescence characteristics of gamma irradiated phlogopite mica. Radiat. Phys. Chem. **87**, 26–30 (2013)
11. D. Deng, R. Chen, W. Feng, H. Guan, Terbium single-doped or terbium and sodium codoped barium zinc phosphate: a novel green phosphor for near ultraviolet-pumped white light emitting diodes. Spectrosc. Lett. **50**(8), 451–455 (2017)
12. S. Sharma, N. Brahme, D.P. Bisen, P. Dewangan, R. Gupta, Generation of cold white light by using energy transfer process in single phase Ce^{3+}/Tb^{3+} co-doped $CaSrAl_2SiO_7$ phosphor. Opt. Laser Technol. **135**, 106682 (2021)
13. P. Parasuraman, J. Rajeev Gandhi, M. Rathnakumari, P. Sureshkumar, Photoluminescence in cerium doped barium aluminium borate difluoride—$BaAlBO_3F_2$ glass ceramics. Optik **127**, 8956–8962 (2016)
14. G. Tiwari, N. Brahme, D.P. Bisen, S.K. Sao, R. Sharma, Thermoluminescence and mechanoluminescence properties of UV-irradiated $Ca_2Al_2SiO_7:Ce^{3+}$, Tb^{3+} phosphor. Phys. Procedia **76**, 53–58 (2015)
15. G. Tiwari, N. Brahme, R. Sharma, D.P. Bisen, S.K. Sao, M. Singh, Fracto-mechanoluminescence and thermoluminescence properties of UV and γ-irradiated $Ca_2Al_2SiO_7:Ce^{3+}$ phosphor. J. Biol. Chem. Lumin. **31**(3), 793–801 (2016)

16. S. Tigga, N. Brahme, D.P. Bisen, Investigations on luminescence behaviour of Ce-activated $BaMgAl_{10}O_{17}$ phosphor. J. Biol. Chem. Lumin. **31**(7), 1306–1312 (2016)

ISSN NO : 0363-8057

GRADIVA REVIEW JOURNAL

A Monthly Publishing Journal

Impact Factor : 6.1

UGC-CARE Group - II Journal ()

1.National Multidisciplinary Conference On Sustainable Development'-NMCSD-2022 (Shri-Pundlik-Maharaj-Mahavidyalaya/)

Shri Pundlik Maharaj Mahavidyalaya, Nandura Dist.Buldana (MS), India (Shri-Pundlik-Maharaj-Mahavidyalaya/)

Home ()

Call For Papers (Call-For-Papers/)

Author's (Authors/)

Present Issue (VOLUME-8-ISSUE-3-2022/)

Special Issue (Special-Issue/)

Previous Issues (Previous-Issue/)

Editorial Board (Editorial-Board/)

Contact (Contact/)

ISSN NO : 0363-8057

GRADIVA REVIEW JOURNAL
A Monthly Publishing Journal

Impact Factor : 6.1

UGC-CARE Group - II Journal ()

24.Sustainable Agricultural Development is the Need of the Present Era (gallery/24.rithe%201.pdf)
Dr. Mahadeo A. Rithe
Raje Chhatrapati Kala Mahavidyalaya, Dhamangaon Badhe, Tq. Motala, Dist. Buldana
PAGE NO: 114-117

25.Nematodes that Affect Plants (gallery/25.sachin%20jadhav%201.pdf)
Sachin Dadarao Jadhav,Tejaswini Ramchandra Marakwad ,Sunnanda Manohar Dekate
Shri Pundlik Maharaj Mahavidyalaya, Nandura,Dist. Buldana (MS), India
PAGE NO: 118-123

26.Transparent Window Layer (ZnS) thin films For Solar cell Application (gallery/26.sachin%20mukhmale%201.pdf)
Sachin V. Mukhamale
Shri Pundlik Maharaj Mahavidyalaya Nandura Rly, India
PAGE NO: 124-130

27.Review of the Non-Aligned Movement (gallery/27.sandip%20shirsath%201.pdf)
Shirsath Sandip Haribhau
Shri Dnyaneshwar Mahavidyalaya, Newasa
PAGE NO: 131-135

28.Diversity of Fresh Water Aquatic Hyphomycetes from Bhandardara Dam in Ahmednagar District (M.S) India (gallery/28.sanjay%20ghanwat%201.pdf)
Ghanwat Sanjay Parshuram
Shri Dnyaneshwar Mahavidyalaya, Newasa
PAGE NO: 136-140

29.Sustainability initiatives of selected family businesses in Gujarat State post pandemic (gallery/29.saraswathi%20moorthy%201.pdf)
Dr Saraswathi Moorthy, Hemanshi Kotai
Ramniranjan Jhunjhunwala College of Arts Science and Commerce (Autonomous) ghatkopar West Mumbai
PAGE NO: 141-147

30.Introductory study on machine learning tool WEKA (gallery/30.saurabh%20ghogare%201.pdf)
Dr. Saurabh Ashok Ghogare,Rodge S.A,Swapnil K. Shelke
J. B. Arts and Birla Commerce Mahavidyalaya, Dhamangaon (Rly), Amravati
PAGE NO: 148-151

31.To Study The Physical Characters Of Soil In Shrirampur Tahsil (gallery/31.sharada%20adik%201.pdf)
DR. SharadaNavnath Adik
Shri.DnyaneshwarMahavidyalaya,Newasa ,District -Ahmednagar,Maharashtra
PAGE NO: 152-159

32.Women Empowerment Through Self Help Groups (Shgs) And Sustainable Development Of Rural India (gallery/32.shivling%20rajmane%201.pdf)
Dr. Shivaling B. Rajmane
Deshbhakta Ratnappa Kumbhar College of Commerce (Autonomous), Kolhapur
PAGE NO: 160-165

33.Sustainable Development of Historical city Varanasi, Uttarpradesh (gallery/33.shouvonik%20bala%201%20(1).pdf)
Shouvonik Bala
Vidyasagar College for women, Calcutta
PAGE NO: 166-171

35.Effective Listening : A way to Language Sustainability (gallery/35.smita%20borade%201.pdf)
Smita Arjun Borade
Ashoka College of Education, Nashik
PAGE NO: 172-176

36.Struggle for Existence: A Realistic Study of the Theme of Existential Dilemma in Bernard Malamud's Fiction The Natural (gallery/36.sobal%20rose%201%20(1).pdf)
Dr. Sobal Rose G.Veliannur
Nutan Adarsh Arts, Commerce & Smt. M.H.Wegad Science College, Umrer, Nagpur District
PAGE NO: 177-181

38.Pharmacognostic Study Of Angiospermic Medicinal Plants With Emphasis On Standerdization Parameters (gallery/38.suchita%20dighe%201.pdf)
S.W. Dighe
Shri Pundlik Maharaj Mahavidyalaya , Nandura ,Dist. Buldana
P.S.Kokate
Shri. Shivaji College of Arts , Commerce and Science Akola
S.V. Pundkar
Shri Shivaji Science College , Amravati
PAGE NO: 182-188

GRADIVA REVIEW JOURNAL

ISSN NO : 0363-805

Introductory study on machine learning tool WEKA

Dr. Saurabh Ashok Ghogare
Assistant Professor,
Department of Computer Science,
Adarsha Science, J. B. Arts and Birla Commerce Mahavidyalaya,
Dhamangaon (Rly), Amravati.

Rodge S.A.
Associate Professor,
Department of Electronics
Adarsha Science, J. B. Arts and Birla Commerce Mahavidyalaya,
Dhamangaon (Rly), Amravati.

Mr. Swapnil K. Shelke
Assistant Professor,
Department of Electronics
Adarsha Science, J. B. Arts and Birla Commerce Mahavidyalaya,
Dhamangaon (Rly), Amravati.

Abstract:
Data mining is the process of identifying or extracting new patterns from massive datasets or databases, and it is a powerful new branch of computer science with a lot of potential. It's widely utilized in marketing, surveillance, fraud detection, artificial intelligence, scientific research, and a variety of other industries. Today the size of data is increasing day-by-day. To analyze the dataset from different angles and Data mining techniques the WEKA software is used. This paper describes to understand the basic of WEKA. It also explains the basic techniques to use WEKA and how datasets are load into it. WEKA also Supports Varity of Classifier that also explain in this paper.

Keywords: Data mining, data preprocessing, classification, cluster analysis, JRip, Weka tool et.

1. Introduction:

Today the rapid growth of data over the internet, product related word-of-mouth conversation have migrated to online markets, creating active electronic communication that provide a wealth of information. In data mining, the data is stored electronically and the search is computerized or at least augmented by machine. The use data mining is to gain knowledge, not just predictions [8]. Data Mining is the process of extract hidden information from the data set and it is also called as knowledge discovery. This Techniques is used in various applications such as Education, Banking, Market analysis, Telecom industry, Retail Industry, DNA Analysis and Many more. WEKA is open source software an open source software provides tools for data preprocessing, implementation of several Machine Learning algorithms, and visualization tools which help researchers to develop machine learning techniques and apply them to real-world data mining problems. There are some authors who uses WEKA in their dataset.Y. K. Salal, S. M. Abdullaev, Mukesh Kumar (2019), discovers execution forecast in Academic with assistance of Data Mining procedures to improve instruction quality. Gaganjyot Kaur, Amit Chhabra (2014), The paper portrays successful data burrowing frameworks for foreseeing diabetes from therapeutic records of patients. Pima Indians Diabetes dataset of 768 events is used by maker.V. Veeralakshmi, Dr. D. Ramyachitra (2015) investigate execution of three principles classifier algorithms. The calculation is RIDOR, JRIP, and Decision Table. IRIS Dataset is picked for correlation. Dr.S.R.Kalmegh(2017) uses the WEKA with the data set of Indian news and come up with results.

2. Methodology

2.1 WEKA: - WEKA was developed at the University of Waikato in New Zealand. The name stands for Waikato Environment for Knowledge Analysis The system is written in Java and distributed under the terms of the GNU General Public License [12][16]. It runs on almost any platform and has been tested under Linux, Windows, and Macintosh operating systems. It provides a uniform interface to many different learning algorithms, along with methods for pre and post processing and for evaluating the result of learning schemes on any given dataset. This tool also supports the variety file formats for mining include ARFF, CSV, LibSVM, and C4.5[10][13].The easiest way to use WEKA is through a graphical user interface called Explorer as shown in Fig. I. Fig. II Shows the ARFF File Opening by WEKA and Fig. III ARFF file processing by JRip.bThe Step by steps use of WEKA for result purpose is as explain below.

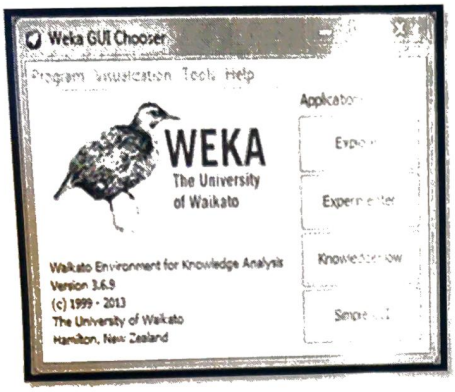

Fig. I: WEKA GUI Explore

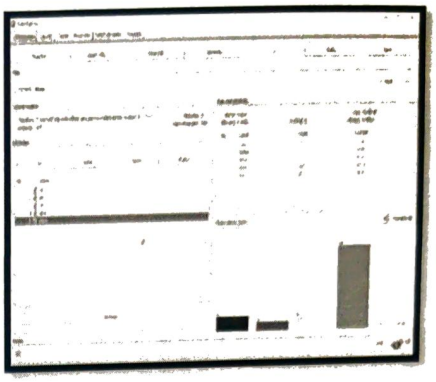

Fig. II: ARFF File Opening by WEKA

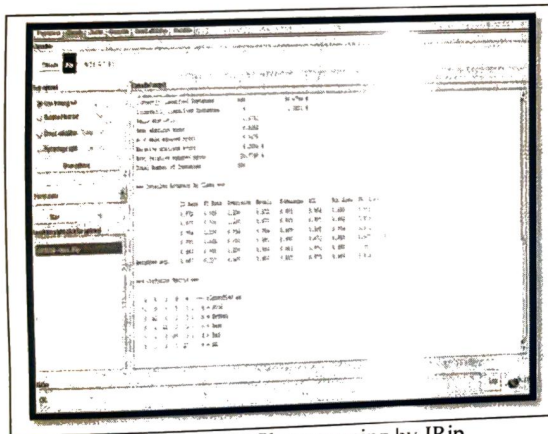

Fig. III: ARFF file processing by JRip

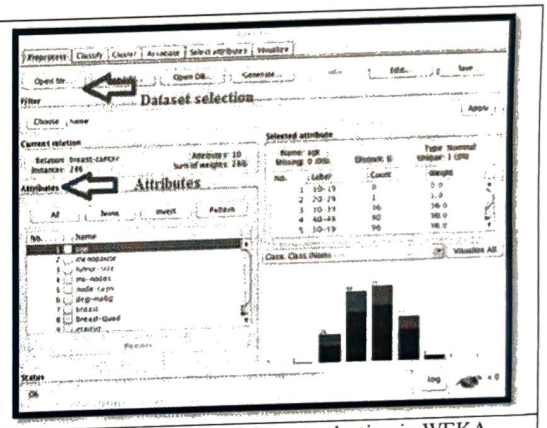

Fig.-IV: Attribute and dataset selection in WEKA

2.1.1 WEKA Application Interfaces

As shown in above Fig-I there are multiple option are available in WEKA application Interface.

- **Explorer:** explorer is environment for exploring data. Explorer contain pre-processing of data, attribute Selection, learning, Visualization.
- **Experimenter:** Experimenter is environment for performing experiments and conducting statistical tests between learning schemes.
- **Knowledge Flow**: Knowledge Flow is Java-Beans-based interface for setting going Machine Learning tests.
- **Simple Command-line**: Provides simple command-line interface that allows direct execution of WEKA commands for operating systems.

2.1.2 Load data into WEKA explorer:

- **Opening Data Set:** In WEKA. the data set taken from explorer window, as shown in fig.I the then click on "open file" and the browse to navigate to the data folder within the WEKA-3.8.5. folder or select dataset supported by WEKA. The data Selection as shown in Fig.IV. After selection of data set the attributes are available on the WEKA screen. By using Attributes, we can visualize the data in graphical form. There are many more options are available to understand the dataset in various ways.

- **Select Classifier:** After Successful Selection of Data set, Next step to select Classifier which is available on next Tab i.e. 'Classify'. Depending upon the use we can select the Classifier and then apply to dataset.

- **Test Option:** The result of applying the chosen classifier will be tested according to the options that are set by clicking in the "Test options" box. There are four test modes: Use training set, supplied test, Cross Validation folds, Percentage split.

- **Use Training Set**: The accuracy of the classifier is based on the class of instances against their actual classes
- **Supplied Test Set:** In the Supplied test a separate file is loaded. Based on this evaluation of the classifier take place on the basis of the authenticity of the prediction of the class of a set of instances loaded from that file
- **Cross-validation:** The cross validation is also called as K-Folds cross Validation. In K-fold Cross – validation, the dataset is divided into k sets. In the first run, k-1 sets are used for training the classifier and the remaining one set is used for testing the classifier. In the next run, another set is held out as the test data and the remaining k-1 sets are used as training sets. Thus, each set is held out in turn as the testing set and the process is repeated k^{th} times. So, each data set used once for testing and k-1 times for training.
- **Percentage Split:** The data set is divided into two sections in Percentage Split based on the value supplied in the percent field. typical split worth is 66% to 34% for train and test sets separately. The classifier is evaluated on how well it predicts the class of the test data.

3. Advantages

1. WEKA is user friendly which helps to develop new machine learning plans.
2. WEKA loads information record in format of ARFF, CSV, C4.5, and binary.
3. It is open source, Free, Extensible can be incorporated into other java bundles.

4. Limitation

1. Worse connectivity to excel spreadsheet and non-Java based databases.
2. CSV reader not as robust as in Rapid Miner.
3. Weka is much weaker in classical statistics.
4. Does not have arrangement to store parameters for scaling to apply to future datasets.
5. Does not have programmed arrangement for Parameter enhancement of learning/statistical techniques

5. Conclusion

WEKA help us researchers to predict the Knowledge from their data set, which help to predict future knowledge from the existing dataset. The basic information provided in this paper may be help new research scholar to gain valuable output from this Software. This paper help to understand the basic working of WEKA, it also shows how data set load into it. Along with this advantages and disadvantages are also discuss.

REFERENCES:

1. Dr.Sushilkumar Rameshpant Kalmegh, Effective classification of indian news using classifier hyperpipes and naivebayes from weka, International Journal of Pure and Applied Research in Engineering and Technology, (2016), ISSN: 2319-507X, Vol4, Iss 9.
2. S. R. Kalmegh, Comparative analysis of WEKA Data Mining Algorithm RandomForest, RandomTree and LADTree for Classification of Indigenous News Data, International Journal of Emerging Technology and Advanced Engineering, (2015), ISSN 250-2459, Vol 5, Iss 1.
3. King,M, A,and Elder,J, F, Evaluation of Fourteen Desktop Data Mining Tools, IEEE International Conference on Systems, Man and Cybernetics , (1998), ISSN: 1062-922X.
4. Wei Peng, Juhua Chen and Haiping Zhou, An Implementation of ID3: Decision Tree, Learning Algorithm Project of Comp 9417: Machine Learning University of New South Wales, School of Computer Science & Engineering, Sydney, NSW 2032, and Australia
5. Uzair Bashir & Manzoor Chachoo, Performance evaluation of j48 and bayes algorithms for intrusion detection system, International Journal of Network Security & Its Applications (IJNSA), (2017), Vol.9, Iss.4.
6. N.Landwehr,M.Hall & E.Frank. Logistic model trees,For Machine Learning, (2005), Vol.59, Iss.12.
7. Mahendra Tiwari, Manu Bhai Jha and OmPrakash Yadav, Performance analysis of Data Mining algorithms in Weka, IOSR Journal of Computer Engineering (IOSRJCE),2012, ISSN 2278-0661, Vol 6, Iss 3.
8. Sushilkumar Rameshpant Kalmegh, Comparative Analysis of WEKA Data Mining Algorithm RandomForest, RandomTree and LADTree for Classification of Indigenous News Data, International Journal of Emerging Technology and Advanced Engineering, ISSN 2250-2459, (2015), Vol 5, Iss1.
9. Sushilkumar Rameshpant Kalmegh, Effective classification of indian news using classifier hyperpipes and naivebayes from WEKA, International journal of pure and applied research in engineering and technology, ISSN 2319-507X, (2016), Vol 4, Iss 9.
10. S.A.Ghogare and Dr.S.R.Kalmegh, Comparative analysis of J48 and LMT classifier using WEKA data mining tool on car Review Data, Research Journey International E- Research Journal, (2019), ISSN:2348-7143, Special Issue 110 (C).

ISSN NO : 0363-8057

11. S.R.Kalmegh & S.N.Deshmukh, Categorical Identification of Indian News Using J48 and Ridor Algorithm, International Refereed Journal of Engineering and Science (IRJES), (2014), ISSN:2319-183X, Vol3, Iss6.
12. Ian H. Witten, Eibe Frank & Mark A. Hall, Data Mining Practical Machine Learning Tools and Techniques, (Third Edition, Morgan Kaufmann Publishers is an imprint of Elsevier, 2016).
13. S.A.Ghogare & Dr. S.R.Kalmegh, performance comparison of RandomForest and Hoeffding Tree classifier using WEKA data Mining tool on car reviews data, international journal of engineering research and Application(IJERA), (2019), ISSN:2248-9622, Vol 9, Issue 3, pp 37-42.
14. S.A.Ghogare, Performance Comparison of Tree based classifier using WEKA, Journal of the Gujarat research Society, ISSN: 0374-8588, Volume 21, Issue 3, PP: 70-75.
15. S.A.Ghogare & Dr.S.R.Kalmegh,(2019), Comparative Analysis of J48 and LMT Classifier Using WEKA Data Mining Tool on Car Reviews Data, 'RESEARCH JOURNEY' International E- Research

VOLUME 8 ISSUE 6 2022

ISSN NO: 0363-8057
Impact Factor: 6.1

22.Quality of Education in Native Ethnic Tribes of Cold Desert Leh-Ladakh (gallery/grj%203432.pdf)
Dr. G. M. Rather
University of Kashmir, Srinagar
PAGE NO: 166-184
DOI:10.37897.GRJ.2021.V7I11.21.49894

23.Implementation Of Eye-controlled Electric Wheelchair (gallery/grj%2034...
D. Nagadevi, C. Hemanth Kumar, R. Sai Teja , K. Gowtham
Chaitanya Bharathi Institute of Technology (CBIT), Gandipet, Hyderaba...
PAGE NO: 185-192
DOI:10.37897.GRJ.2021.V7I11.21.49895

24.Analytical Method Development and Validation of an ICP-MS Method for the Determination of Elemental Impurities in Darunavir Tablets (gallery/grj%203325.pdf)
Jay Bhatt, Dr. Umeshkumar A. Shah, Dr. Hirak Kumar V. Joshi
Nootan Pharmacy College, Sankalchand Patel University, Visnagar,Gujarat, India
PAGE NO: 193-204
DOI:10.37897.GRJ.2021.V7I11.21.49896

26.Solar Street Light ControlSystem using ZigBee Network in all Climatic Conditions (gallery/grj%203421.pdf)
T.Prasanth,T.Mohamed Thameem,M.Kalaiyarasi,A.Sajili,M.Nandhini
AL-Ameen engineering college karundevan palayam,nanjai uthukuli(po),Erode,Tamilnadu
PAGE NO: 220-224
DOI:10.37897.GRJ.2021.V7I11.21.49898

27.Impact Of Covid-19 on India's Stock Market (gallery/grj%203452.pdf)
Dr Amisha Gupta,Dr Bhavneet Kaur,Purnima Verma,Rajat Sehgal, Vanshika Sharma
Jagan institute of management studies
PAGE NO: 225-241
DOI:10.37897.GRJ.2021.V7I11.21.49899

28.Comparative Study Of Flat Slab And Conventional Slab Structure Based On Seismic Behavior: A Review (gallery/grj%203455.pdf)
Yogesh Gajanan Bedre ,Sharif Shaikh
G H Raisoni College of Engineering and Management, Pune
PAGE NO: 242-245
DOI:10.37897.GRJ.2021.V7I11.21.49900

29.Fashion Try-On using Poly-GAN (gallery/grj%203446.pdf)
Shruti Nair,Rajvee Pisey,Meera Narale,Dr. Mrudul Dixit
MKSSS's Cummins College of Engineering for Women, Pune, India
PAGE NO: 246-250
DOI:10.37897.GRJ.2021.V7I11.21.49901

30.Digital Data Storage In Dna (gallery/grj%203397.pdf)
Kbiru Gambo,mitul Patel
PP Savani University, Surat,Gujrat India
PAGE NO: 251-261
DOI:10.37897.GRJ.2021.V7I11.21.49902

31.A Design And Implementaion Of Modified Compact Solar Cell Array Power Production System (gallery/grj%203458.pdf)
V.S. Vedhika,E.Elakkiya,K.Pavithra,K.Akilandaeswari,K.S.Gowthaman
GCE,Thanjavur, Tamilnadu
PAGE NO: 262-276
DOI:10.37897.GRJ.2021.V7I11.21.49902

32.Development of linear array transducer using field _II (gallery/grj%203461.pdf)
Rodge S. A
Adarsha Science J.B.Arts and Birla Commerce Mahavidyalaya,Dhamangaon Rly
PAGE NO: 277-284
DOI:10.37897.GRJ.2021.V7I11.21.49903

33.Shatavri (Asparagus Racemosus) - A Magical Herb For Lactating Female (gallery/grj%203462.pdf)
Muskan Garg,Pratibha Singh,Muskaan Jain,Stuti Sharma
Manav Rachna International Institute of Research and studies, Faridabad, Haryana
PAGE NO: 285-296
DOI:10.37897.GRJ.2021.V7I11.21.49904

34.Cloud Based Intelligent Decision Support Knowledge Based System for Kidney Transplant Patients (CBIDKBS): COVID-19 Response (gallery/grj%203466.pdf)
Dr. Nitin Saraswat,Dr. Deepti Khanna

Development of linear array transducer using field _II

Rodge S. A.
Associate Professor, Dept. of Electronics
Adarsha Science J.B.Arts and Birla Commerce Mahavidyalaya,
Dhamangaon Rly-444709 India)

ABSTRACT

Science past decades, ultrasound imaging technology has satisfied outstanding improvement in obtaining significant diagnostic information from patients in a fast, noninvasive approach. Although the technology has benefited from sophisticated signal processing technology and imaging system integration, much of this progress has been derived from the improvement of ultrasonic transducers. Ultrasonic arrays are used in various applications together with medical imaging. In this particular case is important to accomplish precise information regarding the magnitude and position of the peak pressure and intensity produced by the imaging probe. This paper presents the design of linear array transducers for ultrasonic measurements.

Keywords--Ultrasonic, Linear array Transducer, medical imaging, Field-II GUI, TX/RX Fields.

I INTRODUCTION

For the period of the second half of 20th current century the medical imaging is grown through Ultrasound tool speedily. The part of novel technology is the use of computers to decide problems by simulating theoretical models (Numerical simulations) that has taken place alongside pure theory and experiment during the last few decades. These numerical simulations permit one to resolve problems that may not be accessible to direct experimental study or too complex for theoretical analysis. Computer simulations can link the gap between analysis and experiment **[1].**

These numerical simulations have emerged as a new branch in science and technology complementing both experiments and theory. A simulation can sometimes replace physical experiments, even though most often a simulation and an experiment are complementary. The results of scientific experiments are often explained by simulations and simulations are often calibrated by experiments. The experiments provide input for the simulations, which are viewed as experimenting with theoretical models. The feedback of numerical results into theoretical

ISSN NO : 0363-8057

modeling and continues interaction with laboratory experiments and analytical theory makes computing a vital tool for science. Consequently the increased in computing power in both speed and storage has given computational electronics its significance. Improved computer capacity and the solution algorithms themselves, have a big outcome on the excellence of solution obtained. A numerical model can be used to understand measurements and observations enlarge existing analytical models into new parameter regimes and quantitatively test existing theories that can be done by comparing model predictions to experimental information.

The mutual weak point of both experiment and theory is cover up by the numerical simulations examination and experiment. A third dimension in ultrasonic measurements, of equivalent status and significance to experiment and analysis is nothing but the simulation determination [1]. It has taken an everlasting place in every one aspect of ultrasonic measurements from basic research to engineering design.

A novel and potentially powerful tool is the computer experiment. One can resolve novel and uncertain aspects of usual process, by combining predictable theory, experiment and computer simulation [1]. Such aspects could frequently neither have been understood nor reveled by analysis or experiments alone.

More than the last half century much development has been made in medical device technology. One particular medical technology that has enhanced speedily over the last 30 years is ultrasound. This advancement in technology however has brought with it the rapid obsolescence of system design. The accomplishment of modern electronics is built on the possibility to precisely predict system performance by the use of simulation tools. This model can be extended to components such as piezoelectric transducers attached to the electronics [2]. The ability to simulate both piezoelectric transducer and electronics together renders possible efficient optimizations at system level, i.e. minimizing size, price and power consumption [3].

The systems for images processing in the medical field are very important calling for new techniques, much more superior and performing than they used to be, in order to provide a acceptable analysis and diagnosis. Amongst the medical techniques using computer sciences, it can be mentioned: scintigraphy, echography, tomography, radiography, quantitative microscopy, nuclear magnetic resonance. Ultrasound, widely used in many areas of medicine, provides a secure

ISSN NO : 0363-8057

and efficient means for diagnosis and therapy. When the medium becomes complex solving the wave propagation formula becomes virtually not possible. Modeling becomes much more complex inside the body because the ultrasound propagation speed is different for each tissue and it is known that tissues are not a homogeneous medium for ultrasound wave propagation [4]. Therefore, it is important to know how the ultrasound wave is generated and the ultrasound wave beam shaped.

II Spatial Impulse Theory

The pressure field generated by the aperture is found by the Rayleigh integral [5]

$$p(\vec{r}_1,t)=\frac{\rho_0}{2\pi}\int_s \frac{\partial v_n(\vec{r}_2,t-\frac{|\vec{r}_1-\vec{r}_2|}{c})}{|\vec{r}_1-\vec{r}_2|}ds \qquad (1)$$

Where the field point is denoted by $\vec{r}_1$ and the aperture by $\vec{r}_2$, is the velocity normal to the transducer surface. Using the velocity potential, and assume that the surface velocity is uniform over the aperture making it independent of $\vec{r}_2$, then: where the field point is denoted by $\vec{r}_1$ and the aperture by $\vec{r}_2$, is the velocity normal to the transducer surface. Using the velocity potential, and assume that the surface velocity is uniform over the aperture making it independent of $\vec{r}_2$, then:

$$\Psi(\vec{r}_1,t)=v_n(t)*\int_s \frac{\partial(t-\frac{|\vec{r}_1-\vec{r}_2|}{c})}{2\pi|\vec{r}_1-\vec{r}_2|} \qquad (2)$$

Where * denotes convolution in time. The integral in this equation

$$h(\vec{r}_1,t)=\int_s \frac{\partial(t-\frac{|\vec{r}_1-\vec{r}_2|}{c})}{2\pi|\vec{r}_1-\vec{r}_2|} \qquad (3)$$

Represent the spatial impulse response. The continuous wave field can be found from the Fourier transform of

$$p(\bar{r}_1, t) = \rho_0 \frac{\partial v(t)}{\partial t} * h(\bar{r}_1, t) \qquad (4)$$

The impulse response includes the excitation convolved with both the transducers electro-mechanical impulse response in transmit and receive. The final signal for a collection of scatters is calculated as a linear sum over all signals from the different scatters [6-7].

III LINEAR ARRAY TRANSDUCER

The linear array is the fundamental type of multi-element transducer and it scans the region of interest by exciting the elements situated over the region. The field is focused on the region by introducing time delay in the excitation of the concerned individual elements, so initially concave beam is emitted. Here a Fig.1 shows general design format of 16 element linear array transducer having height, width and kerf of individual element are taken as 5 mm, 0.2 mm and 0.02 mm respectively. The transducers are situated at the center of the coordinate system. To achieve focal length of 30 mm from the center of transducer the electronic focusing is included.

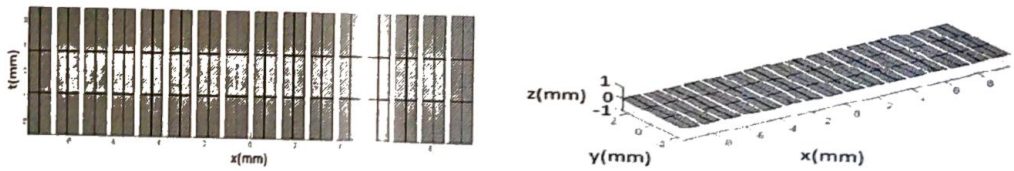

Fig. (1) **Design format of linear array transducer (Height=5mm, Width=0.25mm, Kerf=0.02mm)**

In this paper a linear array transducer of 16 elements is simulated using FIELD-II program with center frequencies 5MHz. For this specified linear array transducer, acoustic field generated is propagated through human body tissues and is observed at a focal distance i.e. (0, 0, 30)

IV RESULT AND DISCUSSION

The calculation of the impulse response is facilitated by projecting the field point onto the plane of the aperture. In this way, the problem became two-dimensional and the field point is given

as a (x, y) coordinate set and a height z above the plane. The spatial impulse response is, thus, determined by the relative length of the part of the arc that intersects the aperture [8]. Thereby it is the crossing of the projected ultrasonic waves with the edges of the aperture that determines the spatial impulse responses as a function of time. In this paper by using FIELD-II program created a 16 element linear array transducer with center frequency fo = 5*MHz*. The speed of sound in tissue is c=*f*0 = 1540*m/s*, The sampling frequency used was *fs* = 100*MHz*. The elements had a width and height of 0.25mm and 5mm respectively. The focal-point was set to 30mm.

Table: 1 shows the parameters for 16 element array transducer, excitation pulse and medium used for this centre frequency (f_0) used is 5MHz. Figs. (a-m) shows; Element impulse response for 16 element array, TX Field image for 16 element array, TX Axial waveform for 16 element array, TX Lateral beam plot for 16 element array, TX/RX Field image for 16 element array, TX/RX Axial waveform for 16 element array, TX/RX Lateral beam plot for 16 element array, K- space TX/RX field image for 16 element array, K-space axial slice for 16 element array, K-space lateral slice for 16 element array, Detected image for 16 element array, Detected image axial slice for 16 element array and Detected image lateral slice for 16 element array.

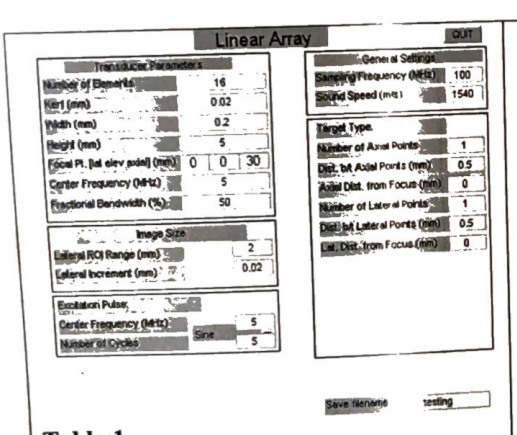

Table:1

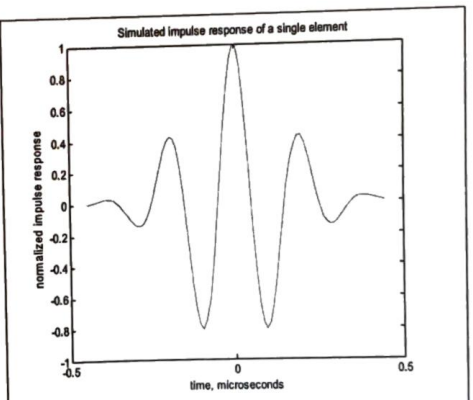

Fig.(a) Element impulse response

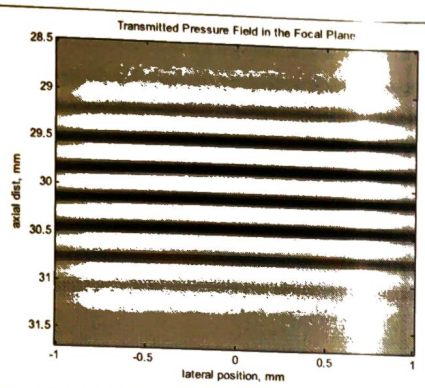

Fig. (b) TX Field image

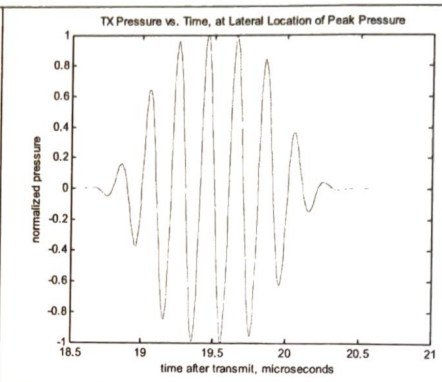

Fig. (c) TX Axial waveform

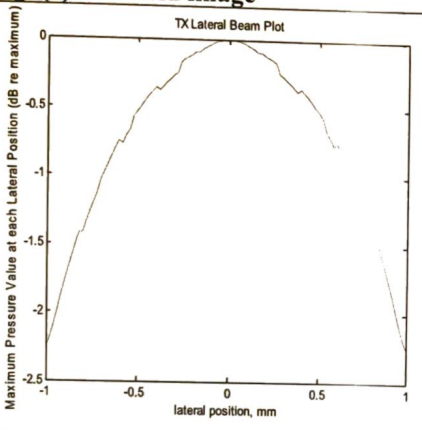

Fig. (d) TX Lateral beamplot

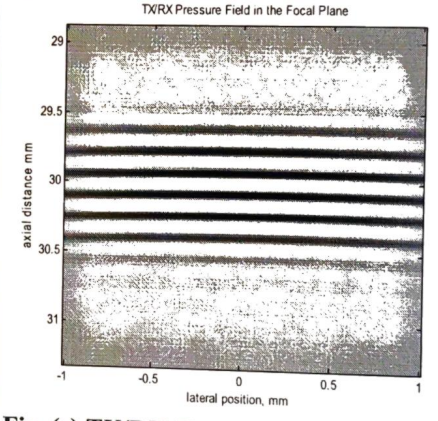

Fig. (e) TX/RX Field image

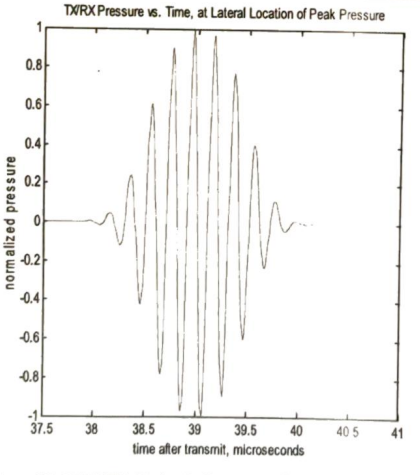

Fig. (f) TX/RX Axial waveform

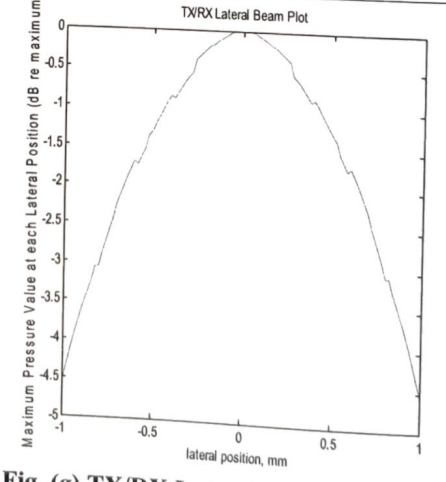

Fig. (g) TX/RX Lateral beam-plot

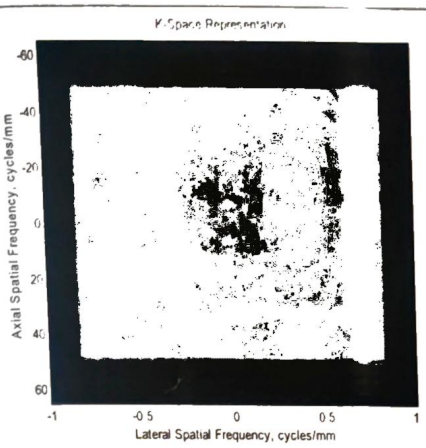

Fig. (h) K space TX/RX field image

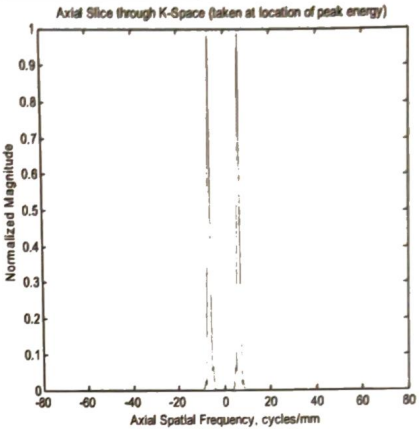

Fig. (i) K space axial slice

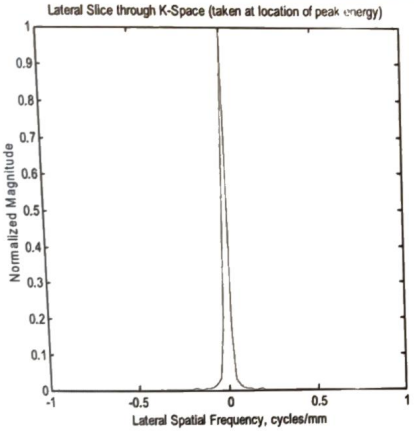

Fig. (j) K space lateral slice

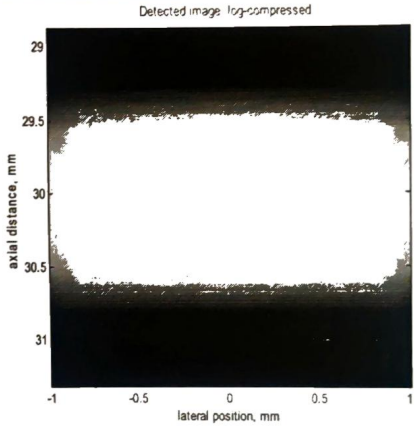

Fig. (k) Detected image

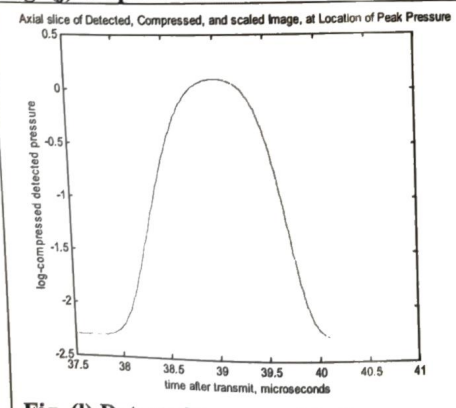

Fig. (l) Detected image axial slice

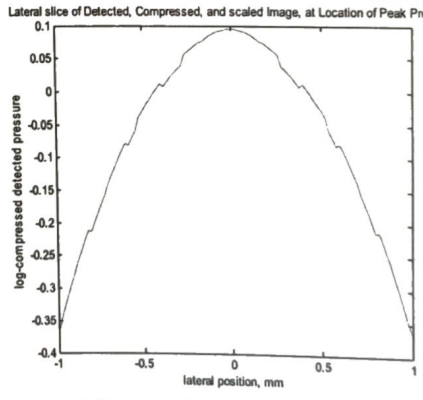

Fig. (m) Detected image lateral slice

V CONCLUSION

The paper attempts to present a coherent analysis of the focusing strategies for 2-D array transducer design and properties, based on linear acoustics. The delays on the individual transducer elements and their relative weight or apodization are changed continuously as a function of depth. This yields near perfect focused images for all depths and has increased the contrast in the displayed image, thus, benefitting the diagnostic importance of ultrasonic imaging.

References:

[1] Gandole, Y. B. (2012). Computer Modeling and Simulation of Ultrasonic System for Material Characterization. http://www.oalib.com/search? kw=Y.%20B.%20Gandole &searchField=authors.

[2] R. Krimholtz, D. Leedom, and G. Matthaci, "New equivalent circuits for elementary piezoelectric transducers," Electron. Lett. **6**, 398–399 ,1970

[3] T. R. Meeker, "Thickness mode piezoelectric transducers," Ultrasonics **10**, 26–36 ,1972.

[4] P. Marchal, F. Levarssort, L.-P. Tran-Huu-Hue, and M. Lethiecq, "Effects of acoustical properties of a lens on the pulse-echo response of a single element transducer," IEEE International Ultrasonics, Ferroelectrics, and Frequency Control Joint 50th Anniversary Conference, pp. 1651–1654,2004.

[5] Jensen, J.A, A New Approach to Calculating Spatial Impulse Responses, IEEE International Ultrasonic Symposium, Toronto, Canada, 1997

[6] P. Marchal, F. Levarssort, L.-P. Tran-Huu-Hue, and M. Lethiecq, "Effects of acoustical properties of a lens on the pulse-echo response of a single element transducer," IEEE International Ultrasonics, Ferroelectrics, and Frequency Control Joint 50th Anniversary Conference, pp. 1651–1654,2004.

[7] JENSEN, J.A., Field: A program for simulating ultrasound systems, 10th Nordic-Baltic Conference on Biomedical Imaging, in: *Medical & Biological Engineering & Computing*, 1996, **34**, Supplement 1, 351–353.

[8] Jensen, J.A., N.B. Svendsen, Simulation of advanced ultrasound systems using field II, Biomedical Imaging: Nano to Macro, 2004. IEEE International Symposiumon, 15-18 April 2004 Page(s):636–639 Vol.-1.

ISSN: 0932-4747 Impact Factor : 4.7

volume 8 issue 4 2022

submit your paper to : editorzeichen@gmail.com

Zeichen Journal

ZEICHEN

UGC Care Group II Journal

UGC APPROVED JOURNAL

VOLUME 8 ISSUE 4 2022

01. Impact of Covid-19 on Migrants and Migrant Families in Siwan District of Bihar (gallery/2501.pdf)
Rani Kumari, ICSSR, ANSISS, Patna, Bihar
Page No: 01- 11
DOI:15.10089.ZJ.2022.V8I04.285311.2751

02. Simulation of 32 Element linear array Transducer using Field-II GUI (gallery/2496.pdf)
Rodge S. A, Adarsha Science J.B.Arts and Birla Commerce Mahavidyalaya,
Page No: 12- 18
DOI:15.10089.ZJ.2022.V8I04.285311.2752

03. A Study on Impact of Covid - 19 Affecting the Buyer Buying Behavior towards Instant Food in Hyderabad (gallery/2497.pdf)
Dr. R Sampath Kumar, Osmania University
Page No: 19- 34
DOI:15.10089.ZJ.2022.V8I04.285311.2753

04. Beyond The Veil of Sisterhood: The Anxieties behind the Unmaking Of the Hero in Things Fall Apart (gallery/2493.pdf)
Oindrila Bhattacharya, Vidyasagar University
Page No: 35- 41
DOI:15.10089.ZJ.2022.V8I04.285311.2754

05. Variation on λmax value of Lawsone (2-hydroxy-1,4-napthoquinone) in different solution in vitro: (gallery/2508.pdf)
A preliminary study (gallery/2508.pdf)
Sharda Mahilkar Sonkar, Anshika Lumb, University of Delhi
Page No: 42- 46
DOI:15.10089.ZJ.2022.V8I04.285311.2755

06. A Study on Expenditure Pattern of Central Government of India (gallery/2506.pdf)
Dr.S.Banusundari, Assistant Professor, Michael Job College of Arts and Science for Women
Page No: 48- 56
DOI:15.10089.ZJ.2022.V8I04.285311.2756

Zeichen Journal
ISSN No: 0932-4747

Simulation of 32 Element linear array Transducer using Field-II GUI

Rodge S. A.
Associate Professor, Dept. of Electronics
Adarsha Science J.B.Arts and Birla Commerce Mahavidyalaya,
Dhamangaon Rly-444709 India)

Abstract-For the duration of the second half of the 20th current century, medical imaging is grown through Ultrasound tools speedily. Its outcome became documented in those areas of imaging in which its unique features present particular advantages over other imaging modalities. It expanded extensive acceptance as a nonionizing form of energy that is useful non-invasively.

The part of novel technology is the utilization of computers to resolve problems by simulating theoretical models (Numerical simulations) that have taken place alongside pure theory and experiment during the last few decades. These numerical simulations allow one to resolve problems that may not be accessible to direct experimental study or are too complex for theoretical analysis. Computer simulations can link the gap between analysis and experiment [1]. This paper presents the simulation of linear array transducers using Field-II GUI.

Keywords--Ultrasonic, Linear array Transducer, medical imaging, Field-II GUI, TX/RX Fields, detected image, TX/RX Axial slice. TX/RX Axial slice.

I INTRODUCTION

These numerical simulations have emerged as a new branch in science and technology complementing both experiments and theory. A simulation can sometimes replace physical experiments, even though most often a simulation and an experiment are complementary. The results of scientific experiments are often explained by simulations and simulations are often calibrated by experiments. The experiments provide input for the simulations, which are viewed as experimenting with theoretical models. The feedback of numerical results into theoretical modeling and continuous interaction with laboratory experiments and analytical theory makes computing a vital tool for science. Consequently, the increase in computing power in both speed and storage has given computational electronics its significance. Improved computer capacity and the solution algorithms themselves have a big outcome on the excellence of the solution obtained. A numerical model can be used to understand measurements and observations enlarge existing analytical models into new parameter regimes and quantitatively test existing theories that can be done by comparing model predictions to experimental information.

ISSN No: 0932-4747

A novel and potentially powerful tool is the computer experiment. One can resolve novel and uncertain aspects of the usual process, by combining predictable theory, experiment, and computer simulation [1]. Such aspects could frequently neither have been understood nor revealed by analysis or experiments alone.

In more than the last half-century, much development has been made in medical device technology. One particular medical technology that has enhanced speedily over the last 30 years is ultrasound. This advancement in technology however has brought with it the rapid obsolescence of system design. The accomplishment of modern electronics is built on the possibility of precisely predicting system performance by the use of simulation tools. This model can be extended to components such as piezoelectric transducers attached to the electronics [2]. The ability to simulate both piezoelectric transducer and electronics together renders possible efficient optimizations at the system level, i.e. minimizing size, price, and power consumption [3].

The systems for images processing in the medical field are very important calling for new techniques, much more superior and performing than they used to be, in order to provide an acceptable analysis and diagnosis. Amongst the medical techniques using computer sciences, it can be mentioned: scintigraphy, echography, tomography, radiography, quantitative microscopy, nuclear magnetic resonance. Ultrasound, widely used in many areas of medicine, provides a secure and efficient means for diagnosis and therapy. When the medium becomes complex solving the wave propagation formula becomes virtually not possible. Modeling becomes much more complex inside the body because the ultrasound propagation speed is different for each tissue and it is known that tissues are not a homogeneous medium for ultrasound wave propagation [4]. Therefore, it is important to know how the ultrasound wave is generated and the ultrasound wave beam is shaped.

II SPATIAL IMPULSE THEORY

The pressure field generated by the aperture is found by the Rayleigh integral [5]

$$p(\vec{r}_1, t) = \frac{\rho_0}{2\pi} \int_s \frac{\partial v_n\left(\vec{r}_2, t - \frac{|\vec{r}_1 - \vec{r}_2|}{c}\right)}{|\vec{r}_1 - \vec{r}_2|} ds \qquad (1)$$

Where the field point is denoted by $\vec{r}_1$ and the aperture by $\vec{r}_2$, is the velocity normal to the transducer surface. Using the velocity potential, and assume that the surface velocity is uniform

ISSN No: 0932-4747

over the aperture making it independent of $\vec{r}_2$, then: where the field point is denoted by $\vec{r}_1$ and the aperture by $\vec{r}_2$, is the velocity normal to the transducer surface. Using the velocity potential, and assume that the surface velocity is uniform over the aperture making it independent of $\vec{r}_2$, then:

$$\Psi(\vec{r}_1, t) = v_n(t) * \int_s \frac{\partial\left(t - \frac{|\vec{r}_1 - \vec{r}_2|}{c}\right)}{2\pi |\vec{r}_1 - \vec{r}_2|} \qquad (2)$$

Where * denotes convolution in time. The integral in this equation

$$h(\vec{r}_1, t) = \int_s \frac{\partial\left(t - \frac{|\vec{r}_1 - \vec{r}_2|}{c}\right)}{2\pi |\vec{r}_1 - \vec{r}_2|} \qquad (3)$$

Represent the spatial impulse response. The continuous wave field can be found from the Fourier transform of

$$p(\vec{r}_1, t) = \rho_0 \frac{\partial v(t)}{\partial t} * h(\vec{r}_1, t) \qquad (4)$$

The impulse response includes the excitation convolved with both the transducers electro-mechanical impulse response in transmit and receive. The final signal for a collection of scatters is calculated as a linear sum over all signals from the different scatters [6-7].

III SIMULATION OF LINEAR ARRAY TRANSDUCER

The linear array is the fundamental type of multi-element transducer and it scans the region of interest by exciting the elements situated over the region. The field is focused on the region by introducing time delay in the excitation of the concerned individual elements, so initially, the concave beam is emitted. Here Fig.1 shows the general design format of 16 elements linear array transducer having height, width, and kerf of the individual element are taken as 5 mm, 0.2 mm, and 0.02 mm respectively. The transducers are situated at the center of the coordinate system. To achieve a focal length of 30 mm from the center of the transducer the electronic focusing is included.

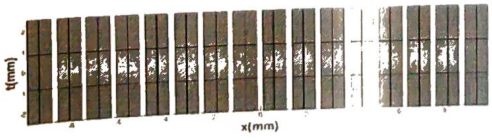

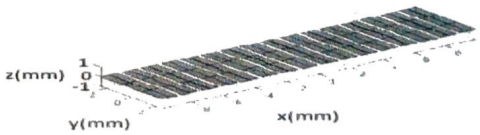

ISSN No: 0932-4747

Fig. (1) Design format of linear array transducer (Height=5mm, Width=0.25mm, Kerf=0.02mm)

In this paper a linear array transducer of 32 elements is simulated using the FIELD-II program with center frequencies 5MHz. For this specified linear array transducer, the acoustic field generated is propagated through human body tissues and is observed at a focal distance i.e. (0, 0, 30)

IV RESULT AND DISCUSSION

The calculation of the impulse response is facilitated by projecting the field point onto the plane of the aperture. In this way, the problem became two-dimensional and the field point is given as an (x, y) coordinate set and a height z above the plane. The spatial impulse response is, thus, determined by the relative length of the part of the arc that intersects the aperture [8]. Thereby it is the crossing of the projected ultrasonic waves with the edges of the aperture that determines the spatial impulse responses as a function of time. In this paper by using the FIELD-II program a 32 element linear array transducer is simulated with center frequency fo = $5MHz$. The speed of sound in tissue is c=$f0$ = $1540m/s$, The sampling frequency used was fs = $100MHz$. The elements had a width and height of 0.25mm and 5mm respectively. The focal point was set to 30mm.

Table: 1 shows the parameters for 32 element array transducer, excitation pulse and the medium used for this center frequency (f_0) used is 5MHz. Figs. (a-m) shows; Element impulse response for 32 element array, TX Field image for 32 element array, TX Axial waveform for 32 element array, TX Lateral beam plot for 32 element array, TX/RX Field image for 32 element array, TX/RX Axial waveform for 32 element array, TX/RX Lateral beam plot for 32 element array, K- space TX/RX field image for 32 element array, K-space axial slice for 32 element array, K-space lateral slice for 32 element array, Detected image for 32 element array, Detected image axial slice for 32 element array and Detected image lateral slice for 32 element array.

ISSN No: 0932-4747

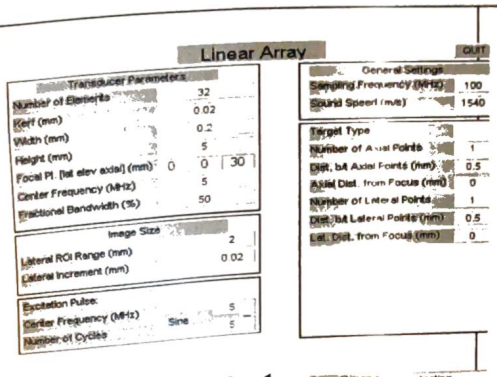

Table: 1

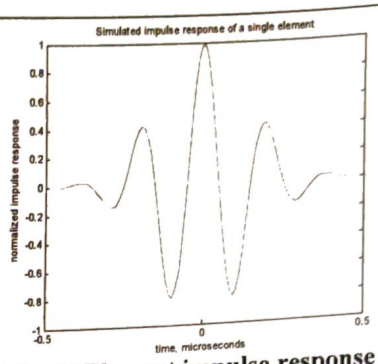

Fig. (a)Element impulse response

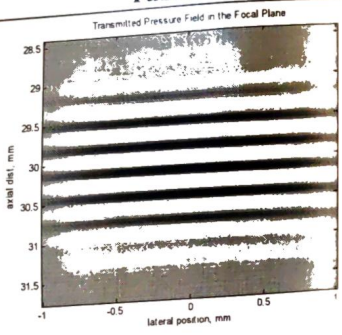

Fig. (b) TX Field image

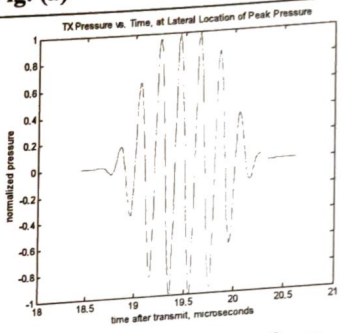

Fig. (c) TX Axial waveform

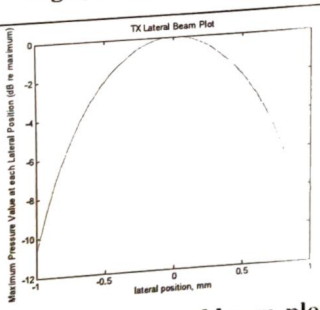

Fig. (d) TX Lateral beam-plot

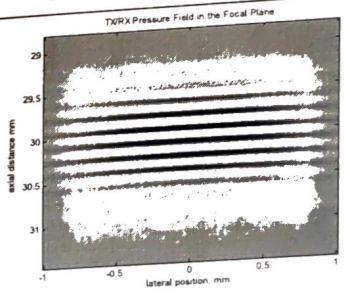

Fig. (e) TX/RX Field image

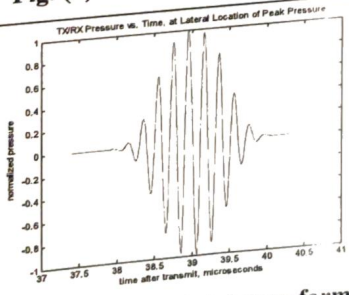

Fig. (f) TX/RX Axial waveform

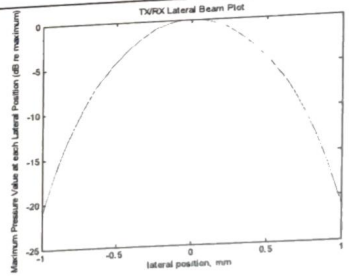

Fig. (g) TX/RX Lateral beam-plot

ISSN No: 0932-4747

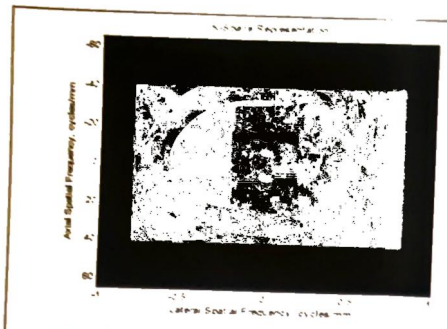

Fig. (h) K space TX/RX field image

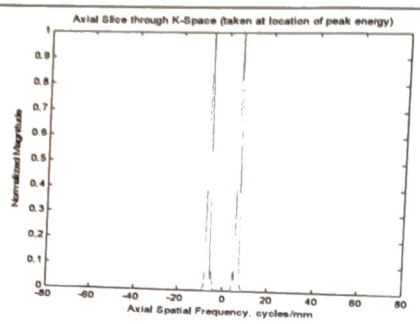

Fig. (i) K space axial slice

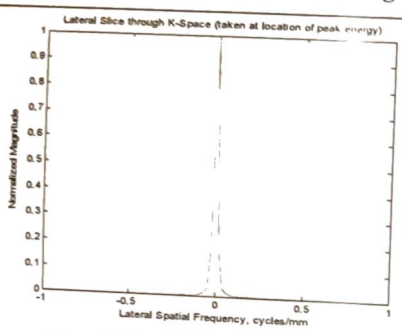

Fig. (j) K space lateral slice

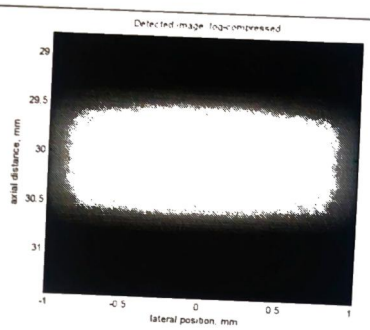

Fig. (k) Detected image

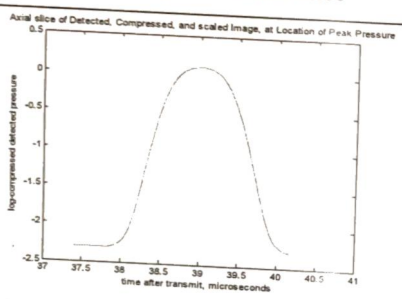

Fig. (l)Detected image axial slice

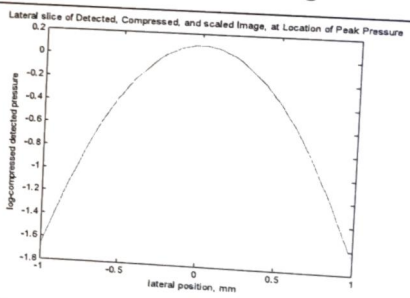

Fig. (m)Detected image lateral slice

V CONCLUSION

The paper attempts to present a coherent analysis of the focusing strategies for 2-D array transducer design and properties, based on linear acoustics. The delays on the individual transducer elements and their relative weight or apodization are changed continuously as a function of depth. This yields near-perfect focused images for all depths. Similarly, if the number of arrays in the transducer is increased then the contrast of the displayed image, has increased thus, benefitting the diagnostic importance of ultrasonic imaging.

ISSN No: 0932-4747

References:

[1] Gandole, Y. B. (2012). Computer Modeling and Simulation of Ultrasonic System for Material Characterization. http://www.oalib.com/search? kw=Y.%20B.%20Gandole &searchField=authors.

[2] R. Krimholtz, D. Leedom, and G. Matthaci, "New equivalent circuits for elementary piezoelectric transducers," Electron. Lett. **6**, 398–399 ,1970

[3] T. R. Meeker, "Thickness mode piezoelectric transducers," Ultrasonics **10**, 26–36 ,1972.

[4] P. Marchal, F. Levarssort, L.-P. Tran-Huu-Hue, and M. Lethiecq, "Effects of acoustical properties of a lens on the pulse-echo response of a single element transducer," IEEE International Ultrasonics, Ferroelectrics, and Frequency Control Joint 50th Anniversary Conference, pp. 1651–1654,2004.

[5] Jensen, J.A, A New Approach to Calculating Spatial Impulse Responses, IEEE International Ultrasonic Symposium, Toronto, Canada, 1997

[6] P. Marchal, F. Levarssort, L.-P. Tran-Huu-Hue, and M. Lethiecq, "Effects of acoustical properties of a lens on the pulse-echo response of a single element transducer," IEEE International Ultrasonics, Ferroelectrics, and Frequency Control Joint 50th Anniversary Conference, pp. 1651–1654,2004.

[7] JENSEN, J.A., Field: A program for simulating ultrasound systems, 10th Nordic-Baltic Conference on Biomedical Imaging, in: *Medical & Biological Engineering & Computing*, 1996, **34**, Supplement 1, 351–353.

[8] Jensen, J.A., N.B. Svendsen. Simulation of advanced ultrasound systems using field II, Biomedical Imaging: Nano to Macro, 2004. IEEE International Symposiumon, 15-18 April 2004 Page(s):636–639 Vol.-1.

Volume 12 Issue 6 JUNE - 2022

ISSN NO: 1934-7197 Submit Article at: submitjournaleca@gmail.com IMPACT FACTOR - 6.1

UGC-CARE Approved (Group - II) Category Journal
(https://www.scopus.com/sourceid/11200153562)

Journal of Engineering, Computing and Architecture

A Peer Reviewed/Referred Open Access Journal

PAPER FORMAT (gallery/jeca%20paper%20format.doc) REGISTRATION FORM (gallery/jeca-%20registration%20form.docx) COPY RIGHT FORM (gallery/jeca-%20copyright-form.docx)

UGC-CARE Group-II Journals Link
https://ugccare.unipune.ac.in/site/Applicant/login.aspx
(https://ugccare.unipune.ac.in/site/Applicant/login.aspx)

USER NAME: careugcpune@gmail.com
PASSWORD: 22334455

VOLUME 12 ISSUE 6 JUNE - 2022

01. Implementation of Information Technology Service Management Using Rasa Chat-Bot and Data Visualizers (gallery/jeca%20-%202776.pdf)
Amaan Akbar Khan, Student - AISSMS College of Engineering, Pune, India.
Bagbande Arun Umakant, Student - AISSMS College of Engineering, Pune, India.
Abdul Aman, Student - AISSMS College of Engineering, Pune, India.
Unnati Manik Chandekar, Student - AISSMS College of Engineering, Pune, India.
Dr. M. A. Pradhan, Professor - AISSMS College of Engineering, Pune, India.
Page No: 1 - 9
DOI:17.0002.JECA.2022.V1206.200786.9901 (gallery/jeca%20-%202776.pdf)

02. UNDERGROUND CABLE FAULT DETECTOR BASED ON ARDUINO (gallery/jeca%20-%202779.pdf)
K. Naresh, HOD & Associate Professor - EEE- Dept., Usha Rama College of Engineering and Technology, A.P, India
K. Himanjan Kumar, K. Durga Prasad, U.Krideva Babu, Y. Kiran Kumar - Final Year B. Tech Students, EEE - Dept., Usha Rama College of Engineering and Technology, A.P, India
Page No: 10 - 24
DOI:17.0002.JECA.2022.V1206.200786.9902 (gallery/jeca%20-%202779.pdf)

03. SMART SOLOR GRASS CUTTER WITH LAWN COVERAGE (gallery/jeca%20-%202780.pdf)
M.RAMBABU, Assistant Professor - EEE-Dept., Usha Rama College of Engineering and Technology, A.P, India
P.VIJAY KUMAR, I.MAHESH BABU, P.SARAN TEJA, S.PAVAN KUMAR - Final Year B.Tech Students, EEE- Dept., Usha Rama College of Engineering and Technology, A.P, India
Page No: 25 - 38
DOI:17.0002.JECA.2022.V1206.200786.9903 (gallery/jeca%20-%202780.pdf)

04. ELECTRIC VEHICLE CHARGING STATION SLOT BOOKING USING ARDUINO (gallery/jeca%20-%202781.pdf)
B.Phani Ranga Raja, Assistant Professor - EEE Dept,Usha Rama College Of Engineering And Technology,AP,India.
S.Lakshmi Satya Dileep, SD.Ibrahim Khalilulla, U.Pandu, R.Jayasree - Final year B.Tech Students EEE Dept.,Usha Rama College Of Engineering And Technology,AP,India.
Page No: 39 - 52
DOI:17.0002.JECA.2022.V1206.200786.9904 (gallery/jeca%20-%202781.pdf)

05. Power Estimation for CMOS VLSI Circuits using Support Vector algorithm for ISCAS'89 benchmark circuit (gallery/jeca%20-%202782.pdf)
Amrita Pahadia, Research Scholar - LNCT University, Bhopal, India.
Dr. Soni Changlani, Professor & Head - LNCT University, Bhopal, India.
Page No: 53 - 66
DOI:17.0002.JECA.2022.V1206.200786.9905 (gallery/jeca%20-%202782.pdf)

06. Quality of Work Life and Job Performance of Employees Working in BPO Industry in Pune (gallery/jeca%20-%202783.pdf)
Sulbha Waghmare, Assistant Professor - Department of Management (MBA), Indira Institute of Management, Pune, India

15. SERVICEABILITY ANALYSIS AND DESIGN IN ULTIMATE STATE OF BRIDGE FOR IRC CLASS 70R VEHICLE (gallery/jeca%20-%202785.pdf)
Dolly Dhomne, Research Scholar - Tulsiramji Gaikwad Patil College of Engineering AND Technology, Nagpur
Amey Khedikar, Professor - Tulsiramji Gaikwad Patil College of Engineering AND Technology, Nagpur
Page No: 173 - 180
DOI:17.0002.JECA.2022.V1206.200786.9915 (gallery/jeca%20-%202785.pdf)

16. EXPERIMENTAL STUDY ON THE POROUS CONCRETE (gallery/jeca%20-%202797.pdf)
Sonali S. Patil, Assistant Professor - SVERI s College of Engineering Pandharpur
Manik G. Deshmukh, Assosiate Professor - SVERI s College of Engineering Pandharpur
Shraddha A. Wangde, Aishwarya V. Adhatrao, Shital S. Dhotre, Kavyanjali C. Mangrule, Bhagyashri R. Bhong, Pooja S. Swami - UG Student - SVERI s College of Engineering Pandharpur
Page No: 181 - 189
DOI:17.0002.JECA.2022.V1206.200786.9916 (gallery/jeca%20-%202797.pdf)

17. ACCIDENT PREVENTION IN HILLY AREAS BY ALERT SYSTEM (gallery/jeca%20-%202793.pdf)
Dr.Kalamani C, Assistant Professor - Dr. Mahalingam College of Engineering and Technology
Subash G K, Kaviyarasu S, Guruprasad K - Students - Dr. Mahalingam College of Engineering and Technology,Pollachi
Page No: 190 - 197
DOI:17.0002.JECA.2022.V1206.200786.9917 (gallery/jeca%20-%202793.pdf)

18. Ultrasonic Study of the Binary Liquid Mixture Consisting of 2-Ethoxyethanol and Methanol at 312.15 °K (gallery/jeca%20-%202799.pdf)
SARWADE M. P., Ware, A. T., Ghuge, D. R., Saif, Ur Raheman - Department of Physics, D. S. M. College, Parbhani - 431401, Maharashtra (India)
Page No: 198 - 211
DOI:17.0002.JECA.2022.V1206.200786.9918 (gallery/jeca%20-%202799.pdf)

19. Design of Super Premium Efficiency Class Induction motors -A Review (gallery/jeca%20-%202800.pdf)
Mr. Omkar Pradip Patil, PG Student - Bharati Vidyapeeth (Deemed to be University),College of Engineering, Pune, [M.S.], India.
Prof. R. S. Ambekar, Assistant Professor - Bharati Vidyapeeth (Deemed to be University), College of Engineering, Pune, [M.S.], India.
Page No: 212 - 230
DOI:17.0002.JECA.2022.V1206.200786.9919 (gallery/jeca%20-%202800.pdf)

20. Weather Prediction Using Machine Learning (gallery/jeca%20-%202801.pdf)
K Jyothirmai, Student (MSc Data Science) - Department of Computer Science, Gandhi Institute Of Technology And Management, Andhra Pradesh, Visakhapatnam, India
M Suresh Kumar, Assistant Professor - Department of Computer Science, Gandhi Institute Of Technology And Management, Andhra Pradesh, Visakhapatnam, India.
K Yasudha, Assistant Professor - Department of Computer Science, Gandhi Institute Of Technology And Management, Andhra Pradesh, Visakhapatnam, India.
Page No: 231 - 235
DOI:17.0002.JECA.2022.V1206.200786.9920 (gallery/jeca%20-%202801.pdf)

21. Linear Array Transducer of 32 Elements with Center Frequency10 MHZ (gallery/jeca%20-%202803.pdf)
Rodge S.A., Associate Professor - Dept. of Electronics Adarsha Science J.B Arts and Birla Commerce Mahavidyalaya, Dhamangaon Rly-444709 India)
S. K Shelke, Assistant Professor - Dept. of Electronics Adarsha Science J.B Arts and Birla Commerce Mahavidyalaya, Dhamangaon Rly-444709 India)
Salve H.E. - Dept. of Electronics Adarsha Science J.B.Arts and Birla Commerce Mahavidyalaya, Dhamangaon Rly-444709 India)
Vishal Gabhane - Dept. of Electronics Adarsha Science J.B Arts and Birla Commerce Mahavidyalaya, Dhamangaon Rly-444709 India)
Page No: 231 - 235
DOI:17.0002.JECA.2022.V1206.200786.9921 (gallery/jeca%20-%202803.pdf)

22. Design and Analysis of (G+5) Residential Building Using Staad.pro (gallery/jeca%20-%202804.pdf)
Girish Falmari, Assistant Professor - SVERI's College of Engineering Pandharpur
Manik Deshmukh, Assosiate Professor - SVERI's College of Engineering Pandharpur
Pritish Aiwale, Ganesh Nimbalkar, Swapnil Kakade, Andeso Pul, Satyam Shinde, Kedar Sikchi - UG Student SVERI's College of Engineering Pandharpur
Page No: 236 - 244
DOI:17.0002.JECA.2022.V1206.200786.9922 (gallery/jeca%20-%202804.pdf)

linear Array Transducer of 32 Elements with Center Frequency10 MHZ

Rodge S.A.[1]
Associate Professor, Dept. of Electronics
Adarsha Science J.B.Arts and Birla Commerce Mahavidyalaya, Dhamangaon Rly-444709 India)
Email:suryakant09@gmail.com

S. K Shelke[2]
Assistant Professor, Dept. of Electronics
Adarsha Science J.B.Arts and Birla Commerce Mahavidyalaya, Dhamangaon Rly-444709 India)
Email:swawpatilkshelke1@gmail.com

Salve H.E[3]
Dept. of Electronics
Adarsha Science J.B.Arts and Birla Commerce Mahavidyalaya, Dhamangaon Rly-444709 India)
Email:hrushadsalve1710@gmail.com

Vishal Gabhane.[4]
Dept. of Electronics
Adarsha Science J.B.Arts and Birla Commerce Mahavidyalaya, Dhamangaon Rly-444709 India)
Email:vishalgabhane2008@gmail.com

ABSTRACT

Ultrasonic arrays are used in many applications including medical imaging. In this specific case is important to achieve precise information about the magnitude and position of the peak pressure, intensity, detected image and various pressure fields produced by the probe. This paper presents the simulation of linear array transducers of 32 elements with center frequency 10 MHz for ultrasonic measurements

Keywords—Ultrasonic, Linear array, Transducer, medical imaging, Field-II GUI, Tx Rx Field images.

1 INTRODUCTION

For the period of the second half of 20th current century the medical imaging is grown through Ultrasound tool speedily. The part of novel technology is the use of computers to decide problems by simulating theoretical models (Numerical simulations) that has taken place alongside pure theory and experiment during the last few decades. These numerical simulations permit one to resolve problems that may not be accessible to direct experimental study or too complex for theoretical analysis. Computer simulations can link the gap between analysis and experiment [2].

More than the last half century much development has been made in medical device technology. One particular medical technology that has enhanced speedily over the last 30 years is ultrasound. This advancement in technology however has brought with it the rapid obsolescence of system design. The accomplishment of modern electronics is built on the possibility to precisely predict system performance by the use of simulation tools. This model can be extended to components such as piezoelectric transducers attached to the electronics [3]. The ability to simulate both piezoelectric transducer and electronics together renders possible efficient optimizations at system level, i.e., minimizing size, price and power consumption [4].

2 SPATIAL IMPULSE THEORY

The pressure field generated by the aperture is found by the Rayleigh integral [5]

$$p(\vec{r}_1,t)=\frac{\rho_0}{2\pi}\int_s \frac{\partial v_n(\vec{r}_2,t-\frac{|\vec{r}_1-\vec{r}_2|}{c})}{|\vec{r}_1-\vec{r}_2|}ds \qquad (1)$$

Where the field point is denoted by $\vec{r}_1$ and the aperture by $\vec{r}_2$, is the velocity normal to the transducer surface. Using the velocity potential, and assume that the surface velocity is uniform over the aperture making it independent of $\vec{r}_2$, then: where the field point is denoted by $\vec{r}_1$ and the aperture by $\vec{r}_2$, is the velocity normal to the transducer surface. Using the velocity potential, and assume that the surface velocity is uniform over the aperture making it independent of $\vec{r}_2$, then:

$$\Psi(\vec{r}_1,t)=v_n(t)*\int_s \frac{\partial(t-\frac{|\vec{r}_1-\vec{r}_2|}{c})}{2\pi|\vec{r}_1-\vec{r}_2|} \qquad (2)$$

Where * denotes convolution in time. The integral in this equation

$$h(\vec{r}_1,t)=\int_s \frac{\partial(t-\frac{|\vec{r}_1-\vec{r}_2|}{c})}{2\pi|\vec{r}_1-\vec{r}_2|} \qquad (3)$$

Represent the spatial impulse response. The continuous wave field can be found from the Fourier transform of

$$p(\vec{r}_1,t)=\rho_0\frac{\partial v(t)}{\partial t}*h(\vec{r}_1,t) \qquad (4)$$

The impulse response includes the excitation convolved with both the transducers electro-mechanical impulse response in transmit and receive. The final signal for a collection of scatters is calculated as a linear sum over all signals from the different scatters [6-7].

3 SIMULATION OF LINEAR ARRAY TRANSDUCER

The linear array is the fundamental type of multi-element transducer and it scans the region of interest by exciting the elements situated over the region. The field is focused on the region by introducing time delay in the excitation of the concerned individual elements, so initially concave beam is emitted.

Here a Fig.1 shows general design format of 16 element linear array transducer having height, width and kerf of individual element are taken as 5 mm, 0.2 mm and 0.02 mm respectively. The transducers are situated at the center of the coordinate system. To achieve focal length of 30 mm from the center of transducer the electronic focusing is included.

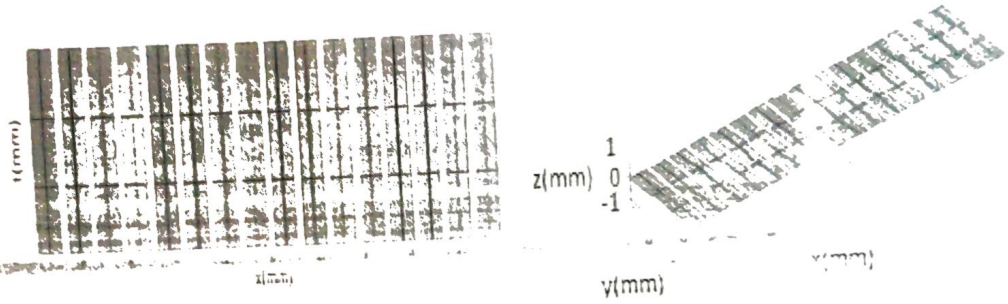

In this paper a linear array transducer of 16 elements is simulated using FIELD-II program with center frequencies 5MHz. For this specified linear array transducer, acoustic field generated is propagated through human body tissues and is observed at a focal distance i.e. (0, 0, 30)

4 RESULT AND DISCUSSION

The calculation of the impulse response is facilitated by projecting the field point onto the plane of the aperture. In this way, the problem became two-dimensional and the field point is given as a (x, y) coordinate set and a height z above the plane. The spatial impulse response is, thus, determined by the relative length of the part of the arc that intersects the aperture [8]. Thereby it is the crossing of the projected ultrasonic waves with the edges of the aperture that determines the spatial impulse responses as a function of time. In this paper by using FIELD-II program created a 32-element linear array transducer with center frequency fo = 10*MHz*. The speed of sound in

tissue is c=$f0$ = 1540m/s, The sampling frequency used was fs = 100MHz. The elements had a width and height of 0.25mm and 5mm respectively. The focal-point was set to 30mm.

Table: 1 shows the parameters for 32element array transducer, excitation pulse and medium used for this center frequency (f_0) used is 10 MHz Figs. (a-m) shows; Element impulse response for 32 element array, TX Field image for 32 element array, TX Axial waveform for 32 element array, TX Lateral beam plot for 32 element array, TX/RX Field image for 32 element array, TX/RX Axial waveform for 32 element array, TX/RX Lateral beam plot for 32 element array, K- space TX/RX field image for 32 element array, K-space axial slice for 32 element array, K-space lateral slice for 32 element array, Detected image for 32 element array, Detected image axial slice for 32 element array and Detected image lateral slice for 32 element array.

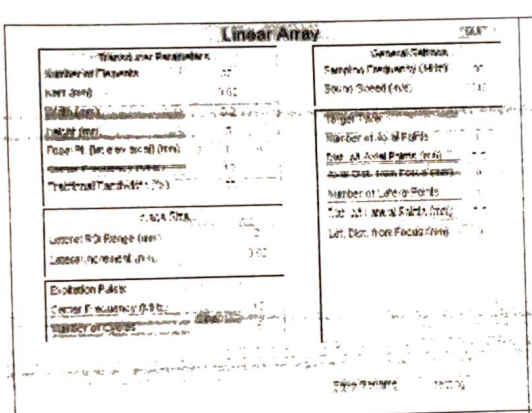

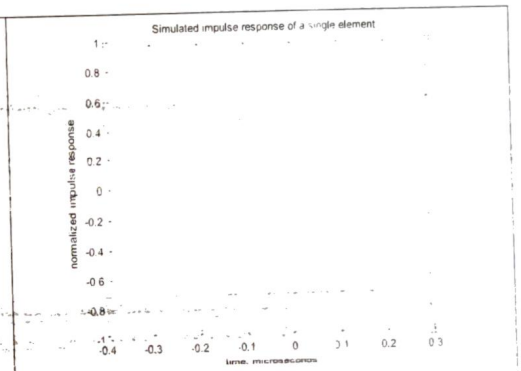

Fig. (a) Element impulse response

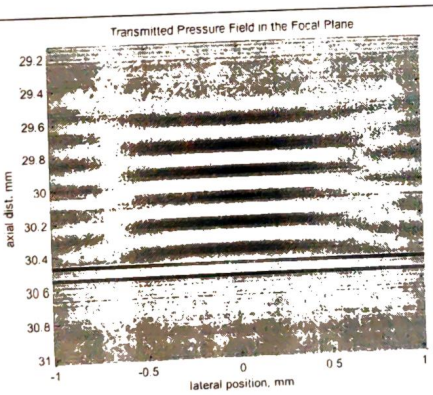

Fig. (b) TX Field image

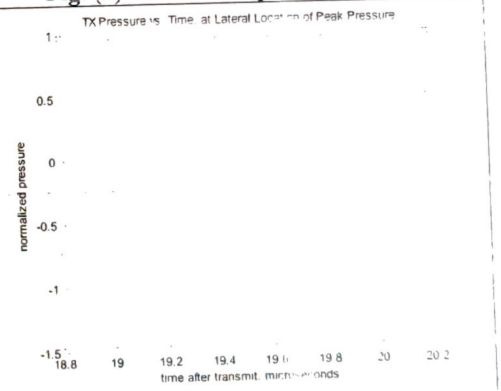

Fig. (c) TX Axial waveform

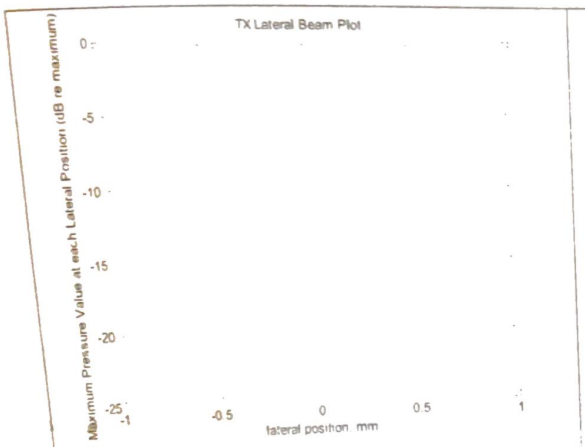

Fig. (d) TX Lateral beam-plot

Fig. (e) TX/RX Field image

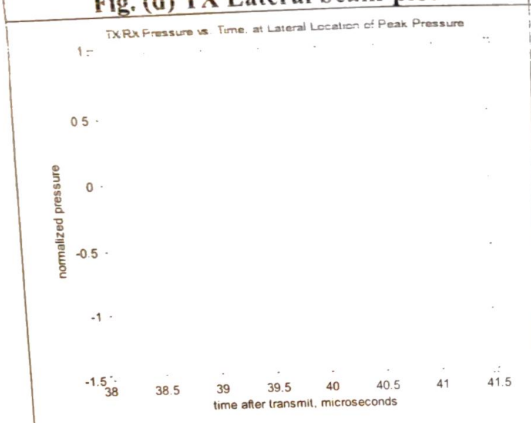

Fig. (f) TX/RX Axial waveform

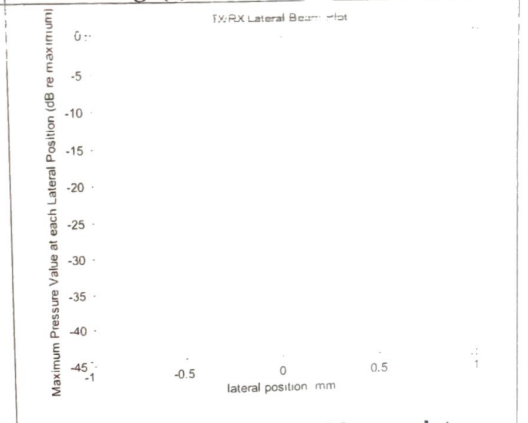

Fig. (g) TX/RX Lateral beam-plot

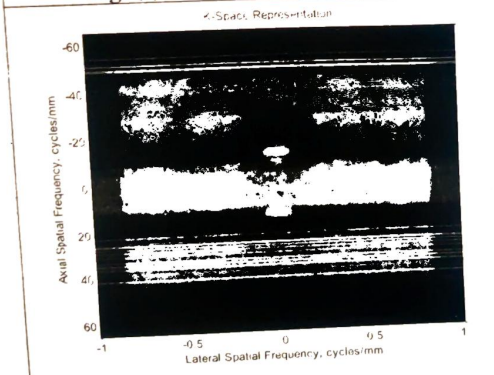

Fig. (h) K space TX/RX Field image

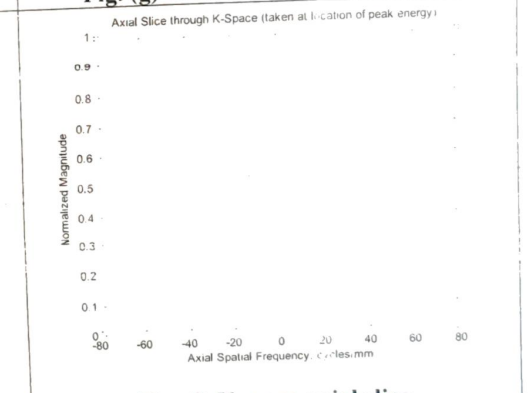

Fig. (i) K space axial slice

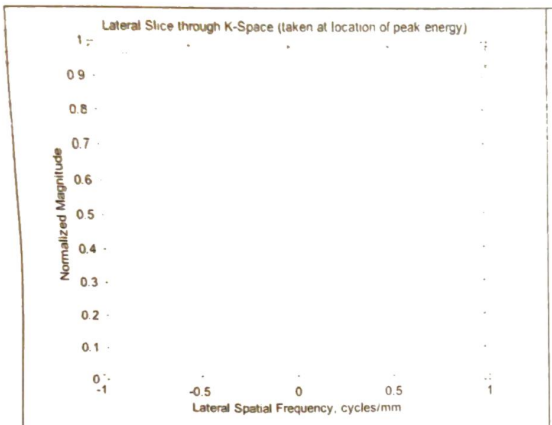

Fig. (j) K space Lateral slice

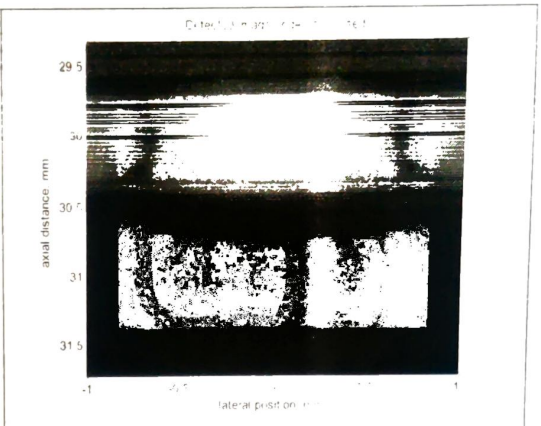

Fig. (k) Detected image

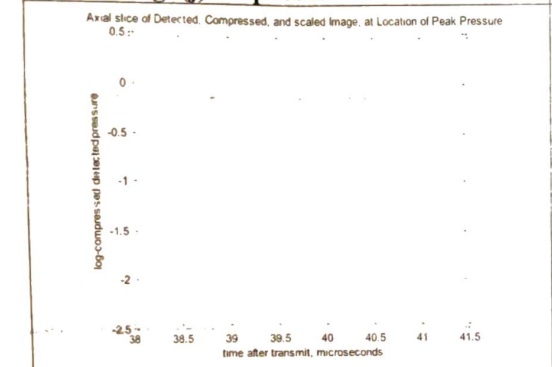

Fig. (l) Detected image axial slice

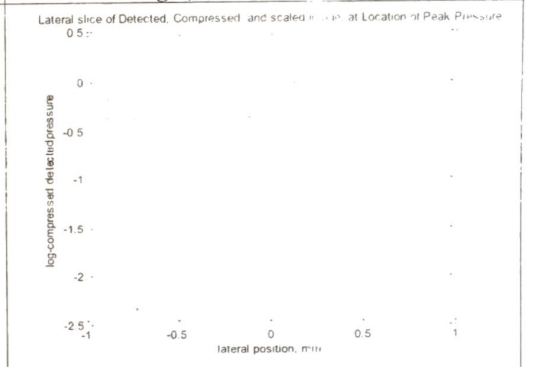

Fig. (m) Detected image lateral slice

5 CONCLUSION

The paper attempts to present a coherent analysis of the focusing strategies for 2-D array transducer design and properties, based on linear acoustics. The delays on the individual transducer elements and their relative weight or apodization are changed continuously as a function of depth. This yields near perfect focused images for all depths and has increased the contrast in the displayed image, thus, benefitting the diagnostic importance of ultrasonic imaging. If the center frequency and number of elements in transducer is increased then contrast in the detected image is increased, this also increases the diagnostic status of ultrasonic imaging

References:

[1] T. R. Meeker, "Thickness mode piezoelectric transducers," Ultrasonics **10**, 26–36 ,1972.

[2] Gandole, Y. B. (2012). Computer Modeling and Simulation of Ultrasonic System for Material Characterization. http://www.oalib.com/search? kw=Y.%20B.%20Gandole &searchField=authors.

[3] R. Krimholtz, D. Leedom, and G. Matthaci, "New equivalent circuits for elementary piezoelectric transducers," Electron. Lett. **6**, 398–399 ,1970

[4] P. Marchal, F. Levarssort, L.-P. Tran-Huu-Hue, and M. Lethiecq, "Effects of acoustical properties of a lens on the pulse-echo response of a single element transducer," IEEE International Ultrasonics, Ferroelectrics, and Frequency Control Joint 50th Anniversary Conference, pp. 1651–1654,2004.

[5] Jensen, J.A, A New Approach to Calculating Spatial Impulse Responses. IEEE International Ultrasonic Symposium, Toronto, Canada, 1997

[6] P. Marchal, F. Levarssort, L.-P. Tran-Huu-Hue, and M. Lethiecq, "Effects of acoustical properties of a lens on the pulse-echo response of a single element transducer," IEEE International Ultrasonics, Ferroelectrics, and Frequency Control Joint 50th Anniversary Conference, pp. 1651–1654,2004.

[7] JENSEN, J.A., Field: A program for simulating ultrasound systems, 10th Nordic-Baltic Conference on Biomedical Imaging, in: *Medical & Biological Engineering & Computing*, 1996, **34**, Supplement 1, 351–353.

[8] Jensen, J.A., N.B. Svendsen, Simulation of advanced ultrasound systems using field II, Biomedical Imaging: Nano to Macro, 2004. IEEE International Symposiumon, 15-18 April 2004 Page(s):636–639 Vol.-1.

VOLUME 8 ISSUE 6 2022

GRADIVA REVIEW JOURNAL

A Monthly Publishing Journal

PAGE NO: 543-553
DOI:10.37897.GRJ.2021.V7I11.21.49936

68.Integrated Solar Drying System (gallery/grj%203527.pdf)
G. Neelavathi,Gangabathina Dhanush Kumar,Akumalli Ameer,M
Mahendra Engineering College
PAGE NO: 554-558
DOI:10.37897.GRJ.2021.V7I11.21.49937

Study on Consumer Attitude and Satisfaction Towards Online Shopping (gallery/grj%203531.pdf)
Dr.C.Nirosha,A.Jaishnavi, B.Susmith, Y.Manjula, T.Shabana
PAGE NO: 559-568
DOI:10.37897.GRJ.2021.V7I11.21.49938

69.Ultrasonic Study of the Binary Liquid Mixture Consisting of Methanol and Acetone 312.15 °K (gallery/grj%203535.pdf)
Sarwade M. P,Bhalerao A. A,Awad P. B.Syeda Tayyaba Sayed
D. S. M. College, Parbhani,Maharashtra (India)
PAGE NO: 578-589
DOI:10.37897.GRJ.2021.V7I11.21.49940

70.Evaluation and study of Acoustics parameters of the Binary Liquid Mixture Containing 2-Ethoxyethanol and Ethanol at 312.15 °K (gallery/grj%203536.pdf)
Sarwade M. P,Bhalerao A. A,Awad P. B.Syeda Tayyaba Sayed
D. S. M. College, Parbhani,Maharashtra (India)
PAGE NO: 590-600
DOI:10.37897.GRJ.2021.V7I11.21.49941

71.An In-depth Study For Application Of Fuzzy Logic In Better Understanding Of Criminal Psychology (gallery/grj%203521.pdf)
Ravi Seeta Sireesha
GVPCE(A),Madhurawada, Visakhapatnam, India
D. Lalitha Bhaskari, P. S. Avadhani
AUCE (A), Andhra University, Visakhapatnam. India
PAGE NO: 601-607
DOI:10.37897.GRJ.2021.V7I11.21.49942

74.Study The Response of Ultrasonic Linear Array Transducer with Different number of Elements (gallery/grj%203542.pdf)
Rodge S.A
Adarsha Science J.B.Arts and Birla Commerce Mahavidyalaya, Dhamangaon Rly India
PAGE NO: 633-636
DOI:10.37897.GRJ.2021.V7I11.21.49945

75.Vibration Analysis for IOT Enabled Predictive Maintenance (gallery/grj%203543.pdf)
SumitKumarGupta,Sushil Kumar Agrawal,Anusuey
Bansal IET Lucknow, India
PAGE NO: 637-643
DOI:10.37897.GRJ.2021.V7I11.21.49946

76.Development Of Health Care And Hygiene Wears Using Amla Leaves (gallery/grj%203538.pdf)
Bharani velayudham v,Elango P,Karthick G,Devanand
K. S. Rangasamy College of Technology
PAGE NO: 644-648
DOI:10.37897.GRJ.2021.V7I11.21.49947

77.Cyber Culture and E-Shopping Behaviour of Millennial Generation in Coimbatore (Tamil Nadu) with Special reference to Big Five Personality Trait Theory – A case study (gallery/grj%203546.pdf)
Dr. K. Vijaya Kumar
Karunya Institute of Technology and Sciences
Dr Challa Ramakrishna,Dr. Challa Krishnaveer Abhishek,Dr. D. Bhanupriya,Dr. Bonda Ramakrishna
Andhra University
PAGE NO: 649-655
DOI:10.37897.GRJ.2021.V7I11.21.49948

78.Antimicrobial Finishing On Socks – Enhanced Freshness And Hygiene (gallery/grj%203550.pdf)
P maheswaran,M.arunkumar, Priyadharshni D, G Sandeep Reddy , Gokulakannan K
KSRangasamyCollegeofTechnology,Tiruchengode,TamilNadu,India
PAGE NO: 656-659
DOI:10.37897.GRJ.2021.V7I11.21.49949

Home (/)
Call for Papers (Call-For-Papers/)
Author's (Authors/)
Publication Charges (Publication-Charges/)
Special Issue (Special-Issue/)
Editorial Board (Editorial-Board/)
Contact (Contact/)

PAPER FORMAT
(HTTPS://DRIVE.GOOGLE.C USP=SHARING)
COPYRIGHT FORM
(HTTPS://DRIVE.GOOGLE.C USP=SHARING)
REGISTRATION FORM
(HTTPS://DRIVE.GOOGLE.C 83AZCKZG87S/VIEW? USP=SHARING)

Study The Response of Ultrasonic Linear Array Transducer with Different number of Elements

Rodge S.A.
Associate Professor, Dept. of Electronics
Adarsha Science J.B.Arts and Birla Commerce Mahavidyalaya,
Dhamangaon Rly-444709 India)

ABSTRACT

Ultrasonic arrays are used in many applications including medical imaging. In this specific case is important to achieve precise information about the magnitude and position of the peak pressure and intensity produced by the probe. This paper presents the simulation of linear array transducers of 16, 32 and 64 elements for ultrasonic measurements

Keywords—Ultrasonic, Linear array, Transducer, medical imaging, Field-II GUI, Tx/Rx Field images.

INTRODUCTION

In the biomedical field, the systems for images processing are very important calling for new techniques, much more advanced and performing than they used to be, in order to provide a correct analysis and diagnosis. Ultrasound, widely used in many areas of medicine, provides a safe and efficient means for diagnosis and therapy. There are considerable efforts in designing transducers and determining the characteristics of the emitted field. To simulate the pressure response from transducers, a model which can predict the volt-to-surface acceleration conversion of multilayered transducers is needed. Methods for modeling piezoelectric transducers are well known in literature. [1-6]. Most of these models are based on electrical equivalent circuits benefiting from transmission line theory to represent the electromechanical coupling and acoustic wave propagation, and others rely on deriving impedance matrices for describing the transducer behavior. All of these methods have their advantage and disadvantages depending on the application of use.

There are considerable efforts in designing transducers and determining the characteristics of the emitted field. Field II program [7], developed by J.A. Jensen, can simulate all kinds of ultrasound transducers using linear acoustics and it utilizes the Tupholme-Stepanishen method for calculating spatial impulse responses. The program is capable of calculating the fields for both the pulsed and continuous wave case for a large number of different transducers and allows visualization of simulating transducers. The calculation of the spatial impulse response assumes linearity [8] and any complex-shaped transducer can therefore be divided into smaller apertures and the response can be found by adding the responses from the sub-apertures.

SPATIAL IMPULSE THEORY

The pressure field generated by the aperture is found by the Rayleigh integral [9]

$$p(\vec{r}_1,t)=\frac{\rho_0}{2\pi}\int_s \frac{\partial v_n(\vec{r}_2,t-\frac{|\vec{r}_1-\vec{r}_2|}{c})}{|\vec{r}_1-\vec{r}_2|}ds \qquad (1)$$

where the field point is denoted by $\vec{r}_1$ and the aperture by $\vec{r}_2$, is the velocity normal to the transducer surface. Using the velocity potential , and assume that the surface velocity is uniform over the aperture making it independent of $\vec{r}_2$, then:

where the field point is denoted by $\vec{r}_1$ and the aperture by $\vec{r}_2$, is the velocity normal to the transducer surface. Using the velocity potential , and assume that the surface velocity is uniform over the aperture making it independent of $\vec{r}_2$. then:

$$\Psi(\vec{r}_1,t)=v_n(t)*\int_s \frac{\partial(t-\frac{|\vec{r}_1-\vec{r}_2|}{c})}{2\pi|\vec{r}_1-\vec{r}_2|} \qquad (2)$$

where * denotes convolution in time. The integral in this equation

$$h(\vec{r}_1,t)=\int_s \frac{\partial(t-\frac{|\vec{r}_1-\vec{r}_2|}{c})}{2\pi|\vec{r}_1-\vec{r}_2|} \qquad (3)$$

represent the spatial impulse response. The continuous wave field can be found from the Fourier transform of

$$p(\vec{r}_1,t)=\rho_0\frac{\partial v(t)}{\partial t}*h(\vec{r}_1,t) \qquad (4)$$

The impulse response includes the excitation convolved with both the transducers

electro-mechanical impulse response in transmit and receive. The final signal for a collection of scatters is calculated as a linear sum over all signals from the different scatters [10].

LINEAR ARRAY TRANSDUCER

The linear array is the fundamental type of multi-element transducer and it scans the region of interest by exciting the elements situated over the region. The field is focused on the region by introducing time delay in the excitation of the concerned individual elements, so initially concave beam is emitted. Here a 16 element linear array transducer is designed using FIELD-II program as shown in the Fig.1, height, width and kerf of individual element are taken as 5 mm, 0.2 mm and 0.02 mm respectively. The transducer is situated at the center of the coordinate system. The electronic focusing is incorporated to achieve focal length of **30** mm from the center of transducer. For the above linear array transducer, an excitation signal of two cycles of sinusoidal pulses is given in Fig. 2(a). The impulse response pattern obtained for each element is shown in Fig. 2(b).

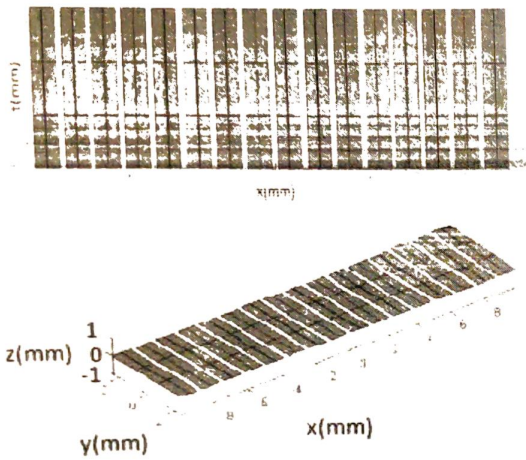

Fig.1 Design of linear array transducer (Height=5mm, Width=0.25mm, Kerf=0.02mm)

For this specified linear array, acoustic field generated is propagated through human body tissues and is observed at a focal distance i.e. (0, 0, 30) whose plot is shown in Fig. 4. Fig. 4(a) shows the field generated while Fig. 4(b) shows the pressure profile at focal distance. Similarly Fig.5 illustrates the lateral beam pattern generated by the assumed linear array transducer. The other simulation parameters chosen are central transducer frequency (f0) =5 MHz, acoustic speed (c0) =1540m/s , fractional bandwith 50%, center frequency of excitation pulse = 7.5 MHz, Number of cycle=5.

IV RESULT AND DISCUSSION

The calculation of the impulse response is facilitated by projecting the field point onto the plane of the aperture. In this way, the problem became two-dimensional and the field point is given as a (x, y) coordinate set and a height z above the plane. The spatial impulse response is, thus, determined by the relative length of the part of the arc that intersects the aperture. Thereby it is the crossing of the projected ultrasonic waves with the edges of the aperture that determines the spatial impulse responses as a function of time.

By using FIELD II program were created three linear arrays with the same characteristics, but with different number of elements: 16 elements, 32 elements and 64 elements. Respectively. For the simulations the transducer center frequency was set to $f_0 = 5MHz$. The speed of sound in tissue is $c=f_0 = 1540m/s$, which gives a wavelength of mm. The sampling frequency used was $f_s = 100MHz$. The elements had a width and height of 0.25mm and 5mm respectively. The focal-point was set to 30mm.

Then the normalized spatial impulse response for this aperture was calculated and plotted by time. Figures 2, 3, 4 and 5 shows the normalized spatial impulse response, Transducer Pressure field, Lateral beam plot and Transmitted Pressure Field in the focal plan for 16 elements. Figures 6, 7, 8 and 9 shows the normalized spatial impulse response, Transducer Pressure field, Lateral beam plot and Transmitted Pressure Field in the focal plan for 32 elements. Figures 10, 11, 12 and 13 shows the normalized spatial impulse response, Transducer Pressure field, Lateral beam plot and Transmitted Pressure Field in the focal plan for 64 elements.

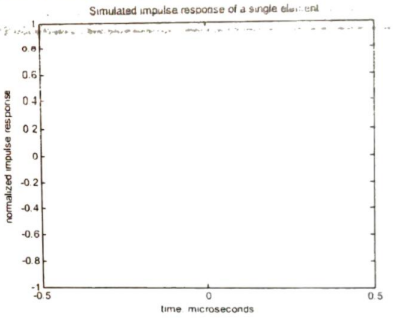

Fig. 2: Normalized impulse response of a single element.

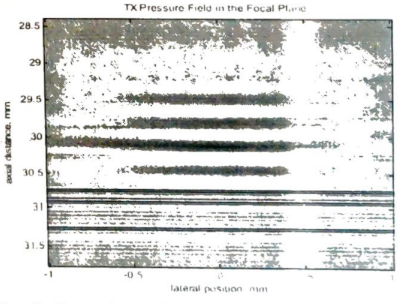

Fig. 3: Transducer Pressure field for 16 elements.

ISSN NO : 0363-8057

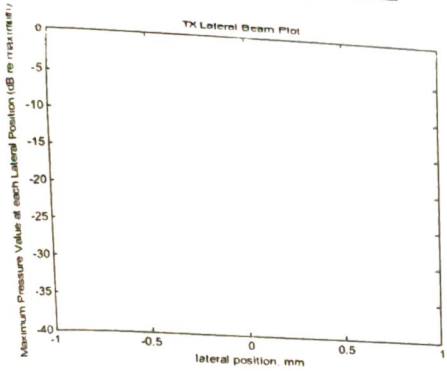

Fig. 4: Lateral beam plot of 16 elements

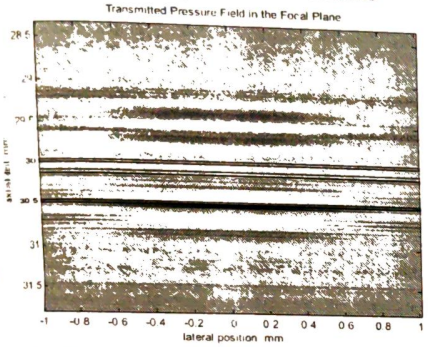

Fig. 5: Transmitted Pressure Field in the focal plan for 16 elements.

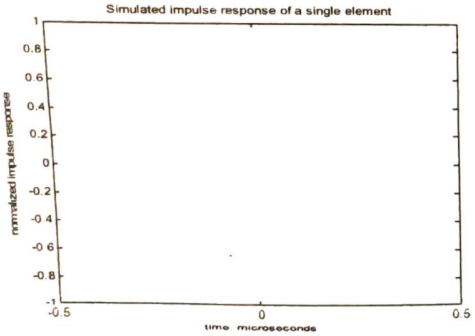

Fig. 6: Normalized impulse response of a32 elements.

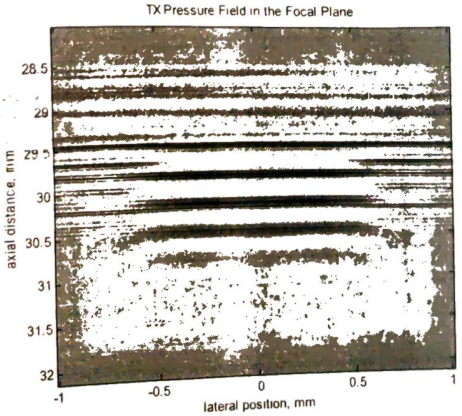

Fig. 7: Transducer Pressure field for 32 elements.

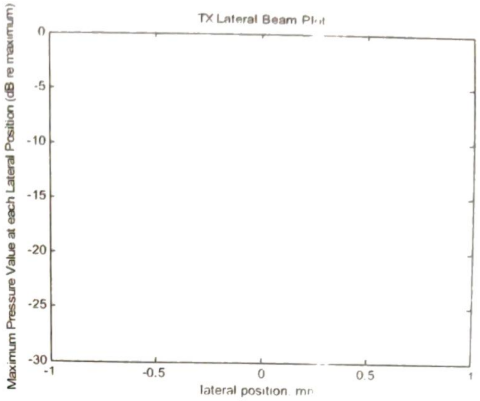

Fig. 8: Lateral beam plot of 32 elements.

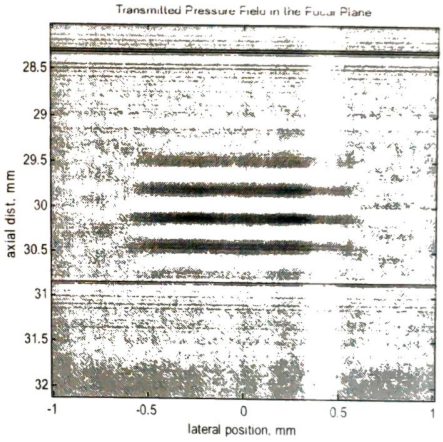

Fig. 9: Transmitted Pressure Field in the focal plan for 32 elements.

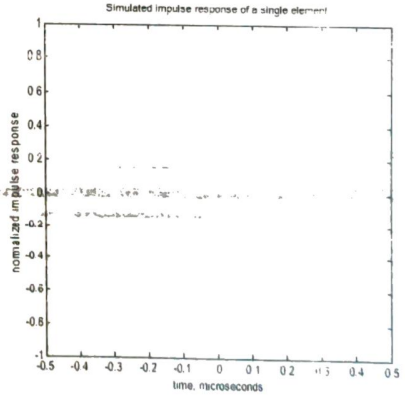

Fig. 10: Normalized impulse response of a64 elements.

ISSN NO : 0363-8057

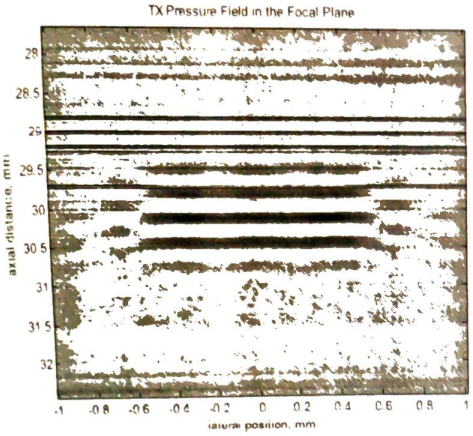

Fig. 11: Transducer Pressure field for 64 elements.

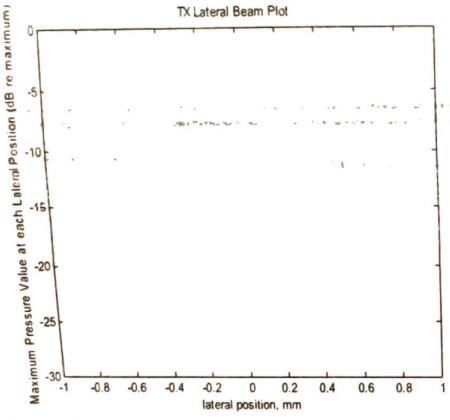

Fig. 12: Lateral beam plot of 64 elements.

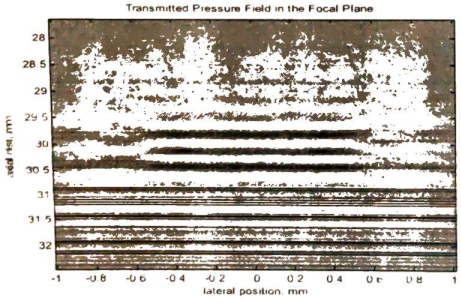

Fig. 13: Transmitted Pressure Field in the focal plan for 64 elements.

V CONCLUSION

The paper attempts to present a coherent analysis of the focusing strategies for 2-D array transducer design and properties, based on linear acoustics. The delays on the individual transducer elements and their relative weight or apodization are changed continuously as a function of depth. This yields near perfect focused images for all depths and has increased the contrast in the displayed image, thus, benefitting the diagnostic value of ultrasonic imaging. If the number of elements in the array transducer is increased then the contrast of detected image and pressure field generated across the transducer is increased, this will increase the diagnostic value of ultrasonic imaging.

REFERENCES

[1] M. Redwood, "Transient performance of a piezoelectric transducer," J Acoust. Soc. Am. **33**, 527–536 ,1961.

[2] E. K. Sittig, "Transmission parameters of thickness-driven piezoelectric transducers arranged in multilayer configurations," IEEE Trans. Sonics Ultrason. **SU-14**, 167–174, 1967.

[3] R. Krimholtz, D. Leedom, and G. Matthaei, "New equivalent circuits for elementary piezoelectric transducers," Electron. Lett. **6**, 398–399 ,1970.

[4] T. R. Meeker, "Thickness mode piezoelectric transducers," Ultrasonics **10**, 26–36 ,1972.

[5] P. Marchal, F. Levarssort, L.-P. Tran-Huu-Hue, and M. Lethiecq, "Effects of acoustical properties of a lens on the pulse-echo response of a single element transducer," IEEE International Ultrasonics, Ferroelectrics, and Frequency Control Joint 50th Anniversary Conference, pp. 1651–1654,2004..

[6] P. Maréchal, F. Levarssort, L.-P. Tran-Huu-Hue, and M. Lethiecq, "Lensfocused transducer modeling using an extended KLM model," Ultrasonics **46**, 155–167, 2007.

[7] JENSEN, J.A., Field: A program for simulating ultrasound systems, 10th Nordic-Baltic Conference on Biomedical Imaging, in: *Medical & Biological Engineering & Computing*, 1996, **34**, Supplement 1, 351–353.

[8] JENSEN, J.A, A New Approach to Calculating Spatial Impulse Responses, *IEEE International Ultrasonic Symposium*, Toronto, Canada, 1997

[9] Jensen, J.A, A New Approach to Calculating Spatial Impulse Responses, IEEE International Ultrasonic Symposium, Toronto, Canada, 1997

[10] Jensen, J.A., N.B. Svendsen, Simulation of advanced ultrasound systems using field II, Biomedical Imaging: Nano to Macro, 2004. IEEE International Symposiumon, 15-18 April 2004 Pages:636–639 Vol 1

GRADIVA REVIEW JOURNAL
A Monthly Publishing Journal
VOLUME 8 ISSUE 6 2022

Home () Call For Papers (Call-For-Papers/) Author's (Author's/) PISSN NO: 0363-8057 (VOLUME-8-ISSUE-11-2022/) Impact Factor: 6.1 Special Issue (Special-Issue/) Editorial Board (Editorial-Board/) Contact (Contact/)

PAPER FORMAT (HTTPS://DRIVE.GOOGLE.C... USP=SHARING)
COPYRIGHT FORM (HTTPS://DRIVE.GOOGLE.C... USP=SHARING)
REGISTRATION FORM (HTTPS://DRIVE.GOOGLE.C... 83AZCKZG87S/VIEW? USP=SHARING)

79.Ultrasonic Technology Used Elasticized Nonwoven And Various Sucking Material Use To Created Adult Diaper (gallery/grj%203553.pdf)
P. maheswaran, M.arunkumar, Swarnajayanthi V, Hariprasath S, Elango M
K.S. Rangasamy College of Technology, Tiruchengode, Tamil Nadu, India
PAGE NO: 660-667
DOI:10.37897.GRJ.2021.V7I11.21.49950

80.Influence of bank-specific and macroeconomic factors in determining non... (gallery/grj%203559.pdf)
Dr. Arun Antony Chully
Vadgaon Sheru, Pune, Maharashtra
Piyush Kumar, Dr Benny J. Godwin
CHRIST (Deemed to be University), Pune Lavasa Campus, Maharashtra
PAGE NO: [illegible]
DOI:10.37897.GRJ.2021.V7I11.21.49951

82.The Emergence Of Stealth Technology (gallery/grj%203545.pdf)
Rithik B, Raghav G, Harshith M, Aravind H S
JSS Academy of Technical Education Bangalore, Karnataka
PAGE NO: 696-702
DOI:10.37897.GRJ.2021.V7I11.21.49953

83.Gdi Based Low Power High Speed 4 Bit Shift Register (gallery/grj%203556.pdf)
P. Surendra Babu, U. Sowmya, N. Usha Sree, P. Sai sree, N. Sasi Rekha
Ravindra College of Engineering for Women
PAGE NO: 703-707
DOI:10.37897.GRJ.2021.V7I11.21.49954

84.Ultrasonic Study of the Binary Liquid Mixture Containing Propanol and Acetone at 312.15 °K (gallery/grj%203565.pdf)
Sarwade M. P, Rokade V. R, Thite M. M
D. S. M. College, Parbhani Maharashtra (India)
PAGE NO: 708-718
DOI:10.37897.GRJ.2021.V7I11.21.49955

85.Mppt Based Battery Charging Using Solar Energy (gallery/grj%203566.pdf)
P.Syed Anwar, V.Vignesh, M.Yashika, Dr. N. Rameshkumar
Al-Ameen Engineering College, Erode, TN, India
PAGE NO: 719-723
DOI:10.37897.GRJ.2021.V7I11.21.49956

86.Protection Of Three Phase Induction Motor Using Virtual System (gallery/grj%203568.pdf)
S.Boopathi, R. Mohamed Basith, J.R. Pugalenthi, K.Manimaran, B.Balajee
Al-Ameen Engineering College, Erode, TN, India
PAGE NO: 724-733
DOI:10.37897.GRJ.2021.V7I11.21.49957

87.Gas Leakage Detection And Auto On Off Gas System (gallery/grj%203569.pdf)
S.Ijaz Ahamed, M.Mohamed Nasrudheen, S.Prakash, S.Syed Abubaker, M.Dinesh Kumar
Al-Ameen Engineering College, Erode, TN, India
PAGE NO: 734-741
DOI:10.37897.GRJ.2021.V7I11.21.49958

88.Hybrid Solar Street Light And Wind Energy System (gallery/grj%203571.pdf)
C.Afsalkhan, R. Mohamed Raiz, Shaik Mohammed Azharudeen, S.Sivaselvam, Dr. A. Sathik Basha
Al-Ameen Engineering College, Erode, TN, India
PAGE NO: 742-745
DOI:10.37897.GRJ.2021.V7I11.21.49959

89.Analysis On Customers Viewpoint Towards Banking Ombusman Scheme (gallery/grj%203576.pdf)
Dr(Smt) A. N. Tamragundi
P G Department of studies in commerce
Seema Badiger, Assistant Professor
Government first grade college for women, K R Nagar- Mysore
PAGE NO: 746-751
DOI:10.37897.GRJ.2021.V7I11.21.49960

90.Simulation of Linear Array Transducer with Center Frequency 5 MHz (gallery/grj%203563.pdf)
Rodge S. A
Adarsha Science J.B.Arts and Birla Commerce Mahavidyalaya, Dhamangaon Rly
PAGE NO: 752-758
DOI:10.37897.GRJ.2021.V7I11.21.49961

GRAD A REVIEW JOURNAL
An UGC-CARE Approved Group-II Journal
ISSN NO : 0363-8057 / Website : http://gradivareview.com/
Email : Submitgrjournal@gmail.Com

Paper ID : GRJ/3563

Certificate of Publication

This is to certify that the paper titled

Simulation of Linear Array Transducer with Center Frequency 5 MHz

Authored by

Rodge S. A

From

Adarsha Science J.B.Arts and Birla Commerce Mahavidyalaya,Dhamangaon Rly

Has been published in

GRADIVA REVIEW JOURNAL Volume 8, Issue 6, June 2022.

UGC APPROVED JOURNAL

DOI: 10.3 7/GRJ
crossref member
CROSSREF.ORG THE CITATION L BACKBONE

Teresa Gallart
Editor-in-Chief
Gradiva Review Journal

6.1 IMPACT FACTOR

Simulation of Linear Array Transducer with Center Frequency 5 MHz

Rodge S. A.
Associate Professor, Dept. of Electronics
Adarsha Science J.B.Arts and Birla Commerce Mahavidyalaya,
Dhamangaon Rly-444709 India)

ABSTRACT

Over the past decades, ultrasound imaging technology has satisfied outstanding improvement in obtaining significant diagnostic information from patients in a fast, noninvasive approach. Piezoelectric transducers are important elements of various broadband ultrasonic systems, either pulse-echo or through-transmission. used for imaging and detection purposes [1]. In ultrasonic broadband applications such as medical imaging, or non-destructive testing, piezoelectric transducers should generate/receive ultrasonic signals with good efficiency over a large frequency range. This implies the use of piezoelectric transducers with high sensitivity, broad bandwidth and short-duration impulse responses. High sensitivity provides large signal amplitudes which determine a good dynamic range for the system and the short duration of the received ultra-sonic signal provides a good axial resolution. This paper presents the simulation of 8-element linear array transducers with center frequency 10 MHZ, using Field-II GUI program for ultrasonic measurements.

Keywords-Detected image, Field-II GUI, Linear array Transducer, medical imaging, TX/RX Fields, TX/RX Axial slice, TX/RX lateral slice, Ultrasonic.

I INTRODUCTION

For the period of the second half of 20th current century the medical imaging is grown through Ultrasound tool speedily. The part of novel technology is the use of computers to decide problems by simulating theoretical models (Numerical simulations) that has taken place alongside pure theory and experiment during the last few decades. These numerical simulations permit one to resolve problems that may not be accessible to direct experimental study or too complex for theoretical analysis. Computer simulations can link the gap between analysis and experiment [2].

More than the last half century much development has been made in medical device technology. One particular medical technology that has enhanced speedily over the last 30 years is ultrasound. This advancement in technology however has brought with it the rapid obsolescence of system

design. The accomplishment of modern electronics is built on the possibility to precisely predict system performance by the use of simulation tools. This model can be extended to components such as piezoelectric transducers attached to the electronics [3]. The ability to simulate both piezoelectric transducer and electronics together renders possible efficient optimizations at system level, i.e. minimizing size, price and power consumption [4].

II SPATIAL IMPULSE THEORY

The pressure field generated by the aperture is found by the Rayleigh integral [5]

$$p(\bar{r}_1,t)=\frac{\rho_0}{2\pi}\int_s \frac{\partial v_n(\bar{r}_2,t-\frac{|\bar{r}_1-\bar{r}_2|}{c})}{|\bar{r}_1-\bar{r}_2|}ds \qquad (1)$$

Where the field point is denoted by $\bar{r}_1$ and the aperture by $\bar{r}_2$, is the velocity normal to the transducer surface. Using the velocity potential, and assume that the surface velocity is uniform over the aperture making it independent of $\bar{r}_2$, then: where the field point is denoted by $\bar{r}_1$ and the aperture by $\bar{r}_2$, is the velocity normal to the transducer surface. Using the velocity potential, and assume that the surface velocity is uniform over the aperture making it independent of $\bar{r}_2$, then:

$$\Psi(\bar{r}_1,t)=v_n(t)*\int_s \frac{\partial(t-\frac{|\bar{r}_1-\bar{r}_2|}{c})}{2\pi|\bar{r}_1-\bar{r}_2|} \qquad (2)$$

Where * denotes convolution in time. The integral in this equation

$$h(\bar{r}_1,t)=\int_s \frac{\partial(t-\frac{|\bar{r}_1-\bar{r}_2|}{c})}{2\pi|\bar{r}_1-\bar{r}_2|} \qquad (3)$$

Represent the spatial impulse response. The continuous wave field can be found from the Fourier transform of

$$p(\bar{r}_1,t)=\rho_0\frac{\partial v(t)}{\partial t}*h(\bar{r}_1,t) \qquad (4)$$

The impulse response includes the excitation convolved with both the transducers electro-mechanical impulse response in transmit and receive. The final signal for a collection of scatters is calculated as a linear sum over all signals from the different scatters [6-7].

III SIMULATION OF LINEAR ARRAY TRANSDUCER

The linear array is the fundamental type of multi-element transducer and it scans the region of interest by exciting the elements situated over the region. The field is focused on the region by introducing time delay in the excitation of the concerned individual elements, so initially concave beam is emitted. Here a Fig.1 shows general design format of 16 element linear array transducer having height, width and kerf of individual element are taken as 5 mm, 0.2 mm and 0.02 mm respectively. The transducers are situated at the center of the coordinate system. To achieve focal length of 30 mm from the center of transducer the electronic focusing is included.

Fig. (1) Design format of linear array transducer (Height=5mm, Width=0.25mm, Kerf=0.02mm)

In this paper a linear array transducer of 8 elements is simulated using FIELD-II program with center frequencies 7.5MHz. For this specified linear array transducer, acoustic field generated is propagated through human body tissues and is observed at a focal distance i.e. (0, 0, 30)

IV RESULT AND DISCUSSION

The calculation of the impulse response is facilitated by projecting the field point onto the plane of the aperture. In this way, the problem became two-dimensional and the field point is given as a (x, y) coordinate set and a height z above the plane. The spatial impulse response is, thus, determined by the relative length of the part of the arc that intersects the aperture [8]. Thereby it is the crossing of the projected ultrasonic waves with the edges of the aperture that determines the spatial impulse responses as a function of time. In this paper by using FIELD-II program created a 32-element linear array transducer with center frequency fo =5*MHz*. The speed of sound in tissue

ISSN NO : 0363-8057

is c=$f0$ = 1540m/s, The sampling frequency used was fs = 100MHz. The elements had a width and height of 0.25mm and 5mm respectively. The focal-point was set to 30mm.

Table: 1 shows the parameters for 8 element array transducer, excitation pulse and medium used, for this center frequency (f_0) used is 5 MHz While Figs. (a-m) shows; Element impulse response for 8 element array, TX Field image for 8 element array, TX Axial waveform for 8 element array, TX Lateral beam plot for 8 element array, TX/RX Field image for 8 element array, TX/RX Axial waveform for 8 element array, TX/RX Lateral beam plot for 8 element array, K- space TX/RX field image for 8 element array, K-space axial slice for 8 element array, K-space lateral slice for 8 element array, Detected image for 8 element array, Detected image axial slice for 8 element array and Detected image lateral slice for 8 element array.

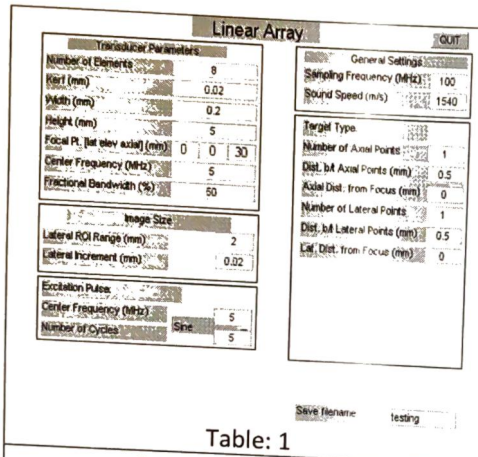

Table: 1

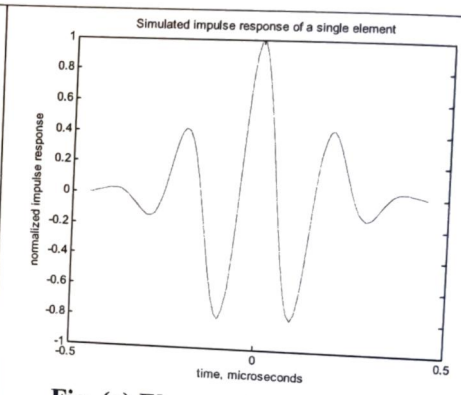

Fig. (a) Element impulse response

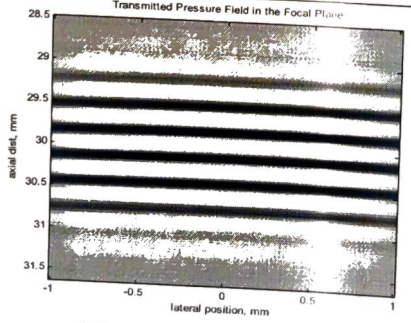

Fig. (b) TX Field image

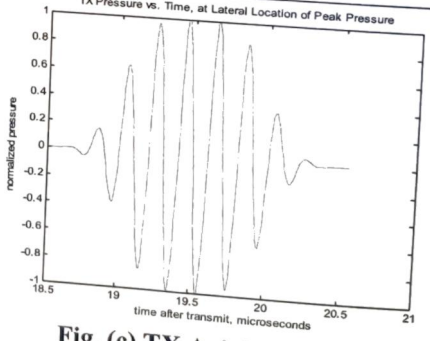

Fig. (c) TX Axial waveform

ISSN NO : 0363-8057

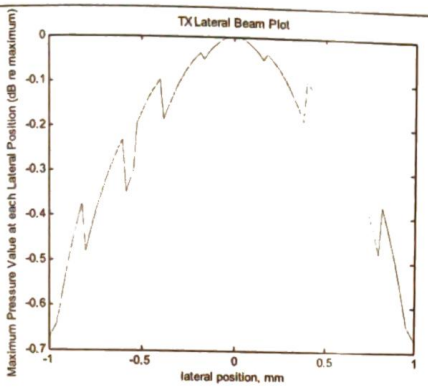

Fig. (d) TX Lateral beam-plot

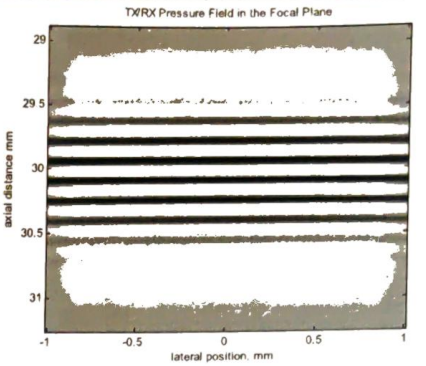

Fig. (e) TX/RX Field image

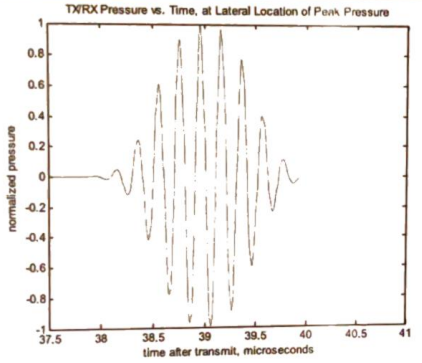

Fig. (f) TX/RX Axial waveform

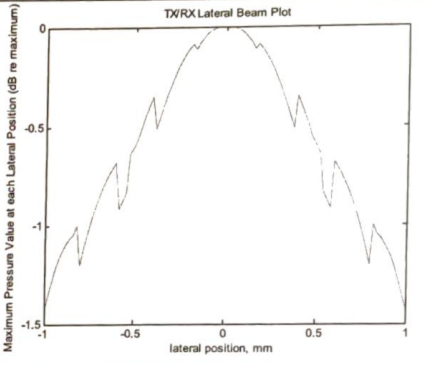

Fig. (f) TX/RX Lateral beam-plot

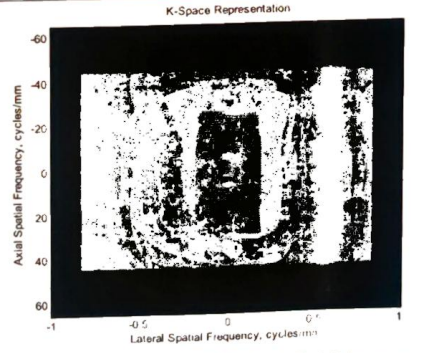

Fig. (g) K space TX/RX field image

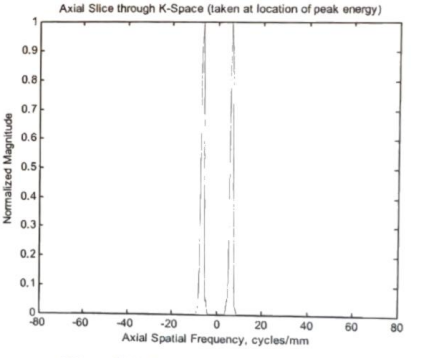

Fig. (h) K space axial slice

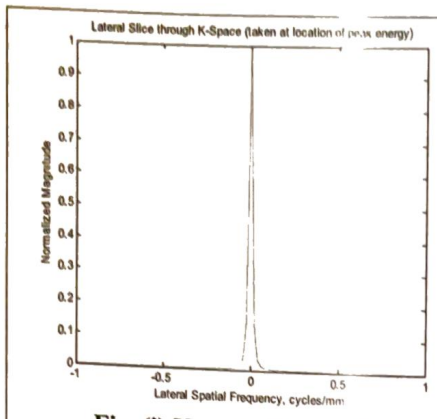

Fig. (i) K space lateral slice

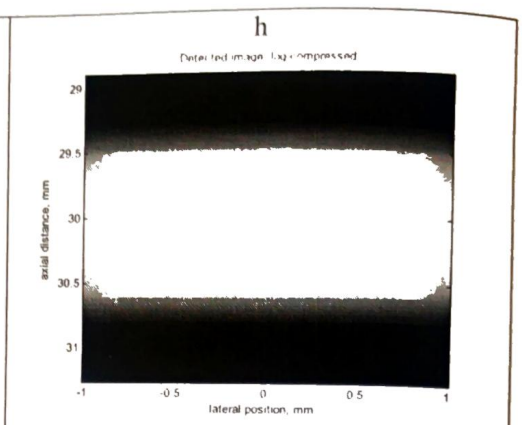

Fig. (j) Detected image

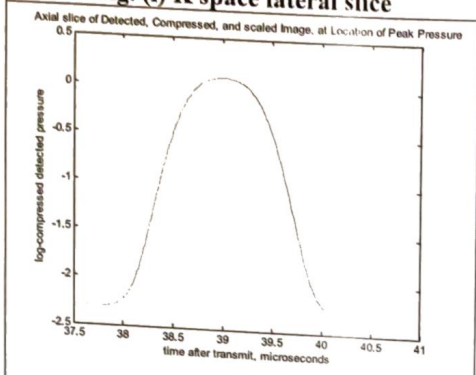

Fig. (l) Detected image axial slice

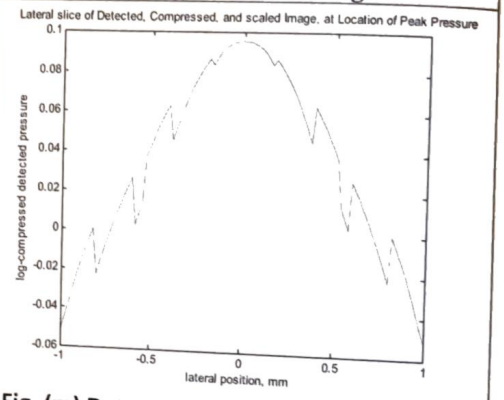

Fig. (m) Detected image lateral slice

V CONCLUSION

The paper attempts to present a coherent analysis of the focusing strategies for 2-D array transducer design and properties, based on linear acoustics. The delays on the individual transducer elements and their relative weight or apodization are changed continuously as a function of depth. This yields near perfect focused images for all depths and has increased the contrast in the displayed image, thus, benefitting the diagnostic importance of ultrasonic imaging. If the center frequency and number of elements in transducer is increased then contrast in the detected image is increased, this also increases the diagnostic status of ultrasonic imaging

References:

[1] Gandole, Y. B. (2012). Computer Modeling and Simulation of Ultrasonic System for Material Characterization. http://www.oalib.com/search? kw=Y.%20B.%20Gandole & searchField=authors.

ISSN NO : 0363-8057

[2] R. Krimholtz, D. Leedom, and G. Matthaci, "New equivalent circuits for elementary piezoelectric transducers," Electron. Lett. **6**, 398–399 ,1970

[3] T. R. Meeker, "Thickness mode piezoelectric transducers," Ultrasonics **10**, 26–36 ,1972.

[4] P. Marchal, F. Levarssort, L.-P. Tran-Huu-Hue, and M. Lethiecq, "Effects of acoustical properties of a lens on the pulse-echo response of a single element transducer," IEEE International Ultrasonics, Ferroelectrics, and Frequency Control Joint 50th Anniversary Conference, pp. 1651–1654,2004.

[5] Jensen, J.A, A New Approach to Calculating Spatial Impulse Responses, IEEE International Ultrasonic Symposium, Toronto, Canada, 1997

[6] P. Marchal, F. Levarssort, L.-P. Tran-Huu-Hue, and M. Lethiecq, "Effects of acoustical properties of a lens on the pulse-echo response of a single element transducer," IEEE International Ultrasonics, Ferroelectrics, and Frequency Control Joint 50th Anniversary Conference, pp. 1651–1654,2004.

[7] JENSEN, J.A., Field: A program for simulating ultrasound systems, 10th Nordic-Baltic Conference on Biomedical Imaging, in: *Medical & Biological Engineering & Computing*, 1996, **34**, Supplement 1, 351–353.

[8] JENSEN, J.A., Users' guide for the Field II program, Technical University of Denmark, DK- 2800 Lyngby, Denmark http://www.es.oersted.dtu.dk/staff/jaj/field/, 2001.

ISSN NO: 1934-7197 Submit Article at: submitjournaleca@gmail.com IMPACT FACTOR - 6.1

UGC-CARE Approved (Group - II) Category Journal
(https://www.scopus.com/sourceid/11200153562)

Journal of Engineering, Computing and Architecture

A Peer Reviewed/Referred Open Access Journal

PAPER FORMAT (gallery/jeca%20paper%20format.doc) REGISTRATION FORM (gallery/jeca-%20registration%20form.docx) COPY RIGHT FORM (gallery/jeca-%20copyright-form.docx) Current Issue (Volume-11-Issue-5-MAY-2021/)

UGC-CARE Group-II Journals Link:
https://ugccare.unipune.ac.in/site/Applicant/login.aspx
(https://ugccare.unipune.ac.in/site/Applicant/login.aspx)

USER NAME: careugcpune@gmail.com
PASSWORD: 22334455

2021

VOLUME 11, ISSUE 12, 2021 (Volume-11-Issue-12-DECEMBER-2021/)
VOLUME 11, ISSUE 11, 2021 (Volume-11-Issue-11-NOVEMBER-2021/)
VOLUME 11, ISSUE 10, 2021 (Volume-11-Issue-10-OCTOBER-2021/)
VOLUME 11, ISSUE 9, 2021 (Volume-11-Issue-9-SEPTEMBER-2021/)
VOLUME 11, ISSUE 8, 2021 (Volume-11-Issue-8-AUGUST-2021/)
VOLUME 11, ISSUE 7, 2021 (Volume-11-Issue-7-JULY-2021/)
VOLUME 11, ISSUE 6, 2021 (Volume-11-Issue-6-JUNE-2021/)
VOLUME 11, ISSUE 5, 2021 (Volume-11-Issue-5-MAY-2021/)
VOLUME 11, ISSUE 4, 2021 (Volume-11-Issue-4-APRIL-2021/)
VOLUME 11, ISSUE 3, 2021 (Volume-11-Issue-3-MARCH-2021/)
VOLUME 11, ISSUE 2, 2021 (Volume-11-Issue-2-FEBRUARY-2021/)
VOLUME 11, ISSUE 1, 2021 (Volume-11-Issue-1-January-2021/)

2020

VOLUME 10, ISSUE 12, 2020 (Volume-10-Issue-12-Dec-2020/)
VOLUME 10, ISSUE 11, 2020 (Volume-10-Issue-11-Nov-2020/)
VOLUME 10, ISSUE 10, 2020 (Volume-10-Issue-10-October-2020/)
VOLUME 10, ISSUE 9, 2020 (Volume-10-Issue-9-2020/)
VOLUME 10, ISSUE 8, 2020 (Volume-10-Issue-8-2020/)
VOLUME 10, ISSUE 7, 2020 (Volume-10-Issue-7-2020/)
VOLUME 10, ISSUE 6, 2020 (Volume-10-Issue-6-2020/)
VOLUME 10, ISSUE 5, 2020 (Volume-10-Issue-5-2020/)
VOLUME 10, ISSUE 4, 2020 (Volume-10-Issue-4-2020/)
VOLUME 10, ISSUE 3, 2020 (Volume-7-Issue-12-2017/)7
VOLUME 10, ISSUE 2, 2020 (Volume-7-Issue-11-2017/)7
VOLUME 10, ISSUE 1, 2020 (Volume-10-Issue-2-2020/)

2019

VOLUME 9, ISSUE 12 2019 (Volume-9-Issue-12-2019/)
VOLUME 9, ISSUE 11, 2019 (Volume-9-Issue-11-2019/)
VOLUME 9, ISSUE 10, 2019 (Volume-9-Issue-10-2019-1/)
VOLUME 9, ISSUE 9, 2019 (Volume-9-Issue-9-2019/)
VOLUME 9, ISSUE 8, 2019 (Volume-9-Issue-8-2019/)
VOLUME 9, ISSUE 7, 2019 (Volume-9-Issue-7-2019/)
VOLUME 9, ISSUE 6, 2019 (Volume-9-Issue-6-2019/)
VOLUME 9, ISSUE 5, 2019 (Volume-9-Issue-5-2019/)
VOLUME 9, ISSUE 4, 2019 (Volume-9-Issue-4-2019/)
VOLUME 9, ISSUE 3, 2019 (Volume-9-Issue-3-2019/)
VOLUME 9, ISSUE 2, 2019 (Volume-9-Issue-2-2019/)
VOLUME 9, ISSUE 1, 2019 (Volume-9-Issue-1-2019/)

2018

VOLUME 8, ISSUE 12, 2018 (Volume-8-Issue-12-2018/)
VOLUME 8, ISSUE 11, 2018 (Volume-8-Issue-11-2018/)
VOLUME 8, ISSUE 10, 2018 (Volume-8-Issue-10-2018/)
VOLUME 8, ISSUE 9, 2018 (Volume-8-Issue-9-2018/)
VOLUME 8, ISSUE 8, 2018 (Volume-8-Issue-8-2018/)
VOLUME 8, ISSUE 7, 2018 (Volume-8-Issue-7-2018/)
VOLUME 8, ISSUE 6, 2018 (Volume-8-Issue-6-2018/)
VOLUME 8, ISSUE 5, 2018 (Volume-8-Issue-5-2018/)
VOLUME 8, ISSUE 4, 2018 (Volume-8-Issue-4-2018/)
VOLUME 8, ISSUE 3, 2018 (Volume-8-Issue-3-2018/)

2017

VOLUME 7, ISSUE 12, 2017 (Volume-7-Issue-12-2017/)
VOLUME 7, ISSUE 11, 2017 (Volume-7-Issue-11-2017/)
VOLUME 7, ISSUE 10, 2017 (Volume-7-Issue-10-2017/)
VOLUME 7, ISSUE 9, 2017 (Volume-7-Issue-9-2017/)
VOLUME 7, ISSUE 8, 2017 (Volume-7-Issue-8-2017/)
VOLUME 7, ISSUE 7, 2017 (Volume-7-Issue-7-2017/)
VOLUME 7, ISSUE 6, 2017 (Volume-7-Issue-6-2017/)
VOLUME 7, ISSUE 5, 2017 (Volume-7-Issue-5-2017/)
VOLUME 7, ISSUE 4, 2017 (Volume-7-Issue-4-2017/)
VOLUME 7, ISSUE 3, 2017 (Volume-7-Issue-3-2017/)
VOLUME 7, ISSUE 2, 2017 (Volume-7-Issue-2-2017/)
VOLUME 7, ISSUE 1, 2017 (Volume-7-Issue-1-2017/)

2016

VOLUME 6, ISSUE 12, 2016 (Volume-6-Issue-12-2016/)
VOLUME 6, ISSUE 11, 2016 (Volume-6-Issue-11-2016/)
VOLUME 6, ISSUE 10, 2016 (Volume-6-Issue-10-2016/)
VOLUME 6, ISSUE 9, 2016 (Volume-6-Issue-9-2016/)
VOLUME 6, ISSUE 8, 2016 (Volume-6-Issue-8-2016/)
VOLUME 6, ISSUE 7, 2016 (Volume-6-Issue-7-2016/)
VOLUME 6, ISSUE 6, 2016 (Volume-6-Issue-6-2016/)
VOLUME 6, ISSUE 5, 2016 (Volume-6-Issue-5-2016/)
VOLUME 6, ISSUE 4, 2016 (Volume-6-Issue-4-2016/)
VOLUME 6, ISSUE 3, 2016 (Volume-6-Issue-3-2016/)

Note: Volume-12 Issue-7 is not showing (i.e., It is not uploaded yet) Hence Indexed page of the same is not available withus.

Comparison of Responses of 2 Element and 4 Element Array Transducer at Center Frequency 5 MHz

Rodge S. A.[1]
Associate Professor, Dept. of Electronics
Adarsha Science J.B.Arts and Birla Commerce Mahavidyalaya,
Dhamangaon Rly-444709 Maharashtra (India)
Email: Suryakantc09@gmail.com

S. K Shelke[2]
Assistant Professor, Dept. of Electronics
Adarsha Science J.B.Arts and Birla Commerce Mahavidyalaya,
Dhamangaon Rly-444709 India)
Email: swapnilkshelke1@gmail.com

ABSTRACT

The systems for images processing in the medical field are very important calling for new techniques, much more advanced and performing than they used to be, in order to provide a correct analysis and diagnosis. Among the medical techniques using computer sciences, it can be mentioned: scintigraphy, echography, tomography, radiography, quantitative microscopy, nuclear magnetic resonance. Ultrasound, widely used in many areas of medicine, provides a safe and efficient means for diagnosis and therapy. When the medium becomes complex solving the wave propagation formula becomes virtually impossible. Modeling becomes much more complex inside the body because the ultrasound propagation speed is different for each tissue and it is known that tissues are not a homogeneous medium for ultrasound wave propagation. Therefore, it is important to know how the ultrasound wave is generated and the ultrasound wave beam shaped. This paper represents the comparison of responses of 2-element 4-element linear array transducers

Key words: Ultrasonic, Linear array Transducer, Field-II GUI, TX/RX Fields, detected image.

I.INTRODUCTION

For the period of the second half of 20th current century the medical imaging is grown through Ultrasound tool speedily. The part of novel technology is the use of computers to decide problems by simulating theoretical models (Numerical simulations) that has taken place alongside pure theory and experiment during the last few decades. These numerical simulations permit one to resolve problems that may not be accessible to direct experimental study or too complex for theoretical analysis. Computer simulations can link the gap between analysis and experiment [1]. These numerical simulations have emerged as a new branch in science and technology complementing both experiments and theory. A simulation can sometimes replace physical experiments, even though most often a simulation and an experiment are complementary. The results of scientific experiments are often explained by simulations and simulations are often calibrated by experiments. The experiments provide input for the simulations, which are viewed as experimenting with theoretical models. The feedback of numerical results into theoretical

modeling and continues interaction with laboratory experiments and analytical theory makes computing a vital tool for science. Consequently, the increased in computing power in both speed and storage has given computational electronics its significance. Improved computer capacity and the solution algorithms themselves, have a big outcome on the excellence of solution obtained. A numerical model can be used to understand measurements and observations enlarge existing analytical models into new parameter regimes and quantitatively test existing theories that can be done by comparing model predictions to experimental information.

The mutual weak point of both experiment and theory is cover up by the numerical simulations' examination and experiment. A third dimension in ultrasonic measurements, of equivalent status and significance to experiment and analysis is nothing but the simulation determination [1]. It has taken an everlasting place in every one aspect of ultrasonic measurements from basic research to engineering design.

II SPECIAL IMPLUSE THEORY

The pressure field generated by the aperture is found by the Rayleigh integral [5]

$$p(\vec{r_1},t)=\frac{\rho_0}{2\pi}\int_s \frac{\partial v_n(\vec{r_2}.t-\frac{|\vec{r_1}-\vec{r_2}|}{c})}{|\vec{r_1}-\vec{r_2}|}ds \qquad (1)$$

Where the field point is denoted by $\vec{r_1}$ and the aperture by $\vec{r_2}$, is the velocity normal to the transducer surface. Using the velocity potential, and assume that the surface velocity is uniform over the aperture making it independent of $\vec{r_2}$, then: where the field point is denoted by $\vec{r_1}$ and the aperture by $\vec{r_2}$, is the velocity normal to the transducer surface. Using the velocity potential, and assume that the surface velocity is uniform over the aperture making it independent of $\vec{r_2}$, then:

$$\Psi(\vec{r}_1,t)=v_n(t)*\int_s \frac{\partial(t-\frac{|\vec{r}_1-\vec{r}_2|}{c})}{2\pi|\vec{r}_1-\vec{r}_2|} \qquad (2)$$

Where * denotes convolution in time. The integral in this equation

$$h(\vec{r}_1,t)=\int_s \frac{\partial(t-\frac{|\vec{r}_1-\vec{r}_2|}{c})}{2\pi|\vec{r}_1-\vec{r}_2|}$$ (3)Represent the spatial impulse

response. The continuous wave field can be found from the Fourier transform of

$$p(\vec{r}_1,t)=\rho_0\frac{\partial v(t)}{\partial t}*h(\vec{r}_1,t) \qquad (4)$$

The impulse response includes the excitation convolved with both the transducers electro-mechanical impulse response in transmit and receive. The final signal for a collection of scatters is calculated as a linear sum over all signals from the different scatters [6-8].

II SIMULATION OF LINEAR ARRAY TRANSDUCER

The linear array is the fundamental type of multi-element transducer and it scans the region of interest by exciting the elements situated over the region. The field is focused on the region by introducing time delay in the excitation of the concerned individual elements, so initially concave beam is emitted. Here a Fig.1 shows general design format of 16 element linear array transducer having height, width and kerf of individual element are taken as 5 mm, 0.2 mm and 0.02 mm respectively. The transducers are situated at the center of the coordinate system. To achieve focal length of 30 mm from the center of transducer the electronic focusing is included.

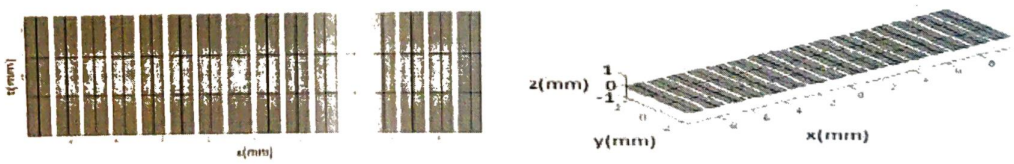

Fig. (1) Design format of linear array transducer (Height=5mm, Width=0.25mm, Kerf=0.02mm)

In this paper a linear array transducer of 16 elements is simulated using FIELD-II program with center frequencies 5MHz. For this specified linear array transducer, acoustic field generated is propagated through human body tissues and is observed at a focal distance i.e. (0, 0, 30)

IV. RESULT AND DISCUSSION

The calculation of the impulse response is facilitated by projecting the field point onto the plane of the aperture. In this way, the problem became two-dimensional and the field point is given as a (x, y) coordinate set and a height z above the plane. The spatial impulse response is, thus, determined by the relative length of the part of the arc that intersects the aperture [8]. Thereby it is the crossing of the projected ultrasonic waves with the edges of the aperture that determines the spatial impulse responses as a function of time. In this paper by using FIELD-II program created a 2-element and 4-element linear array transducer using field -II GUI with center frequency fo = 5*MHz*. The speed of sound in tissue is c=*f*0 = 1540*m/s*, The sampling frequency used was *fs* = 100*MHz*. The elements had a width and height of 0.25mm and 5mm respectively. The focal-point was set to 30mm.

Table: 1and Table: 2 shows the parameters for 2 element and 4- element array transducer, excitation pulse and medium used for this centre frequency (f_0) used is 5MHz. Figs. (a-m) and figs. (a'-m') shows; Element impulse response for 2 and 4-element arrays, TX Field image for 2 and 4 element arrays, TX Axial waveform for 2 and 4 element arrays, TX Lateral beam plot for 2 and 4 element arrays, TX/RX Field image for 2 and 4 element arrays, TX/RX Axial waveform for 2 and 4 element arrays, TX/RX Lateral beam plot for 2 and 4 element arrays, K- space TX/RX field image for 2 and 4 element arrays, K-space axial slice for 2 and 4 element arrays, K-space lateral slice for 2 and 4 element arrays, Detected image for 2 and 4 element arrays, Detected image axial slice for 2 and 4 element arrays and Detected image lateral slice for 2 and 4element arrays. image axial slice for 2 and 4 element arrays and Detected image lateral slice for 2 and 4 element arrays.

IV. RESULT AND DISCUSSION

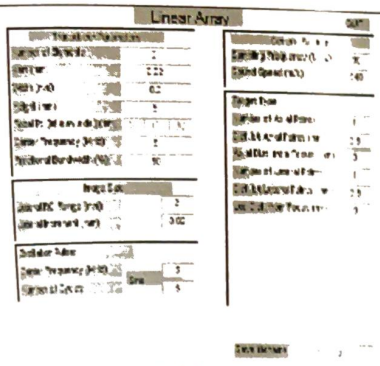

Table: 1

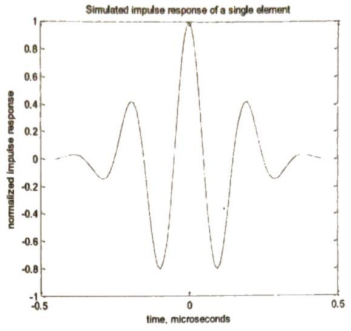

Fig. (a) Element impulse response

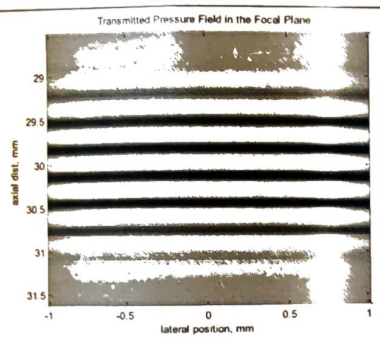

Fig.(b) TX Field image

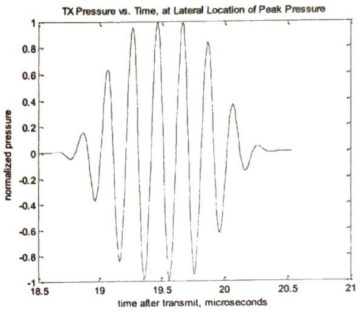

Fig. (c) TX Axial waveform

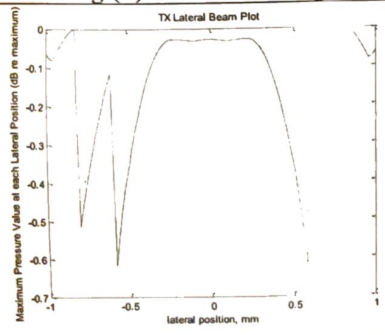

Fig. (d) TX Lateral beam-plot

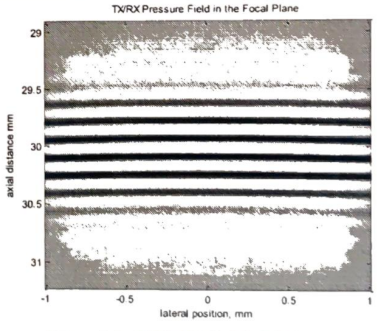

Fig. (e) TX/RX Field image

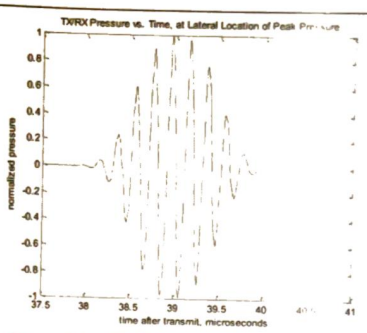

Fig. (f) TX/RX Axial waveform

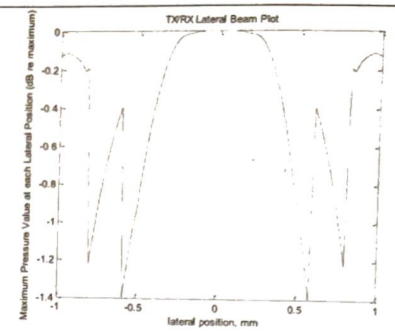

Fig. (g) TX/RX Lateral beam-plot

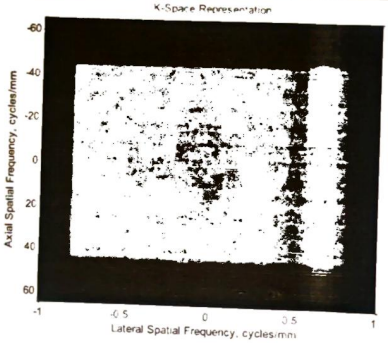

Fig. (h) K space TX/RX field image

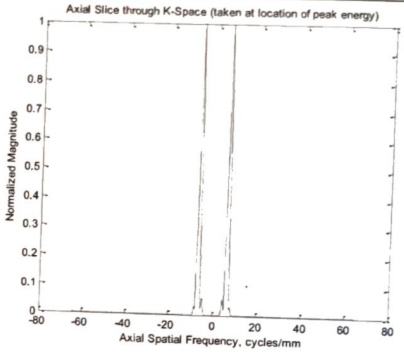

Fig. (i) K space axial slice

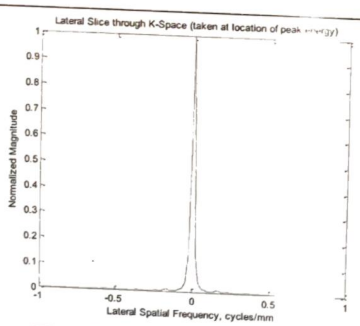

Fig. (j) K space lateral slice

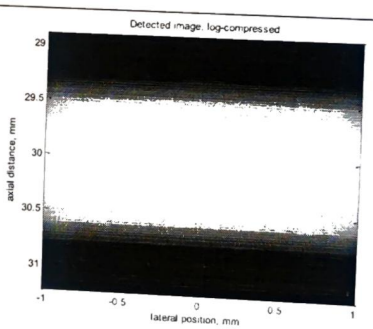

Fig. (k) Detected image

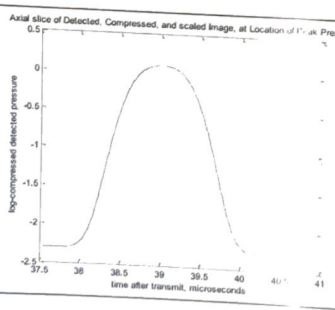

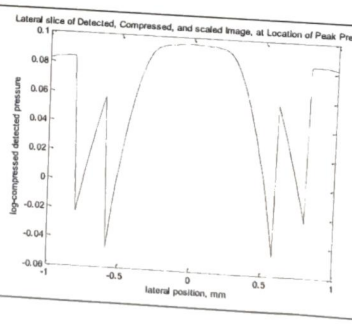

Fig. (l) Detected image axial slice

Fig.(m) Detected image lateral slice

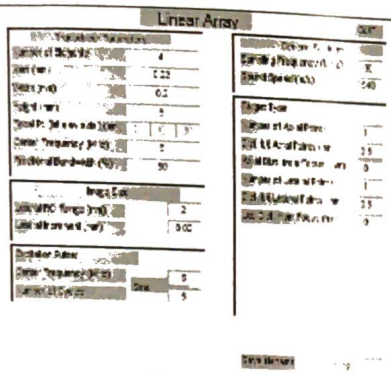

Table: 2

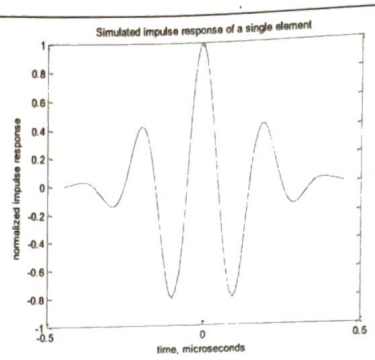

Fig. (a') Element impulse response

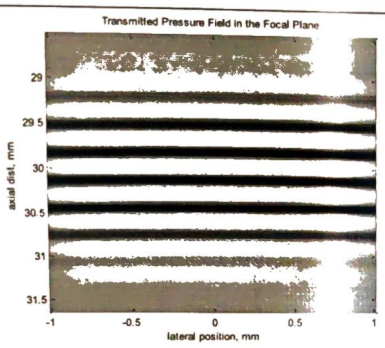

Fig. (b') TX Field image

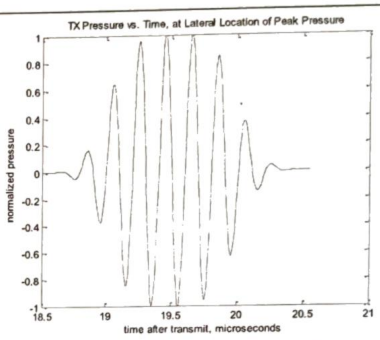

Fig. (c') TX Axial waveform

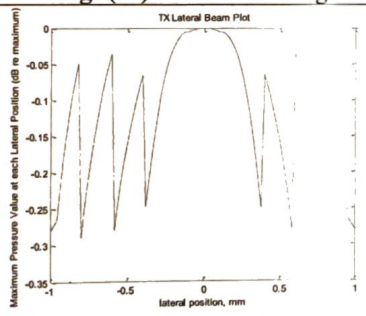

Fig. (d') TX Lateral beam-plot

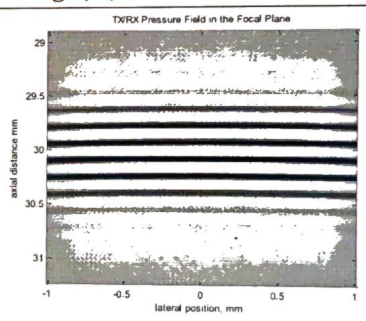

Fig. (e') TX/RX Field image

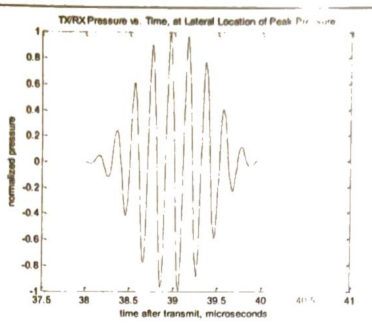

Fig. (f') TX/RX Axial waveform

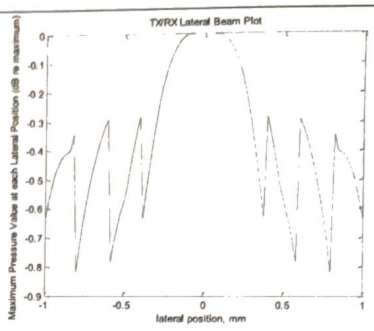

Fig. (g') TX/RX Lateral beam-plot

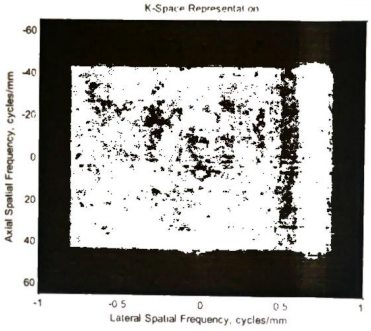

Fig. (h') K space TX/RX Field image

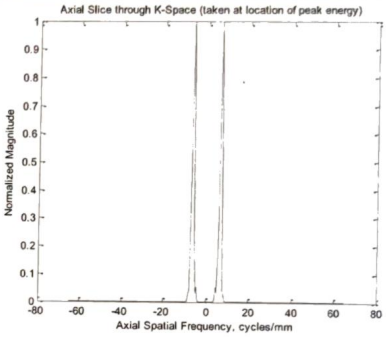

Fig. (I') K space axial slice

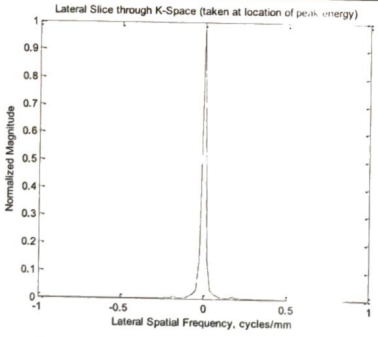

Fig. (j') K space lateral slice

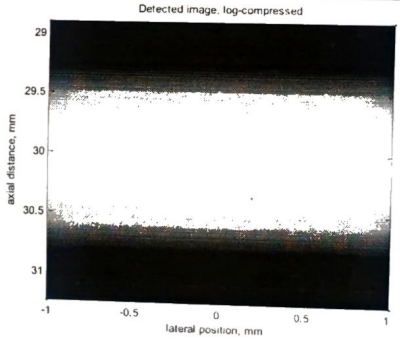

Fig. (k') Detected image

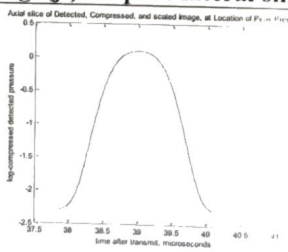

Fig. (l') Detected image axial slice

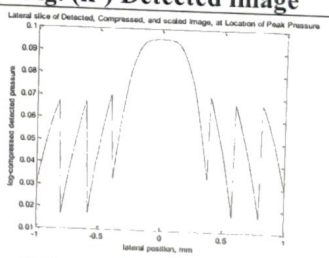

Fig. (m') Detected image Lateral slice

ISSN NO: 1934-7197 Submit Article at: submitjournaleca@gmail.com IMPACT FACTOR - 6.1

UGC-CARE Approved (Group - II) Category Journal
(https://www.scopus.com/sourceid/11200153562)

Journal of Engineering, Computing and Architecture

A Peer Reviewed/Referred Open Access Journal

PAPER FORMAT (gallery/jeca%20paper%20format.doc) REGISTRATION FORM (gallery/jeca-%20registration%20form.docx) COPY RIGHT FORM (gallery/jeca-%20copyright-form.docx) Current Issue (Volume-11-Issue-5-MAY-2021/)

UGC-CARE Group-II Journals Link:
https://ugccare.unipune.ac.in/site/Applicant/login.aspx
(https://ugccare.unipune.ac.in/site/Applicant/login.aspx)

USER NAME: careugcpune@gmail.com
PASSWORD: 22334455

HOME () CALL FOR PAPERS (CALL-FOR-PAPERS/) GUIDELINES (GUIDELINES/) PROPOSAL (PROPOSAL/)
ARCHIVES (ARCHIVES/) EDITORIAL BOARD (EDITORIAL-BOARD/) CONTACT (CONTACT/)

2021

VOLUME 11, ISSUE 12, 2021 (Volume-11-Issue-12-DECEMBER-2021/)
VOLUME 11, ISSUE 11, 2021 (Volume-11-Issue-11-NOVEMBER-2021/)
VOLUME 11, ISSUE 10, 2021 (Volume-11-Issue-10-OCTOBER-2021/)
VOLUME 11, ISSUE 9, 2021 (Volume-11-Issue-9-SEPTEMBER-2021/)
VOLUME 11, ISSUE 8, 2021 (Volume-11-Issue-8-AUGUST-2021/)
VOLUME 11, ISSUE 7, 2021 (Volume-11-Issue-7-JULY-2021/)
VOLUME 11, ISSUE 6, 2021 (Volume-11-Issue-6-JUNE-2021/)
VOLUME 11, ISSUE 5, 2021 (Volume-11-Issue-5-MAY-2021/)
VOLUME 11, ISSUE 4, 2021 (Volume-11-Issue-4-APRIL-2021/)
VOLUME 11, ISSUE 3, 2021 (Volume-11-Issue-3-MARCH-2021/)
VOLUME 11, ISSUE 2, 2021 (Volume-11-Issue-2-FEBRUARY-2021/)
VOLUME 11, ISSUE 1, 2021 (Volume-11-Issue-1-January-2021/)

2020

VOLUME 10, ISSUE 12, 2020 (Volume-10-Issue-12-Dec-2020/)
VOLUME 10, ISSUE 11, 2020 (Volume-10-Issue-11-Nov-2020/)
VOLUME 10, ISSUE 10, 2020 (Volume-10-Issue-10-October-2020/)
VOLUME 10, ISSUE 9, 2020 (Volume-10-Issue-9-2020/)
VOLUME 10, ISSUE 8, 2020 (Volume-10-Issue-8-2020/)
VOLUME 10, ISSUE 7, 2020 (Volume-10-Issue-7-2020/)
VOLUME 10, ISSUE 6, 2020 (Volume-10-Issue-6-2020/)
VOLUME 10, ISSUE 5, 2020 (Volume-10-Issue-5-2020/)
VOLUME 10, ISSUE 4, 2020 (Volume-10-Issue-4-2020/)
VOLUME 10, ISSUE 3, 2020 (Volume-7-Issue-12-2017/)7
VOLUME 10, ISSUE 2, 2020 (Volume-7-Issue-11-2017/)7
VOLUME 10, ISSUE 1, 2020 (Volume-7-Issue-9-2017/)

2019

VOLUME 9, ISSUE 12 2019 (Volume-9-Issue-12-2019/)
VOLUME 9, ISSUE 11, 2019 (Volume-9-Issue-11-2019/)
VOLUME 9, ISSUE 10, 2019 (Volume-9-Issue-10-2019-1/)
VOLUME 9, ISSUE 9, 2019 (Volume-9-Issue-9-2019/)
VOLUME 9, ISSUE 8, 2019 (Volume-9-Issue-8-2019/)
VOLUME 9, ISSUE 7, 2019 (Volume-9-Issue-7-2019/)
VOLUME 9, ISSUE 6, 2019 (Volume-9-Issue-6-2019/)
VOLUME 9, ISSUE 5, 2019 (Volume-9-Issue-5-2019/)
VOLUME 9, ISSUE 4, 2019 (Volume-9-Issue-4-2019/)
VOLUME 9, ISSUE 3, 2019 (Volume-9-Issue-3-2019/)
VOLUME 9, ISSUE 2, 2019 (Volume-9-Issue-2-2019/)
VOLUME 9, ISSUE 1, 2019 (Volume-9-Issue-1-2019/)

2018

VOLUME 8, ISSUE 12, 2018 (Volume-8-Issue-12-2018/)
VOLUME 8, ISSUE 11, 2018 (Volume-8-Issue-11-2018/)
VOLUME 8, ISSUE 10, 2018 (Volume-8-Issue-10-2018/)
VOLUME 8, ISSUE 9, 2018 (Volume-8-Issue-9-2018/)
VOLUME 8, ISSUE 8, 2018 (Volume-8-Issue-8-2018/)
VOLUME 8, ISSUE 7, 2018 (Volume-8-Issue-7-2018/)
VOLUME 8, ISSUE 6, 2018 (Volume-8-Issue-6-2018/)
VOLUME 8, ISSUE 5, 2018 (Volume-8-Issue-5-2018/)
VOLUME 8, ISSUE 4, 2018 (Volume-8-Issue-4-2018/)
VOLUME 8, ISSUE 3, 2018 (Volume-8-Issue-3-2018/)

2017

VOLUME 7, ISSUE 12, 2017 (Volume-7-Issue-12-2017/)
VOLUME 7, ISSUE 11, 2017 (Volume-7-Issue-11-2017/)
VOLUME 7, ISSUE 10, 2017 (Volume-7-Issue-10-2017/)
VOLUME 7, ISSUE 9, 2017 (Volume-7-Issue-9-2017/)
VOLUME 7, ISSUE 8, 2017 (Volume-7-Issue-8-2017/)
VOLUME 7, ISSUE 7, 2017 (Volume-7-Issue-7-2017/)
VOLUME 7, ISSUE 6, 2017 (Volume-7-Issue-6-2017/)
VOLUME 7, ISSUE 5, 2017 (Volume-7-Issue-5-2017/)
VOLUME 7, ISSUE 4, 2017 (Volume-7-Issue-4-2017/)
VOLUME 7, ISSUE 3, 2017 (Volume-7-Issue-3-2017/)
VOLUME 7, ISSUE 2, 2017 (Volume-7-Issue-2-2017/)
VOLUME 7, ISSUE 1, 2017 (Volume-7-Issue-1-2017/)

2016

VOLUME 6, ISSUE 12, 2016 (Volume-6-Issue-12-2016/)
VOLUME 6, ISSUE 11, 2016 (Volume-6-Issue-11-2016/)
VOLUME 6, ISSUE 10, 2016 (Volume-6-Issue-10-2016/)
VOLUME 6, ISSUE 9, 2016 (Volume-6-Issue-9-2016/)
VOLUME 6, ISSUE 8, 2016 (Volume-6-Issue-8-2016/)
VOLUME 6, ISSUE 7, 2016 (Volume-6-Issue-7-2016/)
VOLUME 6, ISSUE 6, 2016 (Volume-6-Issue-6-2016/)
VOLUME 6, ISSUE 5, 2016 (Volume-6-Issue-5-2016/)
VOLUME 6, ISSUE 4, 2016 (Volume-6-Issue-4-2016/)
VOLUME 6, ISSUE 3, 2016 (Volume-6-Issue-3-2016/)

Note: Volume-12 Issue-7 is not showing (i.e. It is not uploaded yet) Hence Indexed page of the same is not available with us.

Comparative Study of 4-Element and 8-Element Array Transducers at Center Frequency 5 MHz

Rodge S. A.[1]
Associate Professor, Dept. of Electronics
Adarsha Science J.B.Arts and Birla Commerce Mahavidyalaya,
Dhamangaon Rly-444709 Maharashtra (India)
Email: Suryakantc09@gmail.com

Rodge Amey[2]
Pursuing M.Sc. Physics from University of Hyderabad
Email: amey.rodge@rodge

ABSTRACT: Ultrasonic arrays are used in many applications including medical imaging. In this specific case is important to achieve precise information about the magnitude and position of the peak pressure, intensity, detected image and various pressure fields produced by the transducer probe. This paper presents the study of responses of 4 element and 8 element linear arrays with center frequency 5MHz for ultrasonic measurements.

KEY WORDS: Detected Image, Field-II GUI, Linear array transducer, TX/RX Pressure field.

I. INTRODUCTION

More than the last half century much development has been made in medical device technology. One particular medical technology that has enhanced rapidly over the last 30 years is ultrasound. This advancement in technology however has brought with it the rapid obsolescence of system design. The achievement of modern electronics is built on the possibility to precisely predict system performance by the use of simulation tools. This model can be extended to components such as piezoelectric transducers attached to the electronics [1]. The capability to simulate both piezoelectric transducer and electronics jointly renders possible efficient optimizations at system level, i.e. minimizing size, price and power consumption [2].

II. SPATIAL IMPULSE THEORY

The pressure field generated by the aperture is found by the Rayleigh integral [5]

$$p(\vec{r}_1,t)=\frac{\rho_0}{2\pi}\int_s \frac{\partial v_n(\vec{r}_2.t-\frac{|\vec{r}_1-\vec{r}_2|}{c})}{|\vec{r}_1-\vec{r}_2|}ds \qquad (1)$$

Where the field point is denoted by $\vec{r}_1$ and the aperture by $\vec{r}_2$, is the velocity normal to the transducer surface. Using the velocity potential, and assume that the surface velocity is uniform over the aperture making it independent of $\vec{r}_2$, then: where the field point is denoted by $\vec{r}_1$ and the aperture by $\vec{r}_2$, is the velocity normal to the transducer surface. Using the velocity potential,

and assume that the surface velocity is uniform over the aperture making it independent of $\vec{r_2}$, then:

$$\Psi(\vec{r_1},t)=v_n(t)*\int \frac{\partial(t-\frac{|\vec{r_1}-\vec{r_2}|}{c})}{2\pi|\vec{r_1}-\vec{r_2}|} \quad (2)$$

Where * denotes convolution in time. The integral in this equation

$$h(\vec{r_1},t)=\int_s \frac{\partial(t-\frac{|\vec{r_1}-\vec{r_2}|}{c})}{2\pi|\vec{r_1}-\vec{r_2}|} \quad (3)$$

Represent the spatial impulse response. The continuous wave field can be found from the Fourier transform of

$$p(\vec{r_1},t)=\rho_0 \frac{\partial v(t)}{\partial t} * h(\vec{r_1},t) \quad (4)$$

The impulse response includes the excitation convolved with both the transducers electro-mechanical impulse response in transmit and receive. The final signal for a collection of scatters is calculated as a linear sum over all signals from the different scatters [3-7].

III. SIMULATION OF LINEAR ARRAY TRANSDUCER

The linear array is the fundamental type of multi-element transducer and it scans the region of interest by exciting the elements situated over the region. The field is focused on the region by introducing time delay in the excitation of the concerned individual elements, so initially concave beam is emitted.

Here a Fig.1 shows general design format of 16 element linear array transducer having height, width and kerf of individual element are taken as 5 mm, 0.2 mm and 0.02 mm respectively. The transducers are situated at the center of the coordinate system. To achieve focal length of 30 mm from the center of transducer the electronic focusing is included.

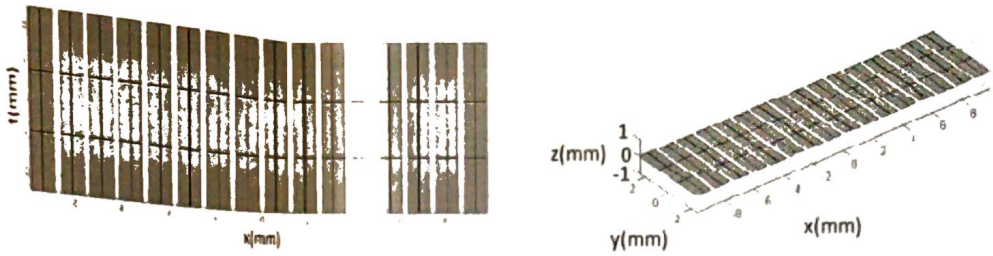

In this paper a linear array transducer of 4-elements and 8-elements is simulated by using FIELD-II GUI program with center frequencies 5MHz. For these specified linear array transducers, acoustic field generated is propagated through human body tissues and is observed at a focal distance i.e. (0, 0, 30)

IV. RESULT AND DISCUSSION

The calculation of the impulse response is facilitated by projecting the field point onto the plane of the aperture. In this way, the problem became two-dimensional and the field point is given as a (x, y) coordinate set and a height z above the plane. The spatial impulse response is, thus, determined by the relative length of the part of the arc that intersects the aperture [8]. Thereby it is the crossing of the projected ultrasonic waves with the edges of the aperture that determines the spatial impulse responses as a function of time. In this paper by using FIELD-II program simulated 4-element and 8-element linear array transducers with center frequency fo = 5*MHz*. The speed of sound in tissue is c=*f*0 = 1540*m/s*, The sampling frequency used was *fs* = 100*MHz*. The elements had a width and height of 0.25mm and 5mm respectively. The focal-point was set to 30mm.

Table: 1 and Table: 2 shows the parameters for 4-element array transducer and 8-element array transducer, excitation pulse and medium used for these center frequency (f_0) used is 5 MHz Figs. (a-m) shows; Element impulse response for 4-element array and figs. (a'-m') Element impulse response for 8-element array transducer, TX Field image, TX Axial waveform, TX Lateral beam plot, TX/RX Field image, TX/RX Axial waveform, TX/RX Lateral beam plot, K- space TX/RX field image, K-space axial slice, K-space lateral slice, Detected image, Detected image axial slice and Detected image lateral slice for 4-element array transducers and 8-element array transducer.

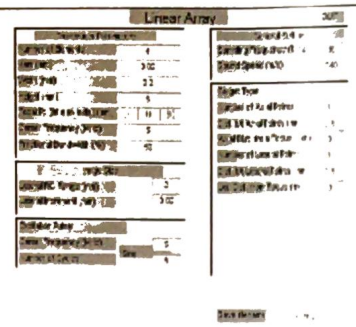

Table: 2

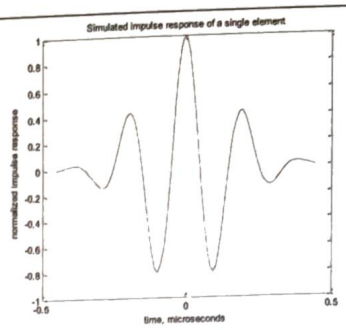

Fig. (a) Element impulse response

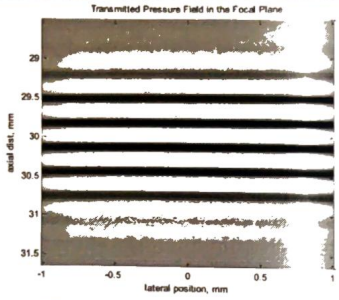

Fig. (b) TX Field image

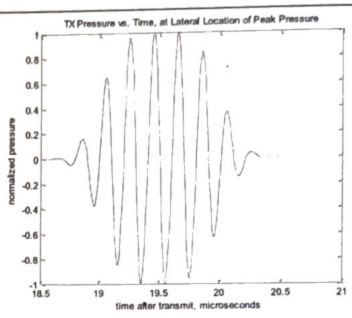

Fig. (c) TX Axial waveform

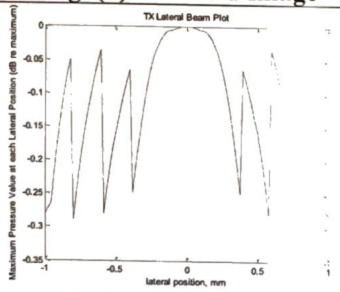

Fig. (d) TX Lateral beam-plot

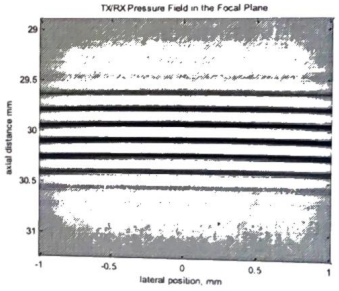

Fig. (e) TX/RX Field image

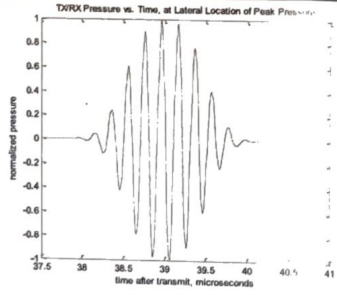

Fig. (f) TX/RX Axial waveform

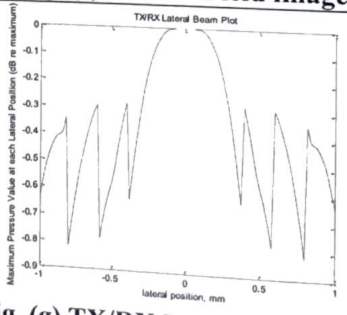

Fig. (g) TX/RX Lateral beam-plot

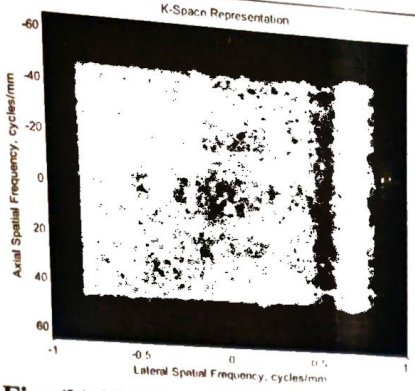

Fig. (h) K space TX/RX Field image

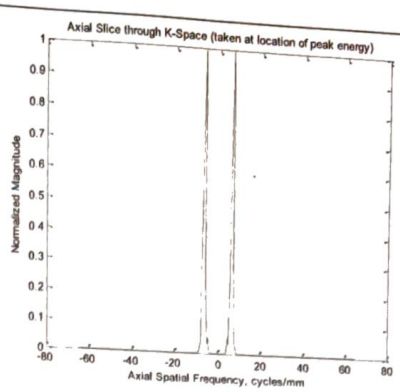

Fig. (i) K space axial slice

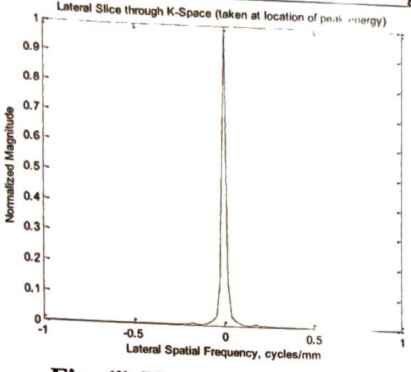

Fig. (j) K space lateral slice

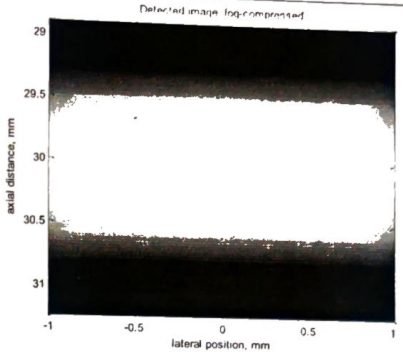

Fig. (k) Detected image

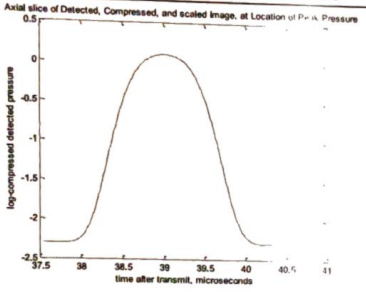

Fig. (l) Detected image axial slice

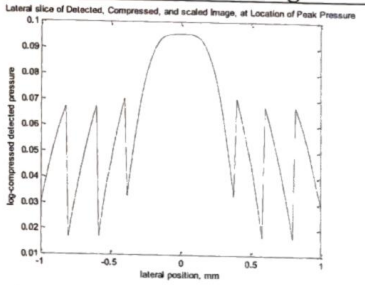

Fig. (m) Detected image Lateral slice

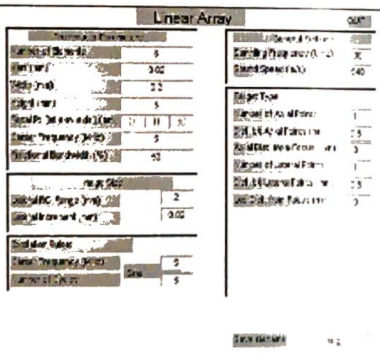

Table: 2

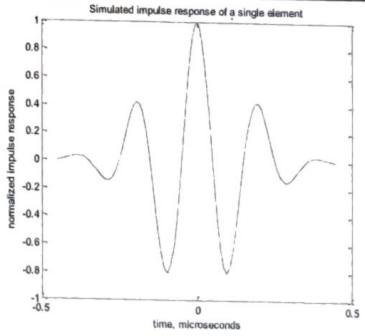

Fig. (a') Element impulse response

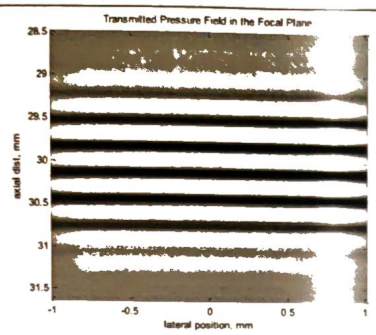

Fig. (b') TX Field image

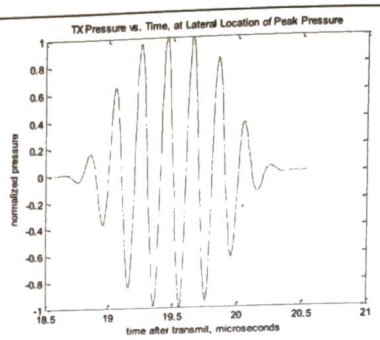

T Fig. (c') X Axial waveform

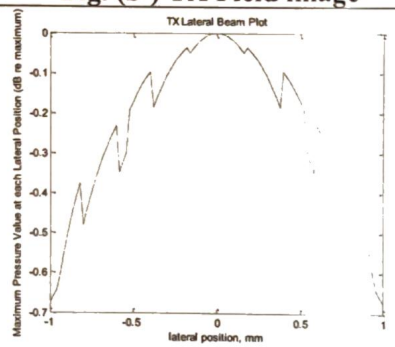

Fig. (d') TX Lateral beam-plot

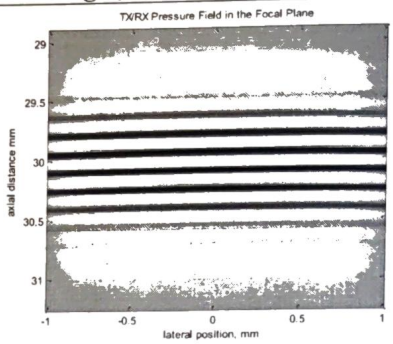

Fig. (e') TX/RX Field image

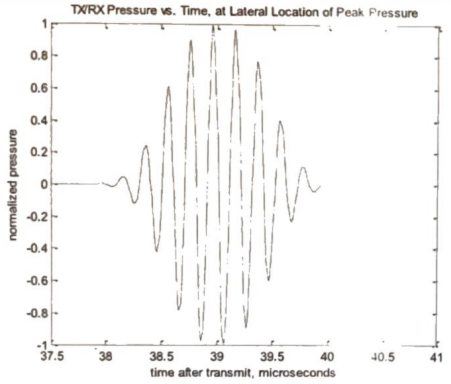

Fig. (f') TX/RX Axial waveform

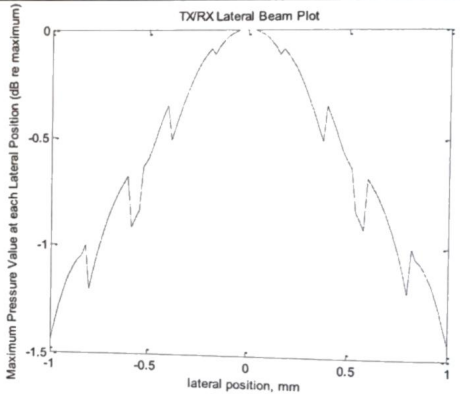

Fig. (g') TX/RX Lateral beam-plot

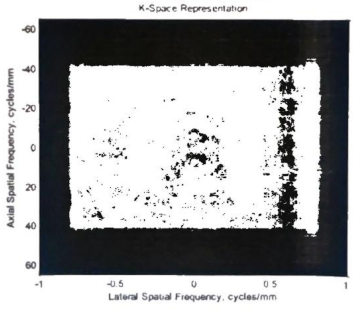

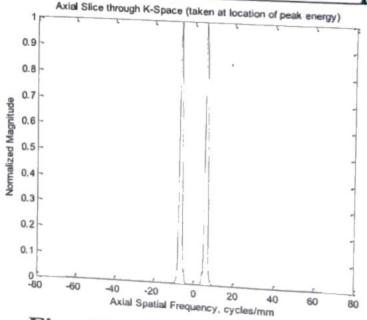

Fig. (I')K space axial slice

Fig. (h') K space TX/RX field image

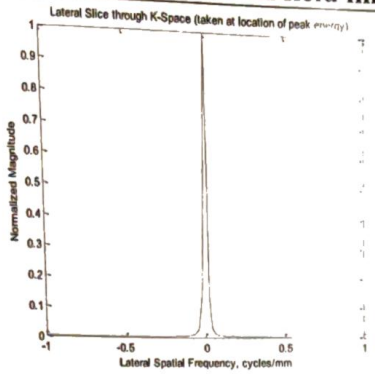

Fig. (j')K space lateral slice

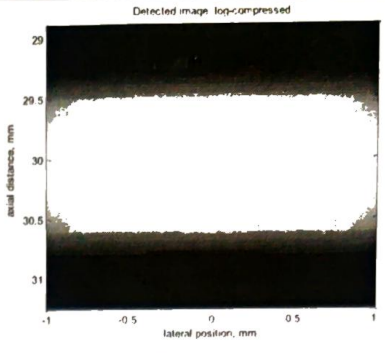

h

Fig. (k')Detected image

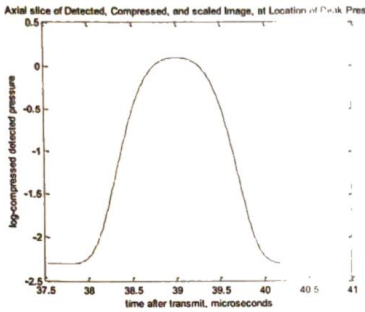

Fig. (l') Detected image axial slice

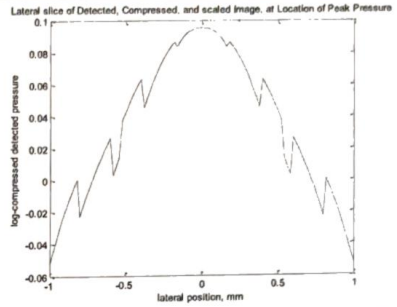

Fig. (m') Detected image lateral slice

V. CONCLUSION

The paper attempts to present a coherent analysis of the focusing strategies for 2-D array transducer design and properties, based on linear acoustics. The delays on the individual transducer elements and their relative weight or apodization are changed continuously as a function of depth. This yields near perfect focused images for all depths. Similarly, if number of arrays in the transducer are increased then contrast of displayed image, is increased thus, benefitting the diagnostic importance of ultrasonic imaging. The detected image response for 8-element array has higher contrast than 4-element array also the pressure filed generated by 8-element is high this increases diagnostic value.

References

[1] *Gandole, Y. B. (2012). Computer Modeling and Simulation of Ultrasonic System for Material Characterization. http://www.oalib.com/search? kw=Y.%20B.%20Gandole &searchField=authors.*

[2] *R. Krimholtz, D. Leedom, and G. Matthaci, "New equivalent circuits for elementary piezoelectric transducers," Electron. Lett. **6**, 398–399 ,1970*

[3] *T. R. Meeker, "Thickness mode piezoelectric transducers," Ultrasonics **10**, 26–36 ,1972.*

[4] P. Marchal, F. Levarssort, L.-P. Tran-Huu-Hue, and M. Lethiecq, "Effects of acoustical properties of a lens on the pulse-echo response of a single element transducer," IEEE International Ultrasonics, Ferroelectrics, and Frequency Control Joint 50th Anniversary Conference, pp. 1651–1654,2004.

[5] Jensen, J.A, A New Approach to Calculating Spatial Impulse Responses, IEEE International Ultrasonic Symposium, Toronto, Canada, 1997

[6] P. Marchal, F. Levarssort, L.-P. Tran-Huu-Hue, and M. Lethiecq, "Effects of acoustical properties of a lens on the pulse-echo response of a single element transducer," IEEE International Ultrasonics, Ferroelectrics, and Frequency Control Joint 50th Anniversary Conference, pp. 1651–1654,2004.

[7] JENSEN, J.A., Field: A program for simulating ultrasound systems, 10th Nordic-Baltic Conference on Biomedical Imaging, in: Medical & Biological Engineering & Computing, 1996, 34, Supplement 1, 351–353.

[8] Jensen, J.A., N.B. Svendsen, Simulation of advanced ultrasound systems using field II, Biomedical Imaging: Nano to Macro, 2004. IEEE International Symposiumon, 15-18 April 2004 Page(s):636–639 Vol.-1.

Not in List

Science, Technology And Development Journal

An UGC CARE APPROVED GROUP - II MULTIDISCIPLINARY JOURNAL

(https://www.scopus.com/sourceid/37750)

editorstdjournal@gmail.com

ISSN NO: 0950-0707

Impact Factor : 6.1

VOLUME XI ISSUE VI JUNE 2022

1. **IoT based Bike fall and theft detection withtracking system (gallery/1-june2022.pdf)**
Rutvik Rajendra Sutar, Tanmay Hitesh Barot, Sanket Rajkumar Chavare, Akib Samsher Shaikh, Darshan Rajendra Chougule - Sharad institute of technology polytechnic yadrav,Kolhapur, Maharashatra,India.
Page No : 1-4
DOI:22.18001.STD.2022.V11I06.22.35600 (gallery/1-june2022.pdf)

2. **Construction of a tree with n taxa on an n−dimensional space where n = 2,3, that preserves distance as (gallery/2-june2022.pdf) in a given (gallery/2-june2022.pdf)distance matrix. (gallery/2-june2022.pdf)**
Renjini Raveendran P, Beena S - SAINTS' COLLEGE, UNIVERSITY OF KERALA, THIRUVANANTHAPURAM., NSS COLLEGE NILAMEL.
Page No : 5-14
DOI:22.18001.STD.2022.V11I06.22.35601 (gallery/2-june2022.pdf)

3. **IoT based massage delievering and Remainder Announcement System (gallery/3-june2022.pdf)**
Megha M Chavan, Sejal R Deshinge, Payal A Hajare, Arpita A Landage, Pratiksha G Lokam, Ms.J.B.Chougule - Sharad institute of technology polytechnic yadrav, Kolhapur, Maharashtra, India.
Page No : 15-20
DOI:22.18001.STD.2022.V11I06.22.35602 (gallery/3-june2022.pdf)

4. **Effect of sewage farming water on ground water (gallery/4-june2022.pdf)**
Mahesh S. Yadav, Jaydeep S. Buchade, Suraj M. Patil, Vishwajeet, S. Shelke, Suyash S. Firange, Aditya C. Mane - Rajarambapu institute of Technology, Rajaramnagar, India.
Page No : 21-24
DOI:22.18001.STD.2022.V11I06.22.35603 (gallery/4-june2022.pdf)

5. **Determinates of Human Developmentregional inequalities in Karnataka (gallery/5-june2022.pdf)**
Niranjan.R and Rajappa.S - Vijayanagara Sri Krishnadevaraya University., VSK University, Ballari.
Page No : 26-49
DOI:22.18001.STD.2022.V11I06.22.35604 (gallery/5-june2022.pdf)

6. **IoT based School Bus Tracking System (gallery/6-june2022.pdf)**
Hujefa A. Dadhiwale, Omkar B. Kamble, Bhuddhagosh M. Kurne, Manish R. Sutar, Miss . M . G . Soundatte - Sharad Institute Of Technology Polytechnic, Yadrav (Ichalkaranji), Maharashtra, India.
Page No : 50-53
DOI:22.18001.STD.2022.V11I06.22.35605 (gallery/6-june2022.pdf)

DOI:22.18001.STD.2022.V11I06.22.35631 (gallery/33-june2022.pdf)

34. **A BRIEF STUDY OF SPECTRAL RESOLUTION OF E3, E BEING A (5,3)- JECTION (gallery/34-june2022.pdf)**
Naveen Kumar Baitha, Dr. L.B. Singh - J.P .University, Chapra, Bihar., J.P. University, Chapra.
Page No : 344-351
DOI:22.18001.STD.2022.V11I06.22.35632 (gallery/34-june2022.pdf)

35. **COMPACT UWB -MIMO TRIPLE NOTCHED ANTENNA FOR ISOLATION REDUCTION. (gallery/35-june2022.pdf)**
Mr. G. Vijaya Kumar, Sk.Razak, G Charan, V.Raja - ALIET, JNTUK, Vijayawada, Andhra Pradesh, India.
Page No : 352-369
DOI:22.18001.STD.2022.V11I06.22.35633 (gallery/35-june2022.pdf)

36. **DESIGN OF RADIX-8 BOOTH MULTIPLIER USING PARALLEL PREFIX ADDERS (gallery/36-june2022.pdf)**
Mr.G.Ravi, Ch.Darsini Ram, V.Divya, E.Teja Sri - ALIET, JNTUK,Vijayawada, Andhra Pradesh , India.
Page No : 370-375
DOI:22.18001.STD.2022.V11I06.22.35634 (gallery/36-june2022.pdf)

37. **Development of 16 Element linear array transducer Using Field-II (gallery/37-june2022.pdf)**
Rodge S.A., R. D. Chaudhari - Adarsha Science J.B.Arts and Birla Commerce Mahavidyalaya, Dhamangaon Rly-444709 Maharashtra (India)., RLT Science College Akola Maharashtra (India).
Page No : 376-382
DOI:22.18001.STD.2022.V11I06.22.35635 (gallery/37-june2022.pdf)

38. **AN IMPROVEDDROOP CONTROL STRATEGY FOR REACTIVE POWER SHARING IN ISLANDED MICRO GRID (gallery/38-june2022.pdf)**
Allam Ruchitha, Dr. K. Sree latha, Dr. P.V.Kishore - St. Peters Engineering College, Hyderabad.
Page No : 383-392
DOI:22.18001.STD.2022.V11I06.22.35636 (gallery/38-june2022.pdf)

39. **Design of Smart Safety System for Women Using IOT (gallery/39-june2022asdf.pdf)**
Mr. Abdul Azeem, Saravakota Sravan Kumar, Gayam Nagendra, Kunchala Tirumala sai - JNTUK, Vijayawada, Andhra Pradesh, India.
Page No : 393-398
DOI:22.18001.STD.2022.V11I06.22.35637 (gallery/39-june2022asdf.pdf)

40. **EMERGENCY PATIENT MONITORING SYSTEM (gallery/40-june2022asdf.pdf)**
K. Appala Raju, K. Sunil, M. Geethabhiram, P. Sai Pavan - Andhra Loyola Institute of Engineering and Technology, Vijayawada, india.
Page No : 399-402
DOI:22.18001.STD.2022.V11I06.22.35638 (gallery/40-june2022asdf.pdf)

41. **Detection of Diabetic Retinopathy Using Convolution Neural Networks (gallery/41-june2022asdf.pdf)**
Appala Raju K, Ravali S, Swathi K, Navya M - Andhra Loyola Institute of Engineering and Technology, Vijayawada (AP), India.
Page No : 403-407
DOI:22.18001.STD.2022.V11I06.22.35639 (gallery/41-june2022asdf.pdf)

42. **A study on weight status Pre and Post Covid -19 among school going children Lucknow City (gallery/42-june2022.pdf)**
Km. Shikha and Neetu Singh - Babasaheb Bhimrao Ambedkar University, Lucknow, (A CENTRAL UNIVERSITY) Vidya vihar, Raebareli Road, Lucknow.
Page No : 408-417
DOI:22.18001.STD.2022.V11I06.22.35640 (gallery/42-june2022.pdf)

43. **SOCIO-ECONOMIC CONDITIONS OF ZARDOZI WORKERS OF RAMNAGAR BLOCK, BARBANKI DISTRICT (gallery/43-june2022.pdf)**
OF UTTAR PRADESH (gallery/43-june2022.pdf)
Sana Aisha, Prof. Rachna Mujoo - UNIVERSITY OF LUCKNOW.
Page No : 418-434

ISSN : 0950-070

Development of 16 Element linear array transducer Using Field-II

Rodge S.A.
Associate Professor, Dept. of Electronics
Adarsha Science J.B.Arts and Birla Commerce Mahavidyalaya,
Dhamangaon Rly-444709 Maharashtra (India)

R. D. Chaudhari
RLT Science College AkolaMaharashtra (India)

Abstract:Piezoelectric transducers are significant elements of many broadband ultrasonic systems, either pulse-echo or through-transmission, used for imaging and detection purposes. In ultrasonic broadband applications such as medical imaging, or non-destructive testing, piezoelectric transducers should generate/receive ultrasonic signals with good efficiency over a large frequency range. This implies the use of piezoelectric transducers with high sensitivity, broad bandwidth and short-duration impulse responses. High sensitivity provides large signal amplitudes which determine a good dynamic range for the system and the short duration of the received ultra-sonic signal provides a good axial resolution. This paper presents the simulation of linear array transducers for ultrasonic measurements.

Keywords--Ultrasonic, Linear array Transducer, medical imaging, Field-II GUI, TX/RX Fields, detected image, TX/RX Axial slice, TX/RX Axial slice.

I. INTRODUCTION

For the period of the second half of 20th current century the medical imaging is grown through Ultrasound tool speedily. The part of novel technology is the use of computers to decide problems by simulating theoretical models (Numerical simulations) that has taken place alongside pure theory and experiment during the last few decades. These numerical simulations permit one to resolve problems that may not be accessible to direct experimental study or too complex for theoretical analysis. Computer simulations can link the gap between analysis and experiment [1].

These numerical simulations have emerged as a new branch in science and technology complementing both experiments and theory. A simulation can sometimes replace physical experiments, even though most often a simulation and an experiment are complementary. The

ISSN : 0950-070

results of scientific experiments are often explained by simulations and simulations are often calibrated by experiments. The experiments provide input for the simulations, which are viewed as experimenting with theoretical models. The feedback of numerical results into theoretical modeling and continues interaction with laboratory experiments and analytical theory makes computing a vital tool for science. Consequently the increased in computing power in both speed and storage has given computational electronics its significance. Improved computer capacity and the solution algorithms themselves, have a big outcome on the excellence of solution obtained. A numerical model can be used to understand measurements and observations enlarge existing analytical models into new parameter regimes and quantitatively test existing theories that can be done by comparing model predictions to experimental information.

The mutual weak point of both experiment and theory is cover up by the numerical simulations examination and experiment. A third dimension in ultrasonic measurements, of equivalent status and significance to experiment and analysis is nothing but the simulation determination **[1].** It has taken an everlasting place in every one aspect of ultrasonic measurements from basic research to engineering design.

A novel and potentially powerful tool is the computer experiment. One can resolve novel and uncertain aspects of usual process, by combining predictable theory, experiment and computer simulation **[1].** Such aspects could frequently neither have been understood nor reveled by analysis or experiments alone.

More than the last half century much development has been made in medical device technology. One particular medical technology that has enhanced speedily over the last 30 years is ultrasound. This advancement in technology however has brought with it the rapid obsolescence of system design. The accomplishment of modern electronics is built on the possibility to precisely predict system performance by the use of simulation tools. This model can be extended to components such as piezoelectric transducers attached to the electronics [2]. The ability to simulate both piezoelectric transducer and electronics together renders possible efficient optimizations at system level, i.e. minimizing size, price and power consumption [3].

The systems for images processing in the medical field are very important calling for new techniques, much more superior and performing than they used to be, in order to provide a

ISSN : 0950-0707

acceptable analysis and diagnosis. Amongst the medical techniques using computer sciences, it can be mentioned: scintigraphy, echography, tomography, radiography, quantitative microscopy, nuclear magnetic resonance. Ultrasound, widely used in many areas of medicine, provides a secure and efficient means for diagnosis and therapy. When the medium becomes complex solving the wave propagation formula becomes virtually not possible. Modeling becomes much more complex inside the body because the ultrasound propagation speed is different for each tissue and it is known that tissues are not a homogeneous medium for ultrasound wave propagation [4]. Therefore, it is important to know how the ultrasound wave is generated and the ultrasound wave beam shaped.

II. Spatial Impulse Theory

The pressure field generated by the aperture is found by the Rayleigh integral [5]

$$p(\vec{r}_1,t)=\frac{\rho_0}{2\pi}\int_s \frac{\partial v_n(r_2.t-\frac{|\vec{r}_1-\vec{r}_2|}{c})}{|\vec{r}_1-\vec{r}_2|}ds \qquad (1)$$

Where the field point is denoted by $\vec{r}_1$ and the aperture by $\vec{r}_2$, is the velocity normal to the transducer surface. Using the velocity potential, and assume that the surface velocity is uniform over the aperture making it independent of $\vec{r}_2$, then: where the field point is denoted by $\vec{r}_1$ and the aperture by $\vec{r}_2$, is the velocity normal to the transducer surface. Using the velocity potential, and assume that the surface velocity is uniform over the aperture making it independent of $\vec{r}_2$, then:

$$\Psi(\vec{r}_1,t)=v_n(t)*\int_s \frac{\partial(t-\frac{|\vec{r}_1-\vec{r}_2|}{c})}{2\pi|\vec{r}_1-\vec{r}_2|} \qquad (2)$$

Where * denotes convolution in time. The integral in this equation

$$h(\vec{r}_1,t)=\int_s \frac{\partial(t-\frac{|\vec{r}_1-\vec{r}_2|}{c})}{2\pi|\vec{r}_1-\vec{r}_2|}$$ (3)Represent the spatial impulse response. The continuous wave field can be found from the Fourier transform of

ISSN : 0950-0707

$$p(\vec{r}_1, t) = \rho_0 \frac{\partial v(t)}{\partial t} * h(\vec{r}_1, t) \quad (4)$$

The impulse response includes the excitation convolved with both the transducers electro-mechanical impulse response in transmit and receive. The final signal for a collection of scatters is calculated as a linear sum over all signals from the different scatters [6-7].

III.SIMULATION OF LINEAR ARRAY TRANSDUCER

The linear array is the fundamental type of multi-element transducer and it scans the region of interest by exciting the elements situated over the region. The field is focused on the region by introducing time delay in the excitation of the concerned individual elements, so initially concave beam is emitted. Here a Fig.1 shows general design format of 16 element linear array transducer having height, width and kerf of individual element are taken as 5 mm, 0.2 mm and 0.02 mm respectively. The transducers are situated at the center of the coordinate system. To achieve focal length of 30 mm from the center of transducer the electronic focusing is included.

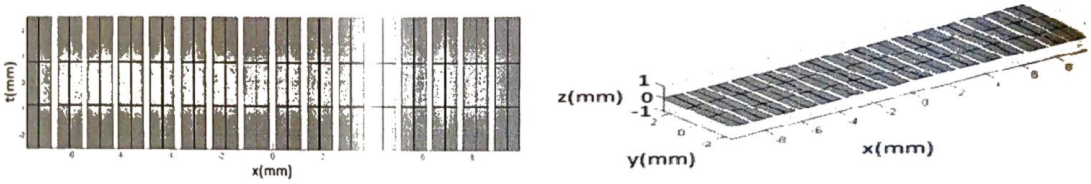

Fig. (1) Design format of linear array transducer (Height=5mm, Width=0.25mm, Kerf=0.02mm)

In this paper a linear array transducer of 16 elements is simulated using FIELD-II program with center frequencies 5MHz. For this specified linear array transducer, acoustic field generated is propagated through human body tissues and is observed at a focal distance i.e. (0, 0, 30)

IV. RESULT AND DISCUSSION

The calculation of the impulse response is facilitated by projecting the field point onto the plane of the aperture. In this way, the problem became two-dimensional and the field point is given as a (x, y) coordinate set and a height z above the plane. The spatial impulse response is, thus, determined by the relative length of the part of the arc that intersects the aperture [8]. Thereby it is the crossing of the projected ultrasonic waves with the edges of the aperture that determines the spatial impulse responses as a function of time. In this paper by using FIELD-II

ISSN : 0950-0707

program created a 16 element linear array transducer with center frequency fo = 5*MHz*. The speed of sound in tissue is c=*f*0 = 1540*m/s*, The sampling frequency used was *fs* = 100*MHz*. The elements had a width and height of 0.25mm and 5mm respectively. The focal-point was set to 30mm.

Table: 1 shows the parameters for 16 element array transducer, excitation pulse and medium used for this centre frequency (f_0) used is 5MHz. Figs. (a-m) shows; Element impulse response for 16 element array, TX Field image for 16 element array, TX Axial waveform for 16 element array, TX Lateral beam plot for 16 element array, TX/RX Field image for 16 element array, TX/RX Axial waveform for 16 element array, TX/RX Lateral beam plot for 16 element array, K- space TX/RX field image for 16 element array, K-space axial slice for 16 element array, K-space lateral slice for 16 element array, Detected image for 16 element array, Detected image axial slice for 16 element array and Detected image lateral slice for 16 element array.

image axial slice for 16 element array and Detected image lateral slice for 16 element array.

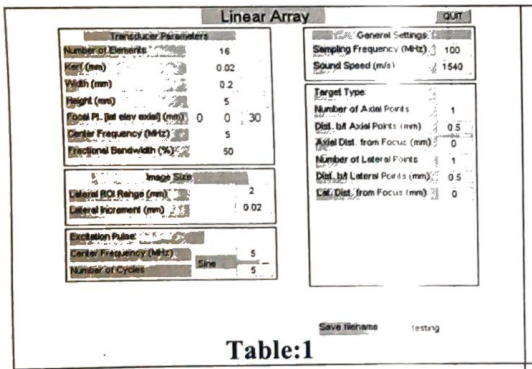

Table:1

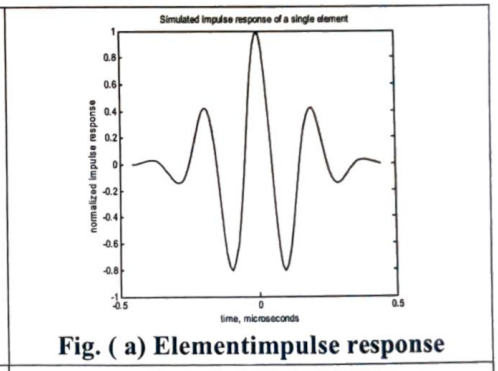

Fig. (a) Elementimpulse response

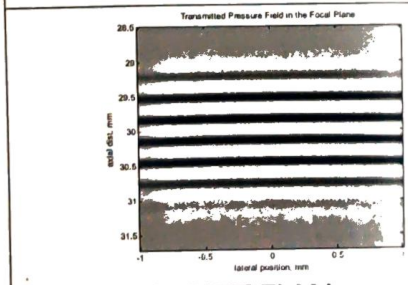

Fig.(b)TX Field image

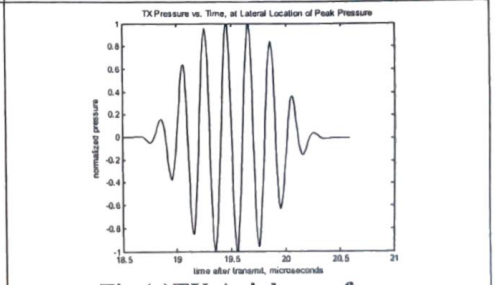

Fig.(c)TX Axial waveform

ISSN : 0950-0707

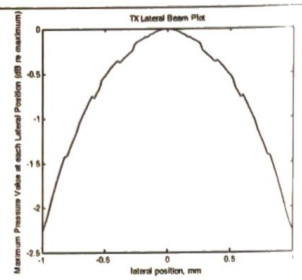

Fig.(d) TX Lateral beam-plot

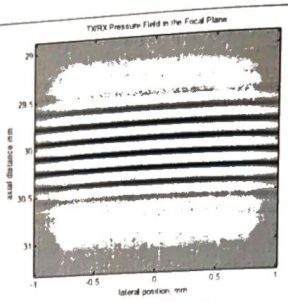

Fig.(e)TX/RX Field image

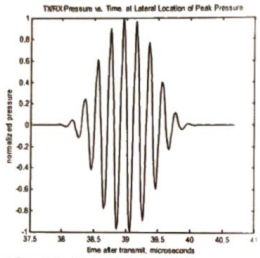

Fig.(f)TX/RX Axial waveform

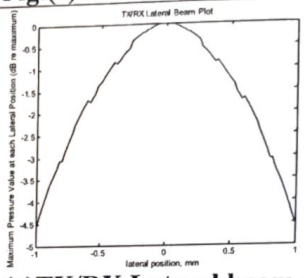

Fig.(g)TX/RX Lateral beam-plot

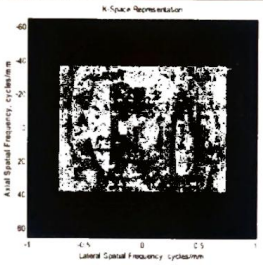

Fig.(h)K space TX/RX field image

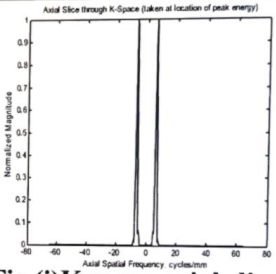

Fig.(i)K space axial slice

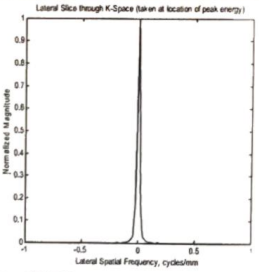

Fig.(j)K space lateral slice

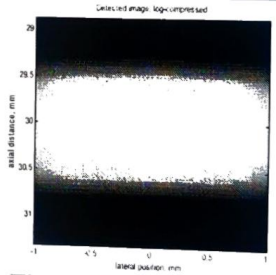

Fig.(k)Detected image

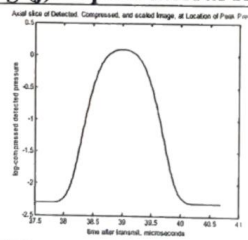

Fig.(l)Detected image axial slice

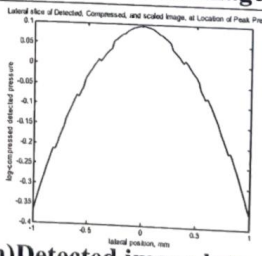

Fig. (m)Detected image lateral slice

V. CONCLUSION

The paper attempts to present a coherent analysis of the focusing strategies for 2-D array transducer design and properties, based on linear acoustics. The delays on the individual transducer elements and their relative weight or apodization are changed continuously as a function of depth. This yields near perfect focused images for all depths. Similarly if number arrays in the transducer are increased then contrast of displayed image, has increased thus, benefitting the diagnostic importance of ultrasonic imaging.

References:

[1] Gandole, Y. B. (2012). Computer Modeling and Simulation of Ultrasonic System for Material Characterization. http://www.oalib.com/search? kw=Y.%20B.%20Gandole &searchField=authors.

[2] R. Krimholtz, D. Leedom, and G. Matthaci, "New equivalent circuits for elementary piezoelectric transducers," Electron. Lett. **6**, 398–399 ,1970

[3] T. R. Meeker, "Thickness mode piezoelectric transducers," Ultrasonics **10**, 26–36 ,1972.

[4] P. Marchal, F. Levarssort, L.-P. Tran-Huu-Hue, and M. Lethiecq, "Effects of acoustical properties of a lens on the pulse-echo response of a single element transducer," IEEE International Ultrasonics, Ferroelectrics, and Frequency Control Joint 50th Anniversary Conference, pp. 1651–1654,2004.

[5] Jensen, J.A, A New Approach to Calculating Spatial Impulse Responses, IEEE International Ultrasonic Symposium, Toronto, Canada, 1997

[6] P. Marchal, F. Levarssort, L.-P. Tran-Huu-Hue, and M. Lethiecq, "Effects of acoustical properties of a lens on the pulse-echo response of a single element transducer," IEEE International Ultrasonics, Ferroelectrics, and Frequency Control Joint 50th Anniversary Conference, pp. 1651–1654,2004.

[7] JENSEN, J.A., Field: A program for simulating ultrasound systems, 10th Nordic-Baltic Conference on Biomedical Imaging, in: *Medical & Biological Engineering & Computing*, 1996, **34**, Supplement 1, 351–353.

[8] Jensen, J.A., N.B. Svendsen, Simulation of advanced ultrasound systems using field II, Biomedical Imaging: Nano to Macro, 2004. IEEE International Symposiumon, 15-18 April 2004 Page(s):636–639 Vol.-1.

ER Publications

ISSN: 2320-8708, New Delhi, India
International Journal of Enhanced Research in Educational Development
UGC Certified International Peer-Reviewed & Refereed Journal
UGC Journal no. 2799

Certificate of Publication

Rodge S. A.

Associate Professor, Dept. of Electronics, Adarsha Science J.B.Arts and Birla Commerce Mahavidyalaya, Dhamangaon Rly-444709 India

TITLE OF PAPER

Linear Array Transducer with Center Frequency 7.5 MHz

has been published in

IJERED, Volume 10, Issue 3, May-June. 2022, Impact Factor 7.326

Paper Id: RED-065202205
Date: 07-06-2022

ER PUBLICATIONS AUTH. SIGNATORY INDIA

Website: www.erpublications.com
Email: erpublications@gmail.com

Authorized Signatory

International Journal of Enhanced Research in Educational Development (IJERED)
ISSN: 2320-8708, Vol. 10 Issue 3, May-June, 2022, Impact Factor: 7.326

Linear Array Transducer with Center Frequency 7.5 MHz

Rodge S. A.

Associate Professor, Dept. of Electronics, Adarsha Science J.B.Arts and Birla Commerce Mahavidyalaya, Dhamangaon Rly-444709 India)

ABSTRACT

Over the past decades, ultrasound imaging technology has satisfied outstanding improvement in obtaining significant diagnostic information from patients in a fast, noninvasive approach. Piezoelectric transducers are important elements of various broadband ultrasonic systems, either pulse-echo or through-transmission, used for imaging and detection purposes[1]. In ultrasonic broadband applications such as medical imaging, or non-destructive testing, piezoelectric transducers should generate/receive ultrasonic signals with good efficiency over a large frequency range. This implies the use of piezoelectric transducers with high sensitivity, broad bandwidth and short-duration impulse responses.High sensitivity provides large signal amplitudes which determine a good dynamic range for the system and the short duration of the received ultra-sonic signal provides a good axial resolution. This paper presents the simulation of 8-element linear array transducers with center frequency 10 MHZ, using Field-II GUI program for ultrasonic measurements.

Keywords-Detected image, Field-II GUI, Linear array Transducer, medical imaging, TX/RX Fields, TX/RX Axial slice, TX/RX lateral slice, Ultrasonic.

INTRODUCTION

For the period of the second half of 20th current century the medical imaging is grown through Ultrasound tool speedily. The part of novel technology is the use of computers to decide problems by simulating theoretical models (Numerical simulations) that has taken place alongside pure theory and experiment during the last few decades. These numerical simulations permit one to resolve problems that may not be accessible to direct experimental study or too complex for theoretical analysis. Computer simulations can link the gap between analysis and experiment [2].

More than the last half century much development has been made in medical device technology. One particular medical technology that has enhanced speedily over the last 30 years is ultrasound. This advancement in technology however has brought with it the rapid obsolescence of system design. The accomplishment of modern electronics is built on the possibility to precisely predict system performance by the use of simulation tools. This model can be extended to components such as piezoelectric transducers attached to the electronics [3]. The ability to simulate both piezoelectric transducer and electronics together renders possible efficient optimizations at system level, i.e. minimizing size, price and power consumption [4].

SPATIAL IMPULSE THEORY

The pressure field generated by the aperture is found by the Rayleigh integral [5]

$$p(\vec{r}_1, t) = \frac{\rho_0}{2\pi} \int_s \frac{\partial v_n\left(\vec{r}_2, t - \frac{|\vec{r}_1 - \vec{r}_2|}{c}\right)}{|\vec{r}_1 - \vec{r}_2|} ds \qquad (1)$$

Where the field point is denoted by $\vec{r_1}$ and the aperture by $\vec{r_2}$, is the velocity normal to the transducer surface. Using the velocity potential, and assume that the surface velocity is uniform over the aperture making it independent of $\vec{r_2}$, then: where the field point is denoted by $\vec{r_1}$ and the aperture by $\vec{r_2}$, is the velocity normal to the transducer surface. Using the velocity potential, and assume that the surface velocity is uniform over the aperture making it independent of $\vec{r_2}$, then:

$$\Psi(\vec{r_1},t)=v_n(t)*\int_s \frac{\partial(t-\frac{|\vec{r_1}-\vec{r_2}|}{c})}{2\pi|\vec{r_1}-\vec{r_2}|} \qquad (2)$$

Where * denotes convolution in time. The integral in this equation

$$h(\vec{r_1},t)=\int_s \frac{\partial(t-\frac{|\vec{r_1}-\vec{r_2}|}{c})}{2\pi|\vec{r_1}-\vec{r_2}|} \qquad (3)$$

Represent the spatial impulse response. The continuous wave field can be found from the Fourier transform of

$$p(\vec{r_1},t)=\rho_0\frac{\partial v(t)}{\partial t}*h(\vec{r_1},t) \qquad (4)$$

The impulse response includes the excitation convolved with both the transducers electro-mechanical impulse response in transmit and receive. The final signal for a collection of scatters is calculated as a linear sum over all signals from the different scatters [6-7].

SIMULATION OF LINEAR ARRAY TRANSDUCER

The linear array is the fundamental type of multi-element transducer and it scans the region of interest by exciting the elements situated over the region. The field is focused on the region by introducing time delay in the excitation of the concerned individual elements, so initially concave beam is emitted. Here a Fig.1 shows general design format of 16 element linear array transducer having height, width and kerf of individual element are taken as 5 mm, 0.2 mm and 0.02 mm respectively. The transducers are situated at the center of the coordinate system. To achieve focal length of 30 mm from the center of transducer the electronic focusing is included.

Fig. (1) Design format of linear array transducer (Height=5mm, Width=0.25mm, Kerf=0.02mm)

In this paper a linear array transducer of 8 elements is simulated using FIELD-II program with center frequencies 7.5MHz. For this specified linear array transducer, acoustic field generated is propagated through human body tissues and is observed at a focal distance i.e. (0, 0, 30)

RESULT AND DISCUSSION

The calculation of the impulse response is facilitated by projecting the field point onto the plane of the aperture. In this way, the problem became two-dimensional and the field point is given as a (x, y) coordinate set and a height z above the plane. The spatial impulse response is, thus, determined by the relative length of the part of the arc that intersects the aperture [8]. Thereby it is the crossing of the projected ultrasonic waves with the edges of the aperture that determines the spatial impulse responses as a function of time. In this paper by using FIELD-II program created a 32-element linear array transducer with center frequency fo = 10*MHz*. The speed of sound in tissue is c=*f*0 = 1540*m/s*, The sampling

frequency used was $fs = 100MHz$. The elements had a width and height of 0.25mm and 5mm respectively. The focal-point was set to 30mm.

Table: 1 shows the parameters for 8 element array transducer, excitation pulse and medium used, for this centre frequency (f_0) used is 7.5 MHz Figs. (a-m) shows; Element impulse response for 8 element array, TX Field image for 8 element array, TX Axial waveform for 8 element array, TX Lateral beam plot for 8 element array, TX/RX Field image for 8 element array, TX/RX Axial waveform for 8 element array, TX/RX Lateral beam plot for 8 element array, K-space TX/RX field image for 8 element array, K-space axial slice for 8 element array, K-space lateral slice for 8 element array, Detected image for 8 element array, Detected image axial slice for 8 element array and Detected image lateral slice for 8 element array.

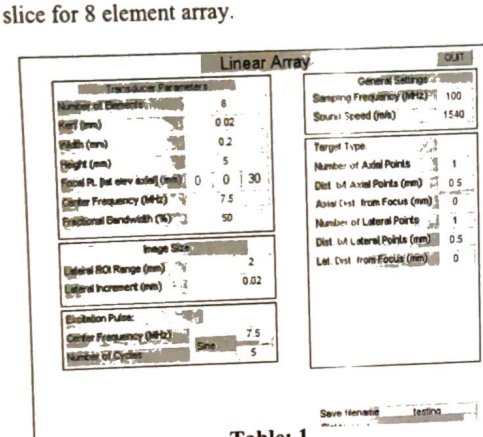

Table: 1

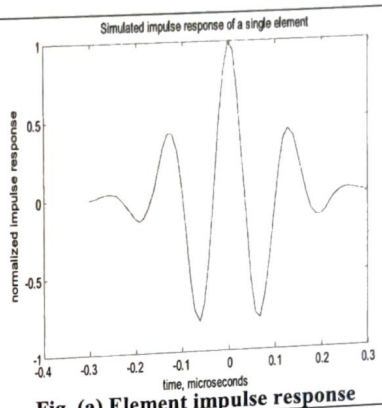

Fig. (a) Element impulse response

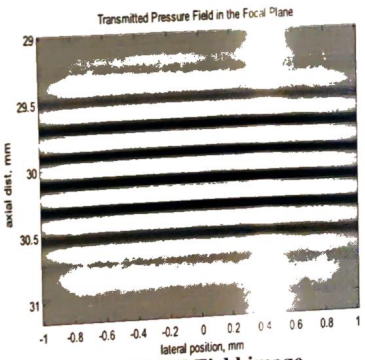

Fig. (b) TX Field image

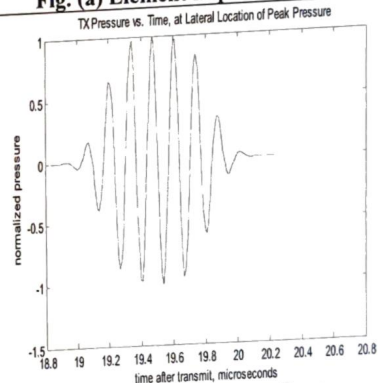

Fig. (c) TX Axial waveform

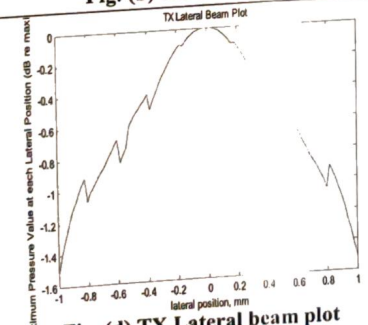

Fig. (d) TX Lateral beam plot

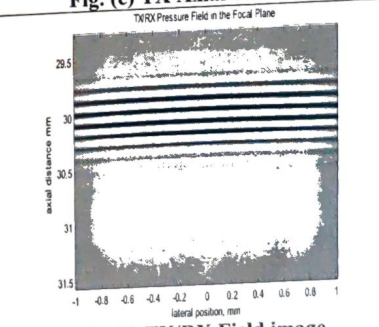

Fig. (e) TX/RX Field image

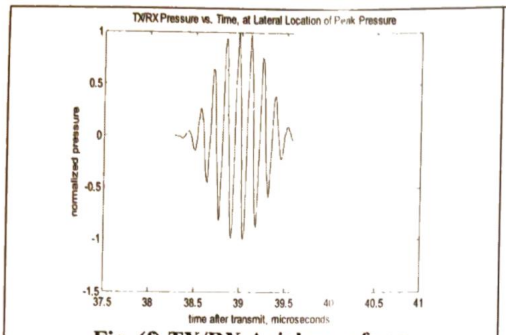

Fig. (f) TX/RX Axial waveform

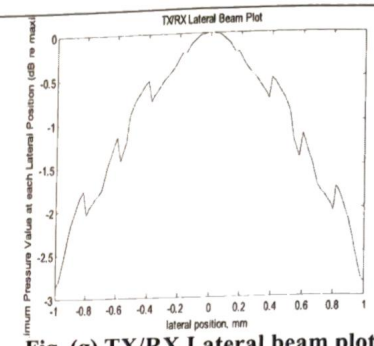

Fig. (g) TX/RX Lateral beam plot

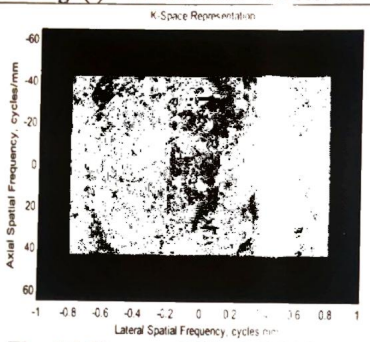

Fig. (h) K space TX/RX field image

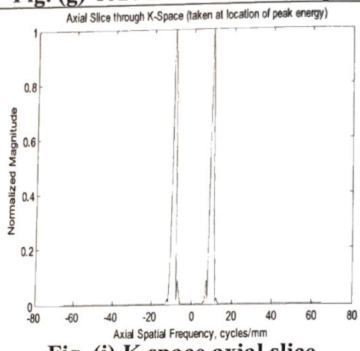

Fig. (i) K space axial slice

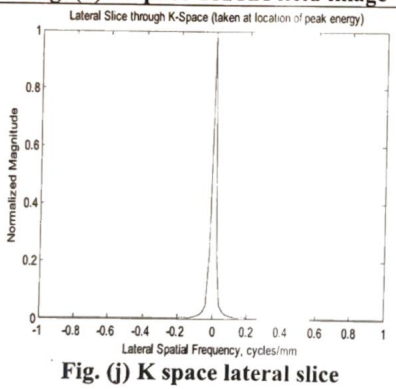

Fig. (j) K space lateral slice

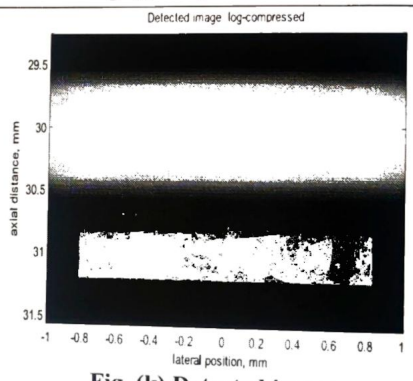

Fig. (k) Detected image

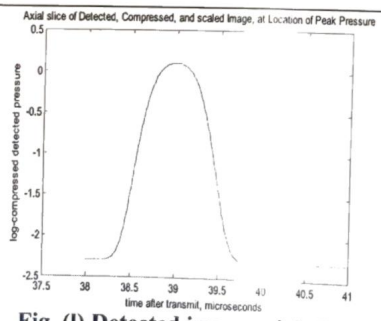

Fig. (l) Detected image axial slice

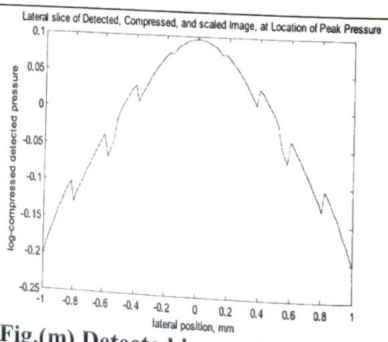

Fig.(m) Detected image lateral slice

CONCLUSION

The paper attempts to present a coherent analysis of the focusing strategies for 2-D array transducer design and properties, based on linear acoustics. The delays on the individual transducer elements and their relative weight or apodization are changed continuously as a function of depth. This yields near perfect focused images for all depths and

has increased the contrast in the displayed image, thus, benefitting the diagnostic importance of ultrasonic imaging.If the center frequency and number of elements in transducer is increased then contrast in the detected image is increased, this also increases the diagnostic status of ultrasonic imaging

REFERENCES

[1]. Gandole, Y. B. (2012). Computer Modeling and Simulation of Ultrasonic System for Material Characterization. http://www.oalib.com/search? kw=Y.%20B.%20Gandole &searchField=authors.

[2]. R. Krimholtz, D. Leedom, and G. Matthaci, "New equivalent circuits for elementary piezoelectric transducers," Electron. Lett. 6, 398–399 ,1970

[3]. T. R. Meeker, "Thickness mode piezoelectric transducers," Ultrasonics 10, 26–36 ,1972.

[4]. P. Marchal, F. Levarssort, L.-P. Tran-Huu-Hue, and M. Lethiecq, "Effects of acoustical properties of a lens on the pulse-echo response of a single element transducer," IEEE International Ultrasonics, Ferroelectrics, and Frequency Control Joint 50th Anniversary Conference, pp. 1651–1654,2004.

[5]. Jensen, J.A, A New Approach to Calculating Spatial Impulse Responses, IEEE International Ultrasonic Symposium, Toronto, Canada, 1997

[6]. P. Marchal, F. Levarssort, L.-P. Tran-Huu-Hue, and M. Lethiecq, "Effects of acoustical properties of a lens on the pulse-echo response of a single element transducer," IEEE International Ultrasonics, Ferroelectrics, and Frequency Control Joint 50th Anniversary Conference, pp. 1651–1654,2004.

[7]. JENSEN, J.A., Field: A program for simulating ultrasound systems, 10th Nordic-Baltic Conference on Biomedical Imaging, in: Medical & Biological Engineering & Computing, 1996, 34, Supplement 1, 351–353.

[8]. JENSEN, J.A., Users' guide for the Field II program, Technical University of Denmark, DK- 2800 Lyngby, Denmark http://www.es.oersted.dtu.dk/staff/jaj/field/, 2001.

DOI:10.37897.GRJ.2021.V7I11.21.49882

GRADIVA REVIEW JOURNAL

A Monthly Publishing Journal

11.Analysis And Design Of Tapered Web Pre-engineered Building(Peb) Structure For Seismic Zone (gallery/grj%203434.pdf)
P. S. Mane, Dr. S. G. Ban
G H Raisoni College of Engineering and Management, Pune
PAGE NO: 77-86
DOI:10.37897.GRJ.2021.V7I11.21.49883

12.Probing new physics in rare decays of b-flavored Hadrons b ! sγ in CMSSM (gallery/grj%203435.pdf)
Gayatri Ghosh
Gauhati University, Jalukbari, Assam
PAGE NO: 87-99
DOI:10.37897.GRJ.2021.V7I11.21.49884

13.Association Of Orthostasia Nervosa with Mental Health Disorders: A Review (gallery/grj%203435.pdf)
Stuti Sharma,Pratibha Singh,Kommi Kalpana,Muskaan Jain,Muskaan Garg
Manav Rachna International Institute of Research and Studies
PAGE NO: 100-116
DOI:10.37897.GRJ.2021.V7I11.21.49885

14.Partial Replacement of Cement by Ground Granulated Blast Slag (GGBS) and Addition of Activated Charcoal Powder (gallery/grj%203437.pdf)
S. P.Khedekar, Shubham bonde , Prathamesh Bacchav , Ajay ingle , Sachin kanoje
All India Shri Shivaji Memorial Society, College Of Engineering, Pune
PAGE NO: 117-124
DOI:10.37897.GRJ.2021.V7I11.21.49886

15.Solar Grass Cutting Machine With Sun Tracking Device (gallery/grj%203438.pdf)
Dr. Udai Chandra Jha,Ayush Gairola,Kulbhushan Dwivedi,AnkurVerma,VikramRanjan Pachauri
Lovely Professional University,Punjab,India
PAGE NO: 125-129
DOI:10.37897.GRJ.2021.V7I11.21.49887

16.Nurturing Entrepreneurial approach among young minds in Higher Technical Educational Institutions (gallery/grj%203440.pdf)
Dr. P. Prabhakar Reddy,Dr. P.V.R. Ravindra Reddy,V. Sandhya, N Jyothirmayi,V. Jaipal Reddy
Chaitanya Bharathi Institute of Technology, Gandipet, Hyderabad, India
PAGE NO: 130-134
DOI:10.37897.GRJ.2021.V7I11.21.49888

17.Online Book Store using Content Based Recommendation System (gallery/grj%203442.pdf)
Alifya Motagamwala,Narendar Gawai
UMIT, SNDT University Mumbai, India
PAGE NO: 135-138
DOI:10.37897.GRJ.2021.V7I11.21.49889

18.Extraction and Purification of essential oil rich in carnosic Acid from Rosemarinus officinalis leaves using one-factor-at-a-time method (gallery/grj%203429.pdf)
S. Kavitha
Adhiyamaan College of Engineering, Hosur, Tamil Nadu, India
C. Logeshwaran,Philip Robinson,B. Mythili Gnanamangai
K. S. Rangasamy College of Technology, Tiruchengode, Tamil Nadu, India
PAGE NO: 139-145
DOI:10.37897.GRJ.2021.V7I11.21.49890

19.Recommendation system using location sensing (LBSN) and sentiment analysis (gallery/grj%203439.pdf)
Kushal Bhoja Suvarna,Dr.Sachin Bojewar
Vidyalankar Institute of Technology, Wadala(E), Maharashtra
PAGE NO: 146-153
DOI:10.37897.GRJ.2021.V7I11.21.49891

20.Design of Hybrid Model of Ultrasonic Transducer (gallery/grj%203449.pdf)
S. A. Rodge
Adarsha Science J.B.Arts and Birla Commerce Mahavidyalaya, Dhamangaon Rly
PAGE NO: 154-158
DOI:10.37897.GRJ.2021.V7I11.21.49892

21.Design, Development, and Testing of Axial Magnetic Coupling for Pump (gallery/grj%203413.pdf)
Maruti M. Khot,Pavan G. Jadhav,Sana M. Bagwan
Walchand college of engineering, Sangli
PAGE NO: 159-165
DOI:10.37897.GRJ.2021.V7I11.21.49893

Home () Call For Papers (Call-for-Papers/)
(Authors/)
Programme Schedule (VOLUME-8-ISSUE-6-11-2022/)
Special Issue (special-issue/)
Editorial Board (Editorial-Board/)
Contact (Contact/)

PAPER FORMAT (HTTPS://DRIVE.GOOGLE.COM/USP=SHARING)
COPYRIGHT FORM (HTTPS://DRIVE.GOOGLE.COM/USP=SHARING)
REGISTRATION FORM (HTTPS://DRIVE.GOOGLE.COM/83AZCKZG87S/VIEW?USP=SHARING)

GRADIVA REVIEW JOURNAL

An UGC-CARE Approved Group-II Journal

ISSN NO : 0363-8057 / Website : http://gradivareview.com/
Email : Submitgrjournal@gmail.Com

Paper ID : GRJ/3449

Certificate of Publication

This is to certify that the paper titled

Design of Hybrid Model of Ultrasonic Transducer

Authored by

S. A. Rodge

From

Adarsha Science J.B.Arts and Birla Commerce Mahavidyalaya, Dhamangaon Rly

Has been published in

GRADIVA REVIEW JOURNAL Volume 8, Issue 6, June 2022.

UGC APPROVED JOURNAL

DOI: 10.3 7/GRJ

crossref member

CROSSREF.ORG THE CITATION BACKBONE

Teresa Gallart
Editor-in-Chief
Gradiva Review Journal

6.1 IMPACT FACTOR

ISSN NO : 0363-8057

Design of Hybrid Model of Ultrasonic Transducer

S. A. Rodge

Department of Electronics
Adarsha Science J.B.Arts and Birla Commerce Mahavidyalaya, Dhamangaon Rly-444709

ABSTRACT: *Newly, ultrasound becomes projecting in several applications especially in medical field to improve the health services either for diagnostic. The advent of ultrasound applications raises the need of reliable transducer to comply with that purpose. As polymer material being popular in medical ultrasound, there are chances to combine it with former piezoelectric ceramic material in designing diagnostic transducer to get hybrid characteristics required for multi-frequency application. In this work, SPICE model of ceramic-polymer piezoelectric has been described. With signal conditioner circuit, complete analog system for ultrasound has also been developed. Initially transducer test for ceramic and polymer model were generated. By filtering and amplifying frequency range from 1 MHz until 10 MHz, the system bargains wideband medical ultrasonic acceptance. It gives smooth result of ultrasound signal for medical purposes.*

KEY WORDS: *Piezoelectric transducer, SPICE model, Hybrid transducer model*

Introduction

Ultrasonic sensing techniques have become mature and are extensively used in the numerous fields of engineering and basic science. Actually, many types of conventional ultrasonic instruments, devices and sophisticated software are commercialized and used for both industrial and medical applications. One of advantages of ultrasonic sensing is its outstanding capability to probe inside objectives nondestructively because ultrasound can propagate through any kinds of media including solids, liquids and gases except vacuum. In typical ultrasonic sensing the ultrasonic waves are travelling in a medium and often focused on evaluating objects so that a useful information on the interaction of ultrasonic energy with the objects are acquired as ultrasonic signals that are the waveforms variations with transit time. Such ultrasonic data provides the fundamental basis for describing the outputs of ultrasonic sensing and evaluating systems. In this work, SPICE model of ceramic-polymer piezoelectric has been described. With signal conditioner circuit, complete analog system for ultrasound has also been developed. Initially transducer test for ceramic and polymer model were generated. By filtering and amplifying frequency range from 1 MHz until 10 MHz, the system offers wideband medical ultrasonic acceptance. It gives smooth result of ultrasound signal for medical purposes.

Model of Piezoelectric transducer

The model developed for piezoelectric transducer is shown in fig.1. The block T_1 represents the transmission line. Independent sources V_1 and V_2 are zero value sources, which are used as ammeters in the circuit. F_1 and F_2 are dependent current sources. The value of F_1 is given by $F_1 = h\ C_0 \times I(V_1)$, where $I(V_1)$ is the current through V_1. The voltage across the dependent voltage source E_1 is given by $E_1 = V(4)$, where $V(4)$ is the voltage at node *4* i.e. the voltage across C_1. The dependent current source F_2 which charges C_1 is given by $F_2 = h \times I(V_2)$, where $I(V_2)$ is the current through V_2 and h is the ratio of the piezoelectric stress constant in the direction of propagation and the permittivity with constant strain . Resistor R_1 is included to prevent node 4 from being a floating node. From the mechanical side (i.e. transmission line T1), the difference between the velocity of each surface normal to the propagation path, represented by the currents u_1 and u_2 controls the current source F_1. The node labels E, B and F, respectively, denote the electrical, back, and front ports.

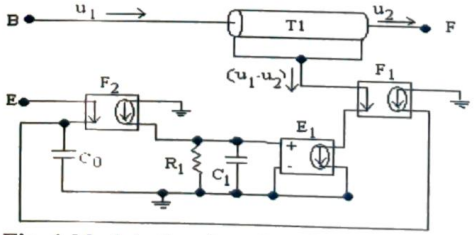

Fig. 1 Model of a piezoelectric transducer

MODEL OF PZT 5A- PVDF HYBRID TRANSDUCER

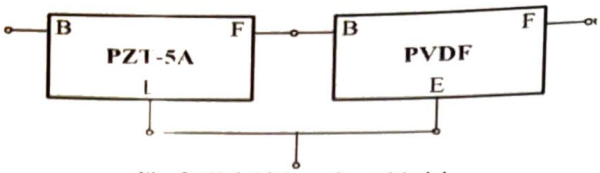

Fig. 2 : Hybrid Transducer Model

Fig. 2 shows series configuration of two material's equivalent models. Although in this model lossy characteristics (mechanical, dielectric, and electromechanical) of piezoelectric are considered, it must be taken to note that polymer material has complex additional losses than those of ceramic material.

The piezoelectric material PZT-5A and PVDF whose material data was obtained from [1], [2], [3], and [6] was chosen and given in table I

TABLE 1. PHYSICAL PROPERTIES OF TRANSDUCERS AT 25 ^{O} C

S.No	Physical properties at 25^{0}C	PZT-5A	PVDF
1	Density (ρ) (kg/m^3)	7750 [3]	1780 [2]
2	Mechanical Q (Q_m)	75 [3]	19 [6]
3	Sound velocity (c) (m/s)	4350 [3]	2200 [2]
4	Permitivity with constant strain (ε^S) (C^2/Nm^2)	7.35 ×10^{-9} [3]	55.78 x 10^{-9} [6]
5	Piezoelectric stress constant (e^{33}) (C/m^2)	15.8 [3]	0.16 [6]
6	Acoustic Impedance (MRayl)	33.7 [3]	2.7 [2]
7	Piezoelectric Constant (10^{-12} C/N)	d_{33} = 374 [1] d_{15} = 584 [1]	d31=23 [6] d32=4 [6] d33=-33 [6]
8	Coupling factor (K_{33})	0.66 [3]	0.2 [6]

Assisted with the definition of the low loss characteristic impedances equation, following relationships can be obtained

$$L = A \cdot \rho \tag{1}$$

$$C = \frac{1}{A\rho c^2} \tag{2}$$

$$R = 2\rho c A \alpha_v \tag{3}$$

$$G = \frac{2\alpha_{tc}}{\rho c A} \tag{4}$$

Mechanically, a transmission line T of length *len* (m) represents the acoustical layer. The length is selected to achieve the desired center frequency *f* (Hz) of the transducer. With fixed ends, the piezoelectric plate has a fundamental resonant frequency as

$$f = \frac{c(T)}{2 \cdot len} \tag{5}$$

Where *c(T)* is the velocity of sound through it at temperature *T*.

Using equations (1), (2) and (3) the piezoelectric material density ρ, required for transmission line, *L* and *C* values can be calculated. The mechanical factor Q_m describes the shape of the resonance peak in the frequency domain. The relation between angular frequency ω, inductance *L* and the resistance *R* is given as [5]:

$$Q_m(T) = \frac{\omega L}{R} \tag{6}$$

In the electrical section, the static capacitance C_0 (T) at temperature T is calculated as

$$C_0(T) = \frac{\varepsilon^S(T) \cdot A}{len} \tag{7}$$

where ε^S(T) (C^2/Nm^2) is the permittivity with constant strain at temperature T [3]. The latter is related to the

permittivity with constant stress (free) ε^1 as :

$$\frac{\varepsilon^T(T)}{\varepsilon^S(T)} = \frac{1}{1-k^2(T)} \quad (8)$$

Where k (T) is the piezoelectric coupling constant at temperature T.

The mechanical and electrical sections interact with two current controlled sources. From the mechanical side, the deformation itself is not measurable, but the current representing the rate of deformation is the difference between the velocity of each surface normal to the propagation path, represented by the currents u_1 and u_2, is the rate of deformation. This current (u_1 - u_2) controls the current source F_1. It has a gain equal to the product of the transmitting constant h (N/C), and the capacitance C_0. h is the ratio of the piezoelectric stress constant e^{33} (C/m^2) in the direction of propagation and the permittivity with zero or constant strain ε^S. In the thickness mode it is [3].

$$h(T) = \frac{e^{33}(T)}{\varepsilon^S(T)} \quad (9)$$

This source's output is in parallel with the capacitor C_0(T). The result is a potential difference across the capacitor that is proportional to the deformation. In the electrical section, the current through the capacitor C_0(T) controls the current source F_2. The gain for this second current source is h(T). Its output needs to be integrated to obtain the total charge on the electrodes that proportionally deforms the transducer. The integration is performed by the capacitor C_1. The voltage controlled voltage source E_1 with unity gain is a one-way isolation for the integrator.

To evaluate the model, the model parameters of PZT-5A and PVDF transducers were calculated using equations (1, 2, 3, 5, 6, 7, 9) and given in table 2.

TABLE 2 MODEL PARAMETERS OF TRANSDUCERS

S.No.	Model parameters	PZT-5A	PVDF
	Physical parameters		
1	Diameter (mm)	12.7	12.5
2	Cross sectional area (A) (m^2)	0.0001267	0.0001227
3	Center frequency (MHz)	5MHz	5MHz
	Equivalent lossy transmission line parameters (Mechanical section)		
4	C	53.8nF	945.8nF
5	R	411kΩ	361.18 kΩ
6	L	981mH	218 mH
7	G	0	0
8	len	435μm	220 μm
	Electrical section parameter		
9	Static capacitance C_0	2.14nF	31.14nF
	Controlled sources parameter		
10	Transmitting constant (h) (N/C)	2.15×10^9	2.87×10^6
11	Current source gain (F_2)	2.15×10^9	2.87×10^6
12	Dependant current source gain (F_1)	4.60	0.09
13	Voltage control voltage source gain (E_1)	1	1
14	R_1	1 KΩ	1 KΩ
15	C_1	1F	1F

SIMULATION SETUP FOR ULTRASONIC SYSTEM

The analogous simulation schematic setup is described in figure 3, with the transducer sub circuit shown in figure 1. In this schematic an ultrasonic probe with acoustic matching layer is symbolized by the two three-port blocks X1 and X2, which involve established PSPICE piezoelectric model. The measuring cell is modeled using lossy transmission line.

ISSN NO : 0363-8057

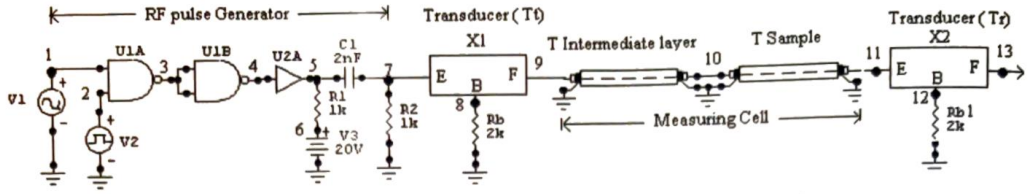

Fig.3 : Simulation setup Schematic for ultrasonic test system.

RESULT AND DISCUSSION

Transient analysis of the transducer model was done with the configuration shown in figure 4. An oscillation was observed after excitation of the piezoelectric crystal. The received signal was compared in the time domain. (Fig. 5, 6, 7)

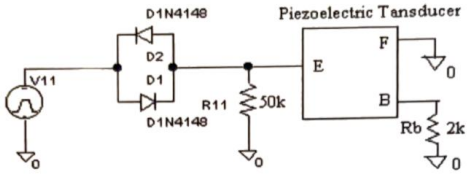

Fig. 4: Simulation setup for analysis of transient behavior of transducers.

Certain polymer characteristic losses are neglected to simplify the preliminary design at this stage. Fig. 6 shows the transient response of series configuration model.

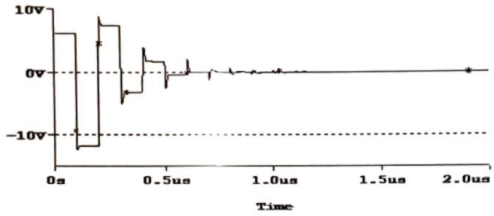

Fig 5 : Transient response of PZT-5A piezoelectric Transducer.

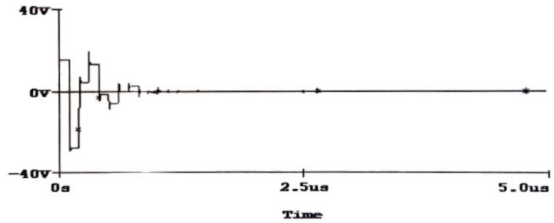

Fig 6: Transient response of PVDF Transducer

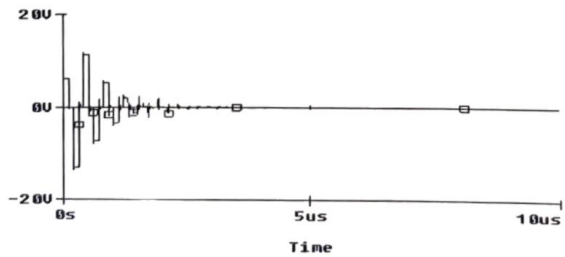

Fig. 7: Transient response of ceramic-polymer piezoelectric transducer (PZT-5A+PVDF) for multi-frequency ultrasonic system

Fig. 8 shows frequency response of transducer. AC analysis was conducted to observe frequency behavior from 1 MHz to 10 MHz. There are three peaks of power spectrums: at 2.8 MHz, 5.5 MHz, and 8 MHz. The last

ISSN NO : 0363-8057

spectrum is higher than another, but for overall dB, bandwidth from 2.5 MHz to 8.5 MHz is considered flat.

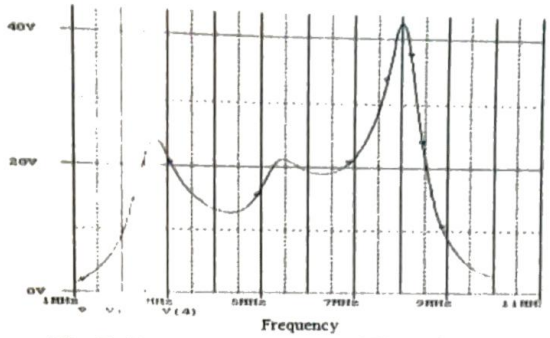

Fig. 8: Frequency response of Transducer

Electrical impedance of transducer was observed as in Fig.9. It gives turning point at about 1 MHz.

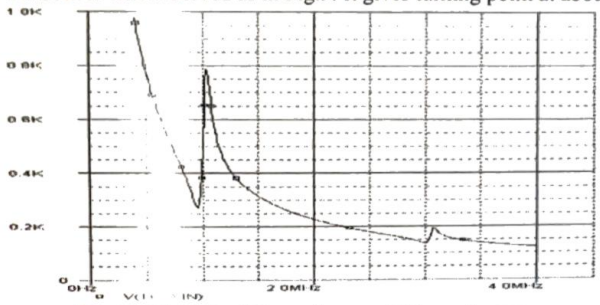

Fig. 9: Electrical Impedance of Transducer

Experimental validation for water sample is shown in fig. 10

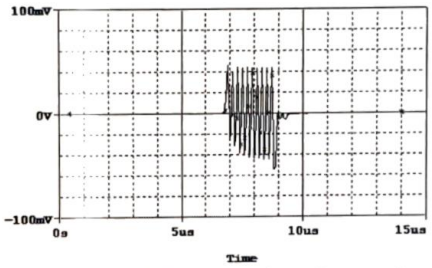

Fig. 10: Complete transient received by 5MHz ceramic-polymer piezoelectric transducer (PZT-5A+PVDF) for multi-frequency ultrasonic system at 25°C in distilled water at d= 1 cm.

CONCLUSION

A model of ceramic-polymer piezoelectric has been described. Simulation level shows that by hybridization, characteristics of both materials are providing a satisfying performance for multi-frequency transducer. Future work would be in detailed design which includes matching element, backing and loading consideration, also single or array configuration. Furthermore, the model could be improved so that it would be prepared for fabrication of hybrid multi-frequency ultrasound transducer.

REFERENCES:

[1] *Berlincourt D., Krueger H.A., and Near C. Important Properties of Morgan Electroceramics, Morgan Electroceramics, Technical Pub., 2001, TP-226.*

[2] *Brown LF. IEEE Trans Ultrason Ferroelect Freq Contr. 2000;47:1377*

[3] *Kino G.S., Acoustic Waves: Devices, Imaging, and Analog Signal Processing. Englewood cliffs, N.J: Prentice-Hall, 1988. 601.*

[4] *Mattiat O. E. ,Ultrasonic Transducer Materials, Plenum Press, London, New York, 1971. 102-105.*

[5] *Puttmer A., Hauptmann P., Lucklum R., Krause O. and Henning B., IEEE Trans. Ultrason., Ferroelect., Freq. Contr., 44, 1997, 60-66.*

[6] *Webster John G., Mechanical Variables Measurement - Solid, Fluid, and Thermal, CRC Press, 1999,Page 7-49.*

9. A Study Of Semi-symmetric Metric Connection In A Riemannian Manifold (gallery/9.grj%204044.pdf)
S C Rastogi
NOT APPLICABLE (RETIRED)
PAGE NO: [illegible]
DOI:10.37897.GRJ.2022.V8I8.22.50270

10.Estimating The Feasibility Of Converting The Food Waste Into The Feed [illegible] /10.[illegible]
PriyaDarshini. K, Reega.R ,Aarthi.N
PSGR Krishnammal college for women, Coimbatore
PAGE NO: [illegible]
DOI:10.37897.GRJ.2022.V8I8.22.50271

11.[illegible] And [illegible] uction Management (gallery/11.grj%204034.pdf)
ShijinRamesh PT
RVS Technical campus Coimbatore
PAGE NO: 126-130
DOI:10.37897.GRJ.2022.V8I8.22.50272

12.Analysis of 4 element and 16 element linear array Transducers5 MHz (gallery/12.grj%204057.pdf)
Rodge S. A
Adarsha Science J.B.Arts and Birla Commerce Mahavidyalaya Maharashtra (India)
PAGE NO: 131-138
DOI:10.37897.GRJ.2022.V8I8.22.50273

13.Effect Of Cutting Fluids On Surface Roughness On Machining Of Al12si Alloy (gallery/13.grj%203967.pdf)
Anil Waghmode,Sanjay Pawar,Sahebagouda Sanganagoudar
Fabtech Technical Campus College of Engineering and Research Sangola
PAGE NO: 139-147
DOI:10.37897.GRJ.2022.V8I8.22.50274

14.Influence of PVD Coated Tools on surface roughness of Al alloy during the wet machining process (gallery/14.grj%204038.pdf)
Dattatray Narale,Sanjay Pawar,Sahebagouda Sanganagoudar
Fabtech Technical Campus College of Engineering and Research Sangola
PAGE NO: 148-156
DOI:10.37897.GRJ.2022.V8I8.22.50275

15.Development and Validation of UV Spectrophotometric Method for Routine Estimation of Neem seed oil in Bulk and Cosmeceutical Formulation – A Quality by Design (QbD) Approach (gallery/15.grj%204064.pdf)
B.P. Manjula,V.G. Joshi,R.S. Siddam Setty,M. Geetha
Rajiv Gandhi University f Health Sciences,Bengaluru-560027, Karnataka, India
PAGE NO: 157-166
DOI:10.37897.GRJ.2022.V8I8.22.50276

16.Wireless Charging Of Elecrtic Vehicles Using Solar Energy (gallery/16.grj%204062.pdf)
Dr B.G.Sujatha,Aruna.Y.V
Cambridge Institute Of Technology, Bengaluru, India
PAGE NO: 167-172
DOI:10.37897.GRJ.2022.V8I8.22.50277

17.Visualization of Nerves, Blood Vessels and Hair Follicles in Human Skin Model (gallery/17.grj%204067.pdf)
Dr.Jayasudha K
Atria Institute of Technology, VTU, Bangalore
Dr.Mohan K.G
Gitam University, Bangalore
PAGE NO: 173-178
DOI:10.37897.GRJ.2022.V8I8.22.50278

18.An Ensemble Prediction Technique and Comparative Analysis on Cardiovascular Disease using Multiple Classifiers (gallery/18.grj%204068.pdf)
Veena Kumari H M
VTU, Belagavi
Dr. Suresh D S
Channabasaveshwara Institute of Technology, Gubbi Tumkur, India
PAGE NO: 179-188
DOI:10.37897.GRJ.2022.V8I8.22.50279

19.Closed Loop Supply Chain and Work Capital Management Efficiency: A Review to Explore the Future Directions (gallery/19.grj%204069.pdf)
Divya D,Dr. Arunkumar O.N
Symbiosis International University (Deemed University), Bangalore
PAGE NO: 189-243

Analysis of 4 element and 16 element linear array Transducers5 MHz

Rodge S. A.[1]
Associate Professor, Dept. of Electronics
Adarsha Science J.B.Arts and Birla Commerce
Mahavidyalaya,
Dhamangaon Rly-444709 Maharashtra (India)

ABSTRACT: Ultrasonic arrays are used in numerous applications including medical imaging. In this specific case is imperative to achieve precise information about the magnitude and position of the peak pressure, intensity, detected image and various pressure fields produced by the transducer probe. This paper presents the analysis of 4-element and 16-element linear arrays with center frequency 5MHz for ultrasonic measurements.

KEY WORDS: Detected Image, Field-II GUI, Linear array transducer, TX/RX Pressure field.

I. INTRODUCTION

More than the last half century widely development has been made in medical device technology. One particular medical technology that has improved rapidly over the last 30 years is ultrasound. This development in technology however has brought with it the rapid obsolescence of system design. The achievement of modern electronics is built on the possibility to precisely predict system performance by the use of simulation tools. This model can be extended to components such as piezoelectric transducers attached to the electronics [1]. The capability to simulate both piezoelectric transducer and electronics jointly renders possible efficient optimizations at system level, i.e., minimizing size, price and power consumption [2].

II. SPATIAL IMPULSE THEORY

The pressure field generated by the aperture is found by the Rayleigh integral [5]

$$p(\vec{r}_1,t)=\frac{\rho_0}{2\pi}\int_s \frac{\partial v_n(\vec{r}_2,t-\frac{|\vec{r}_1-\vec{r}_2|}{c})}{|\vec{r}_1-\vec{r}_2|}ds \qquad (1)$$

Where the field point is denoted by $\vec{r}_1$ and the aperture by $\vec{r}_2$, is the velocity normal to the transducer surface. Using the velocity potential, and assume that the surface velocity is uniform over the aperture making it independent of $\vec{r}_2$, then: where the field point is denoted by $\vec{r}_1$ and

the aperture by $\vec{r_2}$, is the velocity normal to the transducer surface. Using the velocity potential, and assume that the surface velocity is uniform over the aperture making it independent of $\vec{r_2}$, then:

$$\Psi(\vec{r_1},t) = v_n(t) * \int \frac{\partial\left(t - \frac{\left|\vec{r_1} - \vec{r_2}\right|}{c}\right)}{2\pi\left|\vec{r_1} - \vec{r_2}\right|} \tag{2}$$

Where * denotes convolution in time. The integral in this equation

$$h(\vec{r_1},t) = \int_s \frac{\partial\left(t - \frac{\left|\vec{r_1} - \vec{r_2}\right|}{c}\right)}{2\pi\left|\vec{r_1} - \vec{r_2}\right|} \tag{3}$$

Represent the spatial impulse response. The continuous wave field can be found from the Fourier transform of

$$p(\vec{r_1},t) = \rho_0 \frac{\partial v(t)}{\partial t} * h(\vec{r_1},t) \tag{4}$$

The impulse response includes the excitation convolved with both the transducers electro-mechanical impulse response in transmit and receive. The final signal for a collection of scatters is calculated as a linear sum over all signals from the different scatters [3-7].

III. SIMULATION OF LINEAR ARRAY TRANSDUCER

The linear array is the fundamental type of multi-element transducer and it scans the region of interest by exciting the elements situated over the region. The field is focused on the region by introducing time delay in the excitation of the concerned individual elements, so initially concave beam is emitted.

Here a Fig.1 shows general design format of 16 element linear array transducer having height, width and kerf of individual element are taken as 5 mm, 0.2 mm and 0.02 mm respectively. The transducers are situated at the center of the coordinate system. To achieve focal length of 30 mm from the center of transducer the electronic focusing is included.

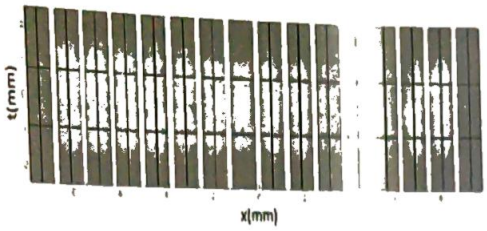

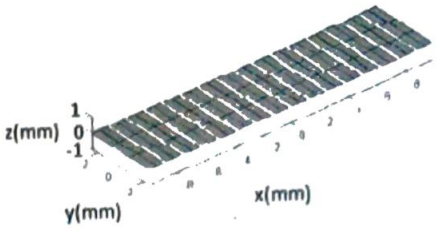

In this paper a linear array transducer of 4-elements and 16-elements is simulated by using FIELD-II GUI program with center frequencies 5MHz. For these specified linear array transducers, acoustic field generated is propagated through human body tissues and is observed at a focal distance i.e. (0, 0, 30)

IV. RESULT AND DISCUSSION

The calculation of the impulse response is eased by projecting the field point onto the plane of the aperture. In this way, the problem became two-dimensional and the field point is given as a (x, y) coordinate set and a height z above the plane. The spatial impulse response is, thus, determined by the relative length of the part of the arc that intersects the aperture [8]. Thereby it is the crossing of the projected ultrasonic waves with the edges of the aperture that determines the spatial impulse responses as a function of time. In this paper by using FIELD-II program simulated 4-element and 16-element linear array transducers with center frequency fo = $5MHz$. The speed of sound in tissue is c=$f0$ = $1540m/s$. The sampling frequency used was fs = $100MHz$. The elements had a width and height of 0.25mm and 5mm respectively. The focal-point was set to 30mm.

Table: 1 and Table: 2 shows the parameters for 4-element and 16-element linear array transducers respectively, excitation pulse and medium used for this center frequency (f0) used is 5 MHz. Figs. (a-m) shows; element impulse responses for 4-element array and figs. (a'-m') shows; element impulse responses for 16-element array transducer (i.e. TX Field image, TX Axial waveform, TX Lateral beam plot, TX/RX Field image, TX/RX Axial waveform, TX/RX Lateral beam plot, K-space TX/RX field image, K-space axial slice, K-space lateral slice, Detected image, Detected image axial slice and Detected image lateral slice).

ISSN NO : 0363-

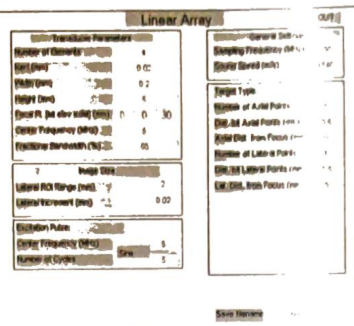

Table: 1

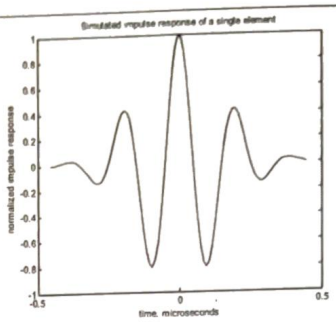

Fig. (a) Element impulse response

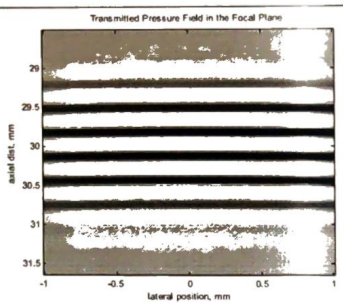

Fig. (b) TX Field image

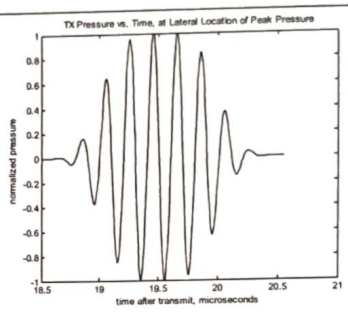

Fig. (c) TX Axial waveform

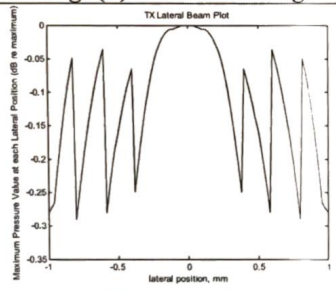

Fig. (d) TX Lateral beam-plot

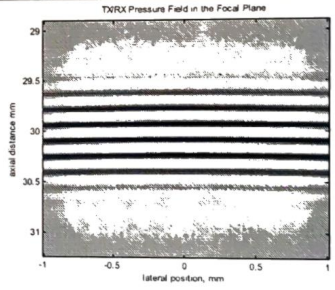

Fig. (e) TX/RX Field image

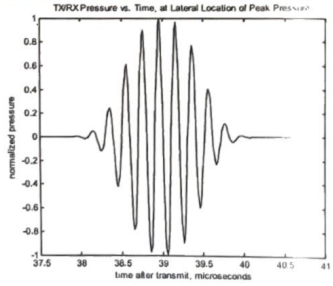

Fig. (f) TX/RX Axial waveform

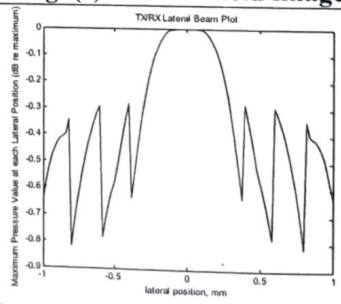

Fig. (g) TX/RX Lateral beam-plot

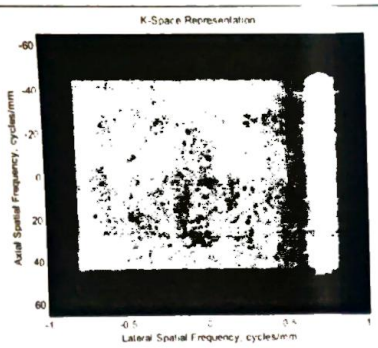

Fig. (h) K space TX/RX Field image

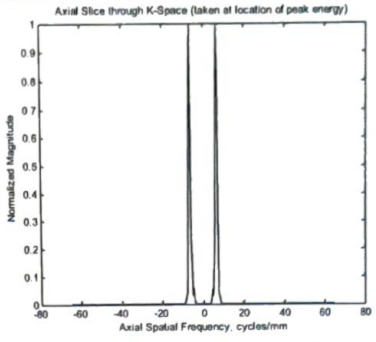

Fig. (i) K space axial slice

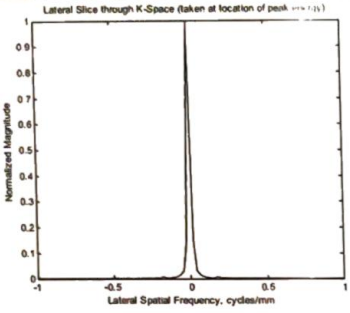

Fig. (j) K space lateral slice

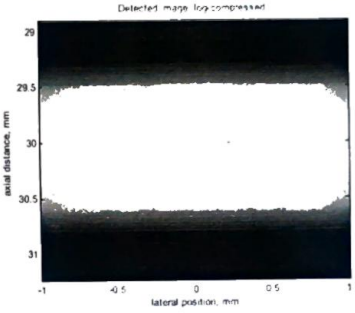

Fig. (k) Detected image

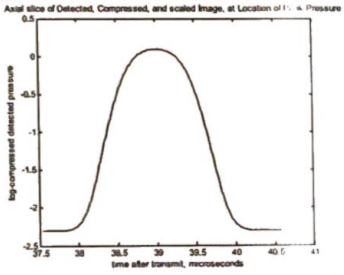

Fig. (l) Detected image axial slice

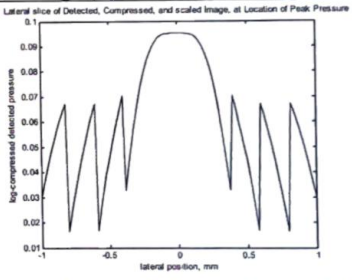

Fig. (m) Detected image Lateral slice

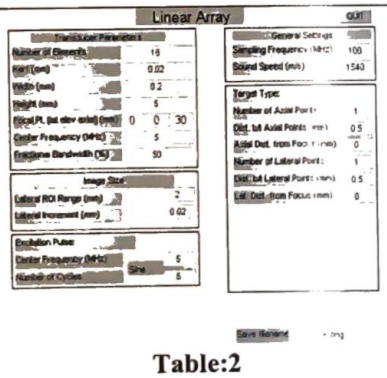

Table:2

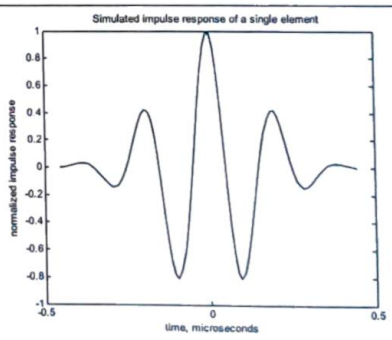

Fig. (a') Element impulse response

ISSN NO : 0363-

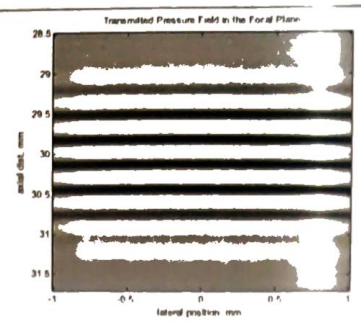

Fig. (b') TX Field image

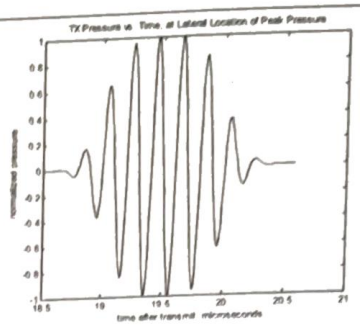

Fig. (c') TX Axial waveform

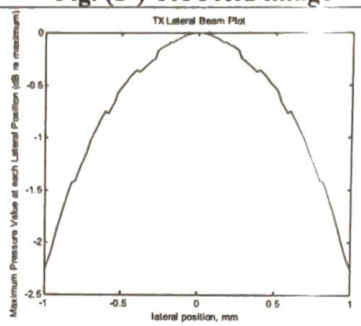

Fig. (d') TX Lateral beam-plot

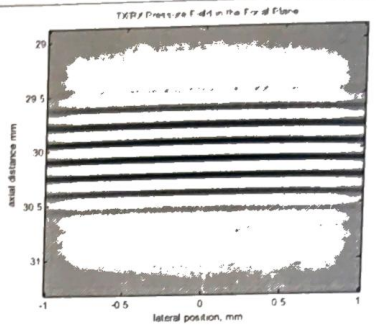

Fig. (e') TX/RX Field image

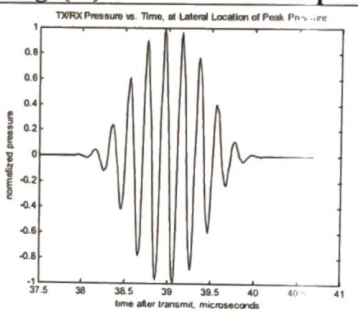

Fig. (f') TX/RX Axial waveform

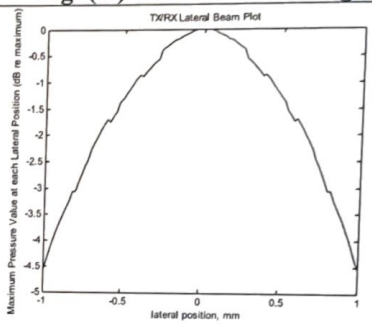

Fig. (g') TX/RX Lateral beam-plot

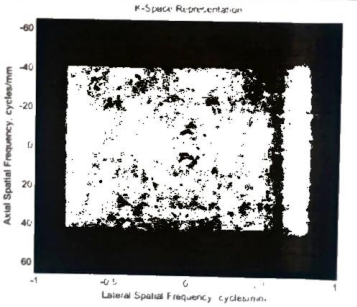

Fig. (h') K space TX/RX field image

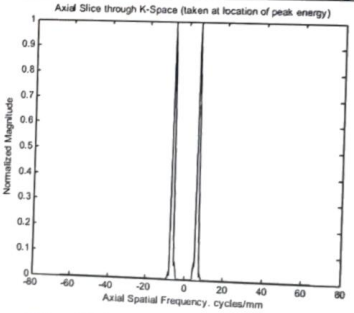

Fig. (I') K space axial slice

ISSN NO : 0363-8

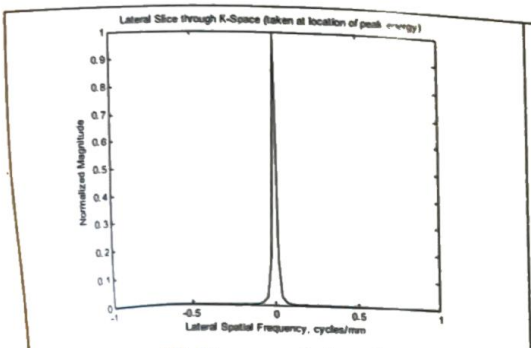

Fig. (j') K space lateral slice

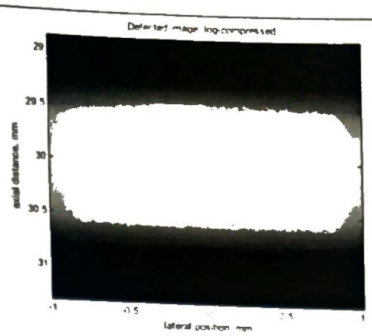

Fig. (k') Detected image

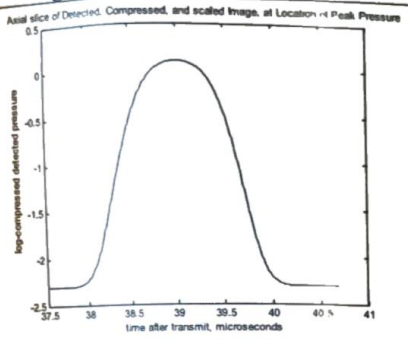

Fig. (l') Detected image axial slice

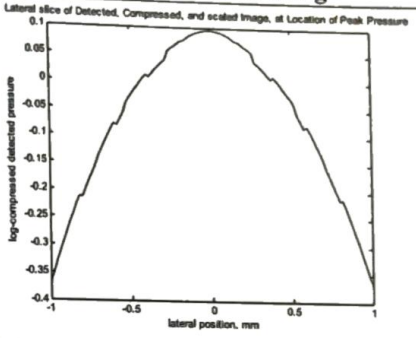

Fig. (m') Detected image lateral slice

V. CONCLUSION

The paper attempts to present a coherent analysis of the focusing strategies for 2-D array transducer design and properties, based on linear acoustics. The delays on the individual transducer elements and their relative weight or apodization are changed continuously as a function of depth. This yields near perfect focused images for all depths. Similarly, if number of arrays in the transducer are increased then contrast of displayed image, is increased thus, benefitting the diagnostic importance of ultrasonic imaging. The detected image response for 16-element array has higher contrast than 4-element array also the pressure filed generated by 16-element is high this increases diagnostic value.

References:

[1] Gandole, Y. B. (2012). Computer Modeling and Simulation of Ultrasonic System for Material Characterization. http://www.oalib.com/search? kw=Y.%20B.%20Gandole &searchField=authors.

[2] R. Krimholtz, D. Leedom, and G. Matthaci, "New equivalent circuits for elementary piezoelectric transducers," Electron. Lett. **6**, 398–399 ,1970

[3] T. R. Meeker, "Thickness mode piezoelectric transducers," Ultrasonics **10**, 26–36 ,1972.

[4] P. Marchal, F. Levarssort, L.-P. Tran-Huu-Hue, and M. Lethiecq, "Effects of acoustical properties of a lens on the pulse-echo response of a single element transducer," IEEE International Ultrasonics, Ferroelectrics, and Frequency Control Joint 50th Anniversary Conference, pp. 1651–1654,2004.

[5] Jensen, J.A, A New Approach to Calculating Spatial Impulse Responses, IEEE International Ultrasonic Symposium, Toronto, Canada, 1997

[6] P. Marchal, F. Levarssort, L.-P. Tran-Huu-Hue, and M. Lethiecq, "Effects of acoustical properties of a lens on the pulse-echo response of a single element transducer," IEEE International Ultrasonics, Ferroelectrics, and Frequency Control Joint 50th Anniversary Conference, pp. 1651–1654,2004.

[7] JENSEN, J.A., Field: A program for simulating ultrasound systems, 10th Nordic-Baltic Conference on Biomedical Imaging, in: *Medical & Biological Engineering & Computing*, 1996, **34**, Supplement 1, 351–353.

[8] Jensen, J.A., N.B. Svendsen, Simulation of advanced ultrasound systems using field II, Biomedical Imaging: Nano to Macro, 2004. IEEE International Symposiumon, 15-18 April 2004 Page(s):636–639 Vol.-1.

Japanese Journal of Applied Physics

REGULAR PAPER

Surface charge dependent structure of ionic liquid/alkali halide interfaces investigated by atomic force microscopy

Japanese Journal of Applied Physics **61**, SL1009 (2022) **REGULAR PAPER**
https://doi.org/**10.35848/1347-4065/ac528e**

Surface charge dependent structure of ionic liquid/alkali halide interfaces investigated by atomic force microscopy

Harshal P. Mungse[1,3], Saki Okudaira[1], Miho Yamauchi[2], Takashi Ichii[1*], Toru Utsunomiya[1], Shingo Maruyama[2], Yuji Matsumoto[2], and Hiroyuki Sugimura[1]

[1]*Department of Materials Science and Engineering, Kyoto University, Yoshida-hommachi, Sakyo, Kyoto 606-8501, Japan*
[2]*Department of Applied Chemistry, Tohoku University, 6-6-07 Aramaki Aza Aoba, Aoba-ku, Sendai 980-8579, Japan*
[3]*Department of Chemistry, Adarsha Science, J. B. Arts and Birla Commerce College Dhamangaon Rly. District- Amravati, 444709, India*

[*]E-mail: ichii.takashi.2m@kyoto-u.ac.jp

Received January 7, 2022; revised February 1, 2022; accepted February 6, 2022; published online June 14, 2022

Ionic liquid (IL)/solid interfaces are relevant to a broad range of physicochemical phenomena and technological processes such as catalysis, corrosion, electrochemistry, and lubrication. Hence, understanding the effect of substrate surface nature on the interfacial properties has a significant impact on improving technological processes in which interfacial properties are dominant. In this work, we investigated interfacial structures between 1-butyl-3-methylimidazolium hexafluorophosphate (BMI-PF_6) IL and KBr crystal surfaces by frequency modulation atomic force microscopy utilizing a quartz tuning fork sensor. KBr(100) and (111) surfaces were used as the substrates, where the (100) surface is electrically neutral, and the (111) surface is highly charged. We investigated the influence of surface charge on their surface structures and interfacial solvation structures by atomic-scale topographic imaging and frequency shift versus distance curve measurement. The behavior of IL at these two interfaces was found to be significantly different due to these different surface properties. © 2022 The Japan Society of Applied Physics

1. Introduction

A new class of ionic salts, ionic liquids (ILs), have been proven to possess considerable potential in electrochemistry, catalysis, solar cell, lubrication applications and also used as green alternative solvents to organic solvents.[1–5] Furthermore, they exhibit several advantages over conventional solvents because they have remarkable properties such as high thermal and chemical stability, low vapor pressure, and high ionic conductivity.[6] Therefore, ILs have attracted great interest in the scientific community. In general, when a liquid is in contact with a solid substrate, the properties of the liquid at the interface are different from those of the bulk liquid.[7] The interfaces between the solids and ILs play a crucial role for some of the applications mentioned above. To enhance the efficiency and selectivity of a particular process, detailed knowledge of the solid/IL interface at the molecular level is required for not only a fundamental understanding point of view but also the industrial applications.

Numerous approaches, such as X-ray reflectivity, resonance shear measurements, neutron reflectometry, sum-frequency generation spectroscopy, and scanning probe microscopy, including scanning tunneling microscopy and atomic force microscopy (AFM), have been applied to study the IL/solid interfaces.[8–11] In particular, AFM is capable of investigating the density distribution of ions composing the IL near the substrate by AFM-based force curve measurement, which revealed the existence of layered structure of ILs, so-called solvation layers.[11–15] However, there is limited knowledge regarding the interfacial structure between ILs/solid and the effects of the nature of solid substrates on the formation of solvation layers. Thus, this subject still has a demand for discussion.

Frequency modulation (FM) AFM, where an AFM force sensor vibrates at its resonance frequency and the force acting to the sensor is detected as its resonance frequency shift (Δf), has a higher resolution imaging capability than the classical AFM mentioned above. Thus, it is gaining particular interest to achieve true atomic-resolution imaging on various materials in different environmental conditions such as in vacuum, ambient conditions, and in liquids.[16–19] It can also characterize the density distribution of liquid molecules on liquid/solid interfaces, and the presence of solvation layers, has been revealed.[20–22] These studies revealed that the FM-AFM technique significantly impacts various research fields like surface science and nanotechnology. However, FM-AFM imaging of the substrates and interfaces in ILs is considered more difficult than in other types of liquid because the quality factor (Q) of the force sensors (Si cantilevers are widely used in FM-AFM) is heavily suppressed due to the high viscosity of ILs. Yokota et al. decreased the sensor noise in FM-AFM by improving the optical beam deflection system and achieved molecular-resolution imaging in IL using a Si cantilever.[19] In contrast, Ichii et al. took another approach; a quartz tuning fork with a sharpened metal probe, the so-called qPlus sensor, was used as a force sensor. Just a tip apex was immersed into the IL to keep the Q factor high, and atomic/molecular-resolution imaging was successfully achieved.[23,24]

Ichii et al. also demonstrated the atomic-resolution imaging and structural analysis of an interface between a KCl (100) surface and 1-butyl-1-methylpyrrolidinium tris(pentafluoroethyl)trifluorophosphate ($Py_{1,4}$-FAP) IL.[25] The two-dimensional Δf mapping revealed a different interfacial structure from other IL/solid interfaces. This difference was explained from the viewpoint of surface charge, i.e. a KCl (100) surface is electrically neutral, whereas charged substrates, such as mica, were used in other reports.[23,26]

In this work, we extended our study with this background to understand the effects of surface nature on the interfacial structure. The KBr(100) and (111) crystal surfaces were investigated in a hydrophobic IL, 1-butyl-3-methylimidazolium hexafluorophosphate (BMI-PF_6), using FM-AFM, in which the (100) surface is electrically neutral, and the (111) surface is highly charged. Both the surface structures in BMI-PF_6 IL were characterized on the atomic scale. Since (100) surfaces of alkali halide crystals can be easily obtained by cleavage, many AFM studies have been carried out on

these surfaces.[27–32] On the other hand, their (111) surfaces are highly charged and have high surface energy, which is difficult to prepare. However, Y. Matsumoto's group has recently developed a method to prepare (111)-oriented alkali halide crystals via IL flux and found that BMI-PF_6 is suitable for this process.[33,34] In addition, the hydrophobicity of the BMI-PF_6 IL minimizes the effect of water molecules even in atmospheric experiments, which is beneficial for AFM analysis. For these reasons, BMI-PF_6 IL was chosen in this study. There have been few examples of AFM observation of alkali halide (111) surfaces, and thus, their atomic-scale structural analysis is both challenging and crucially important in the field of surface science. Furthermore, we carried out Δf versus distance curve measurements on these interfaces and discussed the influence of surface charges on their solvation structures.

2. Experimental

We used an FM-AFM instrument based on a commercial AFM (JEOL JSPM-5200), and the original AFM head was replaced by a home-built AFM head for a qPlus sensor.[35] The qPlus sensor was prepared by attaching one prong of the commercially available quartz tuning fork (STATEK Co. TFW-1165) to the substrate with the help of epoxy adhesive. The probe was made from a tungsten wire with a diameter of 0.1 mm (Nilaco Co.), which was electrochemically etched in a potassium hydroxide solution (1.2 mol L^{-1}) and then glued at the other prong of the tuning fork. The resonance frequency and spring constant of the tuning fork before the probe attachment were 32.768 kHz and 1884 N m^{-1} respectively. After attaching the tungsten probe, the resonance frequency was typically decreased to 13–16 kHz. The qPlus sensor was mechanically vibrated by a piezoelectric zirconate titanate (PZT) plate. The deflection of the qPlus sensors was detected by a transimpedance amplifier with a 100 MΩ feedback register. Then, the deflection signal was amplified by an inverting amplifier with a gain of −10. These electronic circuits were embedded in the AFM head. Δf of the qPlus sensor was detected by a commercial FM demodulator (Kyoto Instruments KI-2001) with some modifications. The vibrating amplitude was kept constant using an amplitude feedback system. Because the vibrating amplitude was detected using root-mean-square (RMS)-DC converter with a bandwidth of more than a few hundred kHz, a band-pass filter was inserted between the transimpedance amplifier and the RMS-DC converter for precise amplitude detection.

All the AFM experiments were performed at room temperature. The AFM topographic images were obtained as the two-dimensional tip trajectories during the tip scanning parallel to the sample surface plane (*xy* plane), where Δf was kept constant, and were processed by WSxM software.[36] Δf versus distance curves were obtained by changing the tip-to-sample distance without the Δf feedback at a constant *xy* position. The atomic models of KBr crystals [Figs. 1 and 2(e), 2(f)] were processed by VESTA software.[37]

BMI-PF_6 IL (Tokyo Chemical Industry Co., LTD, >98%) was purchased and used without further purification. First, we prepared the saturated solution of KBr in BMI-PF_6 IL by adding 1 wt % KBr powder (Nacalai Tesque Inc. >99%). After that, the KBr(100) crystal (Furuuchi Chemical Co.) was cleaved using a sharp knife, and the solution droplet (volume: 0.2 μL) was immediately placed on the cleaved KBr(100) sample with a syringe. This sample containing the IL droplet was kept in a drying chamber (Daikin Industries, ltd., dew point < −50 °C) for 1 day. In contrast, the KBr(111) sample cannot be obtained by cleavage. It was fabricated by Y. Matsumoto's group in Tohoku University using the IL-assisted vacuum deposition method.[33,34] Then, the KBr (111) sample was transferred to H. Sugimura's group in Kyoto University by post. Note that the surface of the KBr (111) sample was covered with BMI-PF_6 IL, which protected the surface from contaminants. The ion arrangement on the (100) and (111) crystal surfaces of KBr is shown in Fig. 1. Alternate K^+ and Br^- ions are present on the KBr(100) surface, while on the KBr(111) surface either K^+ or Br^- ions are present. The KBr-saturated BMI-PF_6 droplet (0.5 μL) was placed on the KBr(111) sample and left in the drying chamber for several weeks. Finally, both the samples were used for topographic imaging and Δf versus distance curve measurement with the FM-AFM instrument.

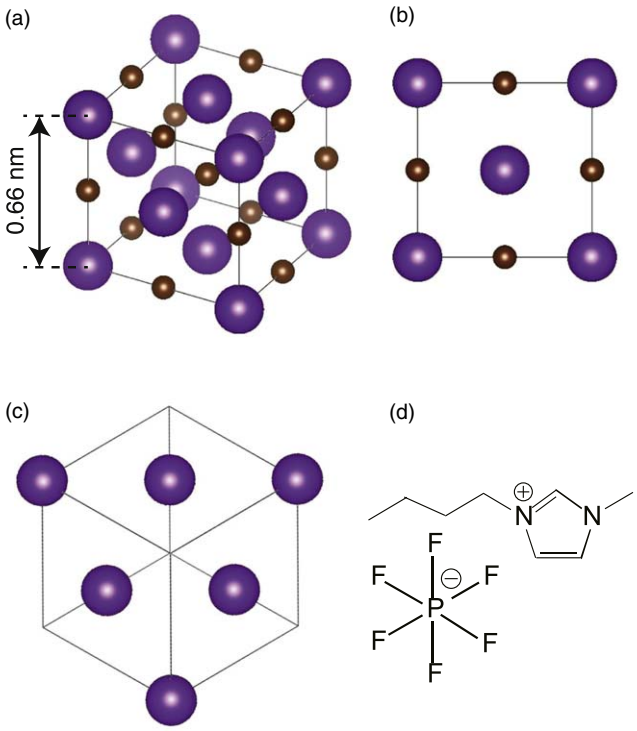

Fig. 1. (Color online) (a) Crystal structure of KBr crystal (purple: Br^-, brown: K^+), (b) atomic arrangement of KBr(100) surface, (c) atomic arrangement of KBr(111) surface assuming the exposure of Br^- ions and (d) molecular structure of BMI-PF_6 IL.

3. Results and discussion

BMI-PF_6 IL possesses a much higher viscosity (308 cP) than water (0.89 cP). We measured the Q factor of a qPlus sensor in air and BMI-PF_6, which were found to be 1700 and 55, respectively. Although the measured Q factor was heavily suppressed in the IL compared to air, it was still much higher than that of Si cantilevers in viscous ILs (∼1).[38,39] The low Q factor of the force sensor increases the frequency noise and reduces the force sensitivity.[40] In this study, only the tip apex was inserted into the IL so that the Q factor was relatively kept high and high force sensitivity was achieved.[25] When the tip apex was sufficiently close to the

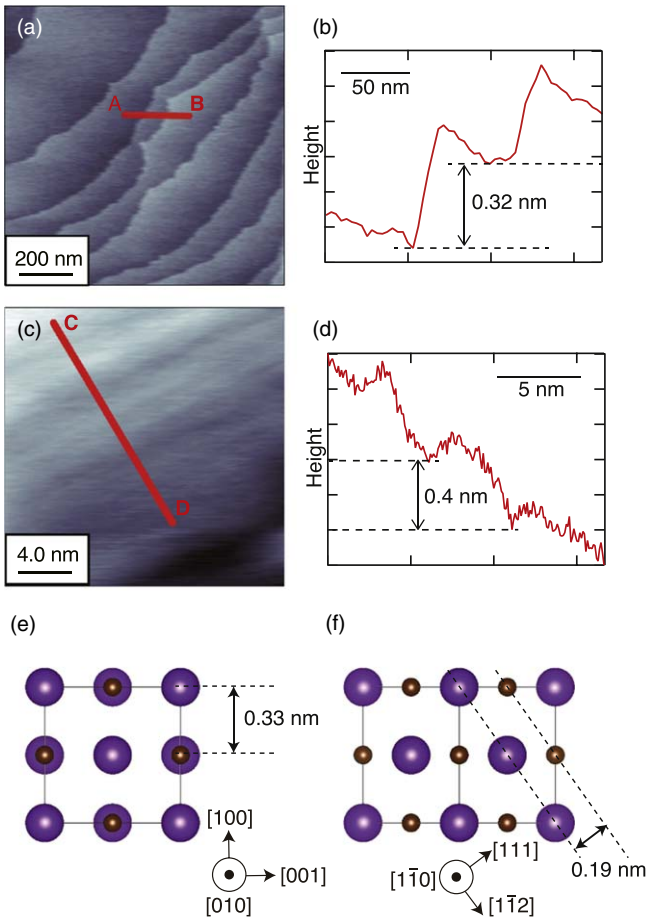

Fig. 2. (Color online) FM-AFM topographic images of (a) KBr(100) [Δf = +5 Hz, A = 1.0 nm] and (c) KBr(111) [Δf = +5 Hz, A = 1.6 nm] obtained in BMI-PF_6. (b) and (d) are the cross-sectional plots obtained along lines AB and CD, respectively. (e) and (f) are the atomic models representing inter planar distance of (100) and (111) KBr crystal surfaces, respectively.

sample surface, the resonance frequency of the qPlus sensor generally changed due to tip-to-sample interaction. The electrostatic and van der Waals forces are suppressed in conductive liquids, and hence positive Δf was usually observed. The Δf of the sensor was responsible for obtaining the topographic images in FM-AFM.

The KBr(100) is known as a natural cleavage plane because it has zero net charges. Figure 2(a) shows a topographic FM-AFM image of (100) surface obtained in BMI-PF_6, in which atomic steps were clearly seen with a step height of ∼0.32 nm [Fig. 2(b)]. This value is in good agreement with the half of the lattice constant $a_0/2$, where $a_0 = 0.66$ nm, as shown in the atomic model of KBr(100) [Fig. 2(e)] and also consistent with the previously reported values by several researchers using AFM.[27,28] As we used the KBr-saturated solution of the IL, the possibility of further dissolution of the KBr(100) crystal in IL was highly suppressed, and hence the stable atomic steps were imaged. In contrast, the KBr(111) surface is electrostatically unstable due to high surface energy and becomes quite difficult to prepare. Y. Matsumoto's group fabricated this sample by growing the KBr(111) microcrystal on α-sapphire(0001) substrate via IL thin film through vacuum deposition method.[34] In our study, we used this KBr(111) sample for the topographic imaging and the interfacial study. We kept the sample in a drying chamber for several weeks because the IL/KBr(111) interface was unstable soon after placing the IL droplet. Figures 2(c) and 2(d) show the topographic image of the (111) surface and the cross-sectional plots obtained along line C–D in Fig. 2(c), respectively. A step structure with a height of ∼0.4 nm was imaged, which was in good agreement with twice of interplanar spacing in the KBr (111) crystal surface, as shown in the atomic model Fig. 2(f). Although we cannot conclude which type of ion (K^+ or Br^-) was exposed to the surface, this result indicates that only one type of ion was exposed. From these low-resolution images of the KBr surface, we obtained a preliminary understanding of the surface topography and atomic arrangement.

Furthermore, we have carried out high-resolution imaging on these surfaces in the IL. Figure 3(a) shows an atomic-resolution topographic image of the KBr(100) surface obtained in KBr-saturated BMI-PF_6. The square lattice with a spacing of 0.46 nm was clearly seen, corresponding to the distance between the nearest equally charged ions (theoretically 0.47 nm). The previous FM-AFM studies on ionic crystals, such as NaCl, KCl, and CaF_2, carried out in UHV and aqueous solution demonstrated that either cations or anions are visible in most cases.[29–32,41] Our previous study on KCl(100) in $Py_{1,4}$-FAP IL and KBr(100) in BMI-PF_6 showed the same result.[25,42] Therefore, the bright spots in the atomic-resolution images could be assigned to K^+ or Br^- ions. Figure 3(b) shows a high-resolution topographic image of the (111) surface of KBr. As shown in Fig. 1(c), on KBr (111), either K^+ or Br^- ions form a triangular lattice with a lattice constant of 0.47 nm. However, the obtained atomic distance was approximately 0.4 nm, revealing the high distortion of atomic arrangement. Figure 3(c) shows another topographic image obtained on a different area on the KBr (111) in BMI-PF_6 IL. It also shows the atomic-scale contrast. The lattice was highly distorted, and the distance between the

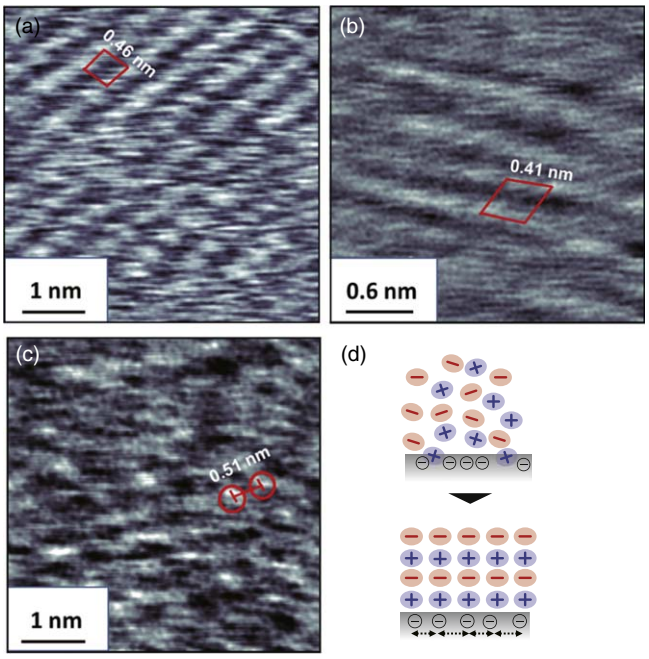

Fig. 3. (Color online) High-resolution AFM topographic images of (a) KBr (100) [Δf = +11 Hz, A = 0.8 nm], (b), (c) KBr(111) [Δf = +5 Hz, A = 1.6 nm for (b) and Δf = +101 Hz, A = 1.6 nm for (c)], obtained in BMI-PF_6. (d) Schematic illustration for explaining the distortion of atomic arrangement of KBr(111) surface in BMI-PF_6.

nearest equally charged ions was ~0.51 nm, obviously not matching the theoretical value (0.47 nm). The (111) surface consists of alternate anions and cations layers, and hence this surface possesses high surface energy, resulting in a distorted surface by surface rearrangement or reconstruction as schematically shown in Fig. 3(d). This may be one of the reasons why the distance between the closest bright spots did not match the theoretical value. It should be noted that from this experimental result, we cannot deny the possibility that the counterions derived from the IL strongly adsorbed on the KBr(111) were imaged, rather than the outermost ions of the KBr(111) surface. However, even if this were the case, it would be due to the high surface charge density of the KBr (111) surface. Thus, it is reasonable to conclude that the difference in the interfacial structure owing to the difference in the physical properties of the (100) and (111) surfaces was imaged on the atomic or molecular scale. At such interfaces where the surface atom reconstruction occurs, the interfacial solvation structure is also likely to be strongly influenced by the surface. Therefore, we analyzed the behavior of the BMI-PF_6 IL at the IL/KBr(100) and IL/KBr(111) interfaces by Δf versus tip-to-sample distance curve measurement.

Figures 4(a) and 4(b) present the Δf versus tip-to-sample distance curves which were obtained at the BMI-PF_6/KBr(100) and BMI-PF_6/KBr(111) interfaces, respectively. At the longer tip-sample distance, no Δf was observed on both the interfaces. On the BMI-PF_6/KBr(100) interface, Δf was positively and monotonically increased without oscillatory profile as the tip approached the surface. In contrast, on the BMI-PF_6/KBr(111) interface, an oscillatory Δf profile was observed. The period of oscillation was 0.65–0.73 nm, which agreed well with the theoretical ion pair diameter of BMI-PF_6 (~0.7 nm). The previous AFM studies

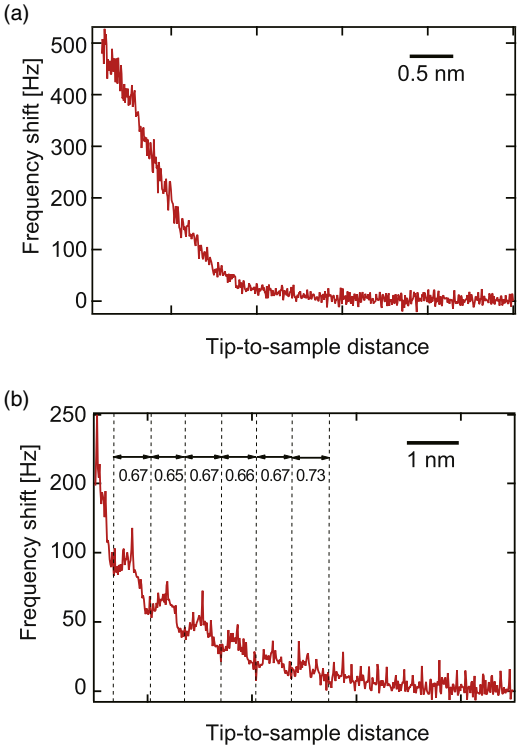

Fig. 4. (Color online) Δf versus tip-to-sample distance curves obtained on (a) a KBr(100)/BMI-PF_6 interface [$A = 0.7$ nm] and (b) a KBr(111) /BMI-PF_6 interface [$A = 5.8$ nm].

also reported that the detected thickness of the layered structure at solid/IL interface matched well with the theoretical ion-pair diameter of the ILs.[11,13–15,26] This is often explained by a model in which the cation and anion layers of the IL are alternately distributed at the interface. Furthermore, the theoretical study on AFM force curves, including Δf versus distance curves in FM-AFM, also supports this model.[43] Thus, our results indicate that the layered distribution of the ions was present only on the BMI-PF_6/KBr(111) interface. The difference in Δf profiles between BMI-PF_6/KBr(100) and BMI-PF_6/KBr(111) interfaces would be due to the different surface charges. The (100) surface is a natural cleavage plane with zero net charges since the number of cations and anions present on the surface is equal. In contrast, the (111) surface of KBr possesses either cations or anions, which leads to a highly charged surface. This would be one of the reasons for the layered solvation structure formation at this interface. When obtaining topographic images at an interface Δf distance curve oscillates, the probe may scan on the solvation layer instead of the outermost surface of the sample because there exist multiple z-positions corresponding to a certain frequency shift. In other words, the KBr(111) surface may have been scanned in Fig. 3(c), which was imaged with the larger Δf, and the solvation layer may have been scanned in Fig. 3(b), which was imaged with the smaller Δf. However, we cannot conclude this at this stage because Figs. 3(b), 3(c), and 4(b) were all obtained with different probes. Topographic imaging at different Δf and the Δf versus distance curve measurements with the same probe and the same amplitude would be a promising way to evaluate the imaging position.

We previously reported two-dimensional Δf mapping on an interface between KCl(100) and $Py_{1,4}$-FAP IL, which were composed of 128 Δf versus distance curves.[25] In that experiment, some of them showed a monotonical increase of Δf as the tip approached the KCl(100) surface, which was similar to the BMI-PF_6/KBr(100) interfacial study (this study). It should be noted that some of Δf profiles on the $Py_{1,4}$-FAP/KCl(100) interfaces showed saw-tooth like oscillations with a period of ~0.3 nm, which agreed well to the height of the atomic step of KCl(100) surface, and obviously smaller than the ion-pair diameter of $Py_{1,4}$-FAP IL. These oscillations were explained by spontaneous and/or tip-induced dissolution of the KCl(100) surface and were considered unrelated to the interfacial solvation structures. Thus, the results on $Py_{1,4}$-FAP/KCl(100) and BMI-PF_6/KBr(100) interfaces both revealed the absence of a layered and alternating cation-anion density distribution at IL/alkali halide(100) interfaces. Recently, FM-AFM studies on water/alkali halide(100) crystal surfaces were reported. Interestingly, the presence of hydration layers at the interfaces was recognized.[31,32] Moreover, the molecular dynamic simulation study also showed the presence of hydration structure at the interface.[32] Our experimental results in this study revealed that the mechanism of IL solvation layer formation is completely different from that of water hydration layers on alkali halide(100) surfaces, suggesting that surface charge is the critical factor for the formation of IL solvation layers.

4. Conclusion

In conclusion, we performed atomic-scale topographic imaging on (100) and (111) surfaces of ionic crystal KBr in viscous BMI-PF_6 IL by FM-AFM utilizing a qPlus sensor. The (100) surface showed a periodic square lattice corresponding well to its atomic arrangement model, whereas the (111) surface showed a strongly distorted atomic-scale contrast. This difference would be attributed to the higher surface charge density and higher surface energy of the (111) surface than the (100) surface. Also, the BMI-PF_6 IL/KBr interfaces for both the surfaces were studied by Δf versus distance curve measurement. The oscillatory Δf profile was only observed on the IL/(111) interface, while the monotonical increase of Δf was observed on the IL/(100) interface. That is, the layered density distribution of the ions was only found on the IL(111) interface, which was also attributed to the high surface charge density of the (111) surface. To the best of our knowledge, this is the first report on atomic-scale imaging on a polar (111) surface of KBr in BMI-PF_6 IL and on surface charge effects on the solvation layers at the interface. The selection of particular solids and liquids and the understanding of their interfacial properties are essential for improving technological processes such as catalysis, lubrication, and electrochemistry. Therefore, we consider the interpretation of the influence of substrate surface nature on interfacial properties to be of great importance, and further knowledge is urgently needed for academic and development of technological processes.

Acknowledgments

This work was supported by a Grant-in-Aid for Scientific Research B (No. 17H02787) from the Japan Society for Promotion of Science (JSPS). The author H.P.M. is grateful to JSPS for a postdoctoral research fellowship (P 16075).

ORCID iDs

Harshal P. Mungse https://orcid.org/0000-0002-8963-9219
Takashi Ichii https://orcid.org/0000-0002-4021-8894
Toru Utsunomiya https://orcid.org/0000-0002-0023-7812
Shingo Maruyama https://orcid.org/0000-0002-6608-2219
Yuji Matsumoto https://orcid.org/0000-0003-1819-5566

1) T. Welton, Chem. Rev. **99**, 2071 (1999).
2) M. J. Earle and K. R. Seddon, Pure Appl. Chem. **72**, 1391 (2000).
3) H. Liu, Y. Liu, and J. Li, Phys. Chem. Chem. Phys. **12**, 1685 (2010).
4) K. R. J. Lovelock, I. J. Villar-garcia, F. Maier, and H. Steinru, Chem. Rev. **110**, 5158 (2010).
5) I. Minami, Molecules **14**, 2286 (2009).
6) N. V. Plechkova and K. R. Seddon, Chem. Soc. Rev. **37**, 123 (2008).
7) H.-J. Butt, B. Cappella, and M. Kappl, Surf. Sci. Rep. **59**, 1–152 (2005).
8) C. Aliaga, C. S. Santos, and S. Baldelli, Phys. Chem. Chem. Phys. **9**, 3683 (2007).
9) M. Mezger et al., Science **322**, 424 (2008).
10) Y. Liu, Y. Zhang, G. Wu, and J. Hu, J. Am. Chem. Soc. **128**, 7456 (2006).
11) R. Atkin, S. Z. El Abedin, R. Hayes, L. H. S. Gasparotto, N. Borisenko, and F. Endres, J. Phys. Chem. C **113**, 13266 (2009).
12) R. Atkin and G. G. Warr, J. Phys. Chem. C **111**, 5162 (2007).
13) H. Hayes, G. G. Warr, and R. Atkin, Phys. Chem. Chem. Phys. **12**, 1709–23 (2010).
14) F. Endres, O. Hofft, N. Borisenko, L. H. Gasparotto, A. Prowald, R. A. Salman, T. Carstens, R. Atkin, A. Bund, and S. Z. El Abedin, Phys. Chem. Chem. Phys. **12**, 1724 (2010).
15) R. Hayes, N. Borisenko, M. K. Tam, P. C. Howlett, F. Endres, and R. Atkin, J. Phys. Chem. C **115**, 6855 (2011).
16) F. J. Giessibl, Science **267**, 68 (1995).
17) T. Fukuma, K. Kobayashi, K. Matsushige, and H. Yamada, Appl. Phys. Lett. **87**, 034101 (2005).
18) D. S. Wastl, A. J. Weymouth, and F. J. Giessibl, ACS Nano **8**, 5233 (2014).
19) Y. Yokota, H. Hara, T. Harada, A. Imanishi, T. Uemura, J. Takeya, and K. Fukui, Chem. Commun. **49**, 10596 (2013).
20) T. Fukuma, Y. Ueda, S. Yoshioka, and H. Asakawa, Phys. Rev. Lett. **104**, 016101 (2010).
21) J. I. Kilpatrick, S.-H. Loh, and S. P. Jarvis, J. Am. Chem. Soc. **135**, 2628 (2013).
22) K. Kobayashi, N. Oyabu, K. Kimura, S. Ido, K. Suzuki, T. Imai, K. Tagami, M. Tsukada, and H. Yamada, J. Chem. Phys. **138**, 184704 (2013).
23) T. Ichii, M. Fujimura, M. Negami, K. Murase, and H. Sugimura, Jpn. J. Appl. Phys. **51**, 08KB08 (2012).
24) T. Ichii, Y. Furutani, M. Negami, T. Utsunomiya, K. Murase, and H. Sugimura, Chem. Lett. **44**, 459 (2015).
25) T. Ichii, M. Negami, and H. Sugimura, J. Phys. Chem. C **118**, 26803 (2014).
26) T. Ichii, S. Ichikawa, Y. Yamada, M. Murata, T. Utsunomiya, and H. Sugimura, Jpn. J. Appl. Phys. **59**, SN1003 (2020).
27) F. J. Giessibl and G. Binnig, Ultramicroscopy **42–44**, 281 (1992).
28) T. Filleter, S. Maier, and R. A. Bennewitz, Phys. Rev. B **73**, 1 (2006).
29) R. Hoffmann, M. A. Lantz, H. J. Hug, P. J. A. Van Schendel, P. Kappenberger, S. Martin, A. Baratoff, and H.-J. Gu Èntherodt, Appl. Surf. Sci. **188**, 238 (2002).
30) R. Hoffmann, L. N. Kantorovich, A. Baratoff, H. J. Hug, and H. J. Güntherodt, Phys. Rev. Lett. **92**, 146103 (2004).
31) T. Arai, M. Koshioka, K. Abe, M. Tomitori, R. Kokawa, M. Ohta, H. Yamada, K. Kobayashi, and N. Oyabu, Langmuir **31**, 3876 (2015).
32) F. Ito, K. Kobayashi, P. Spijker, L. Zivanovic, K. Umeda, T. Nurmi, N. Holmberg, K. Laasonen, A. S. Foster, and H. Yamada, J. Phys. Chem. C **120**, 19714 (2016).
33) S. Kato, Y. Takeyama, S. Maruyama, and Y. Matsumoto, Cryst. Growth Des. **10**, 3608–11 (2010).
34) M. Yamauchi, S. Maruyama, N. Ohashi, K. Toyabe, and Y. Matsumoto, CrystEngComm **18**, 3399 (2016).
35) F. J. Giessibl, Appl. Phys. Lett. **76**, 1470 (2000).
36) I. Horcas, R. Fernández, J. M. Gómez-Rodriguez, J. Colchero, J. Gómez-Herrero, and A. M. Baro, Rev. Sci. Instrum. **78**, 013705 (2007).
37) K. Momma and F. Izumi, J. Appl. Cryst. **44**, 1272 (2011).
38) Y. Yokota, T. Harada, and K. Fukui, Chem. Commun. **46**, 8627–9 (2010).
39) A. Labuda and P. Grutter, Langmuir **28**, 5319 (2012).
40) K. Kobayashi, H. Yamada, and K. Matsushige, Rev. Sci. Instrum **80**, 043708 (2009).
41) S. Fujii and M. Fujihira, Jpn. J. Appl. Phys. **45**, 1986 (2006).
42) Y. Yamada, T. Ichii, T. Utsunomiya, and H. Sugimura, Jpn. J. Appl. Phys. **58**, 095003 (2019).
43) K. Amano, Y. Yokota, T. Ichii, N. Yoshida, N. Nishi, S. Katakura, A. Imanishi, K. Fukui, and T. Sakka, Phys. Chem. Chem. Phys. **19**, 30504 (2017).